Proteomic Profiling of the Corpus Cavernosum Tissue of Rats

By

Catherine Grey Kasper

Submitted in Partial Fulfillment of the Requirements

for the Degree of

Master of Science

in

Biological

Sciences

YOUNGSTOWN STATE UNIVERSITY

November, 2009

Proteomic Profiling of the Corpus Cavernosum Tissue of Rats

Catherine Grey Kasper

I hereby release this thesis to the public. I understand that this thesis will be made available from the OhioLINK ETD Center and the Maag Library Circulation Desk for public access. I also authorize the University or other individuals to make copies of this thesis as needed for scholarly research.

Signature:

Catherine Grey Kasper, Student Date

Approvals:

Dr. Robert Leipheimer, Thesis Advisor Date

Dr. Gary Walker, Thesis Advisor Date

Dr. James Toepfer, Committee Member Date

Peter J. Kasvinsky, Dean of School of Graduate Studies and Research Date

Abstract

These studies were designed to gain a better understanding of the complex cellular processes involved in the regulation of erectile tissue by generating an extensive profile of the proteins present in the smooth muscle cells of the corpus cavernosum. Specifically, this study presents a proteomic profile of corpus cavernosal tissue isolated from intact and castrated rats with a specific focus on the role of androgens. The hypothesis is that castration will alter the protein expression at multiple sites. This proteomic approach provides important insights into protein expression in this tissue and with and without the presence of androgens.

Results of this study demonstrated a variety of proteins expressed in both the castrate and non-castrate tissue. Alterations in the intensity of these polypeptide bands were visible between tissues isolated from intact or castrated rats suggesting either up-regulation or down-regulation of a variety of proteins. Furthermore shifts in these proteins were seen possibly suggesting phosphorylation or dephosphorylation of proteins due to the presence or absence of androgens. Additionally, there were a number of proteins found in gels from either the castrate or non-castrate tissues which did not exist in either's counterpart. These differences suggest that androgens play a critical role in the expression of these proteins in the corpus cavernosum.

Acknowledgments

I would like to express my deepest appreciation to all my committee members and most especially to my committee co-chairs, Dr. Robert Leipheimer and Dr. Gary Walker. Without the guidance, leadership and advice I received from both Dr. Leipheimer and Dr. Walker, as well as Dr. Toepfer, this thesis would not have been possible. The extensive knowledge and continued patience that all of my committee members have given me from the initial pursuit to the final defense of my thesis, and still beyond, has enabled me to further my educational career with a solid background that could only be gotten from the incredible teaching abilities that each of them portray.

Furthermore, I would like to personally extend my sincere gratitude to Dawn Amolsch who continually assisted me beyond what was expected, and enhanced my understanding of processes and procedures that she so patiently showed me. Additionally, I would like to acknowledge Julie Chandler for her assistance and guidance in the lab, which was invaluable to me.

Finally I would like to thank my family and friends for their continued support in my pursuit of higher education.

Table of Contents

List of Figures

Figure Page

List of Figures (cont)

List of Tables

Introduction

Erectile dysfunction (ED) is defined as the chronic inability to attain or maintain a sufficient erection (NIH, 1993). ED differs from impotence in that it is a more precise term defining erectile problems; whereas impotence signifies more of a broad range of problems including sex drive, ejaculation, and/or orgasm, all of which can be an element of erectile disorders (NIH, 1993; Sehgal and Srivastava, 2003). ED affects approximately 152 million men worldwide including 20-30 million men within the United States alone, many of which have not sought treatment (NIH, 1993; Aytac et al., 1999). Prevalence and severity of ED tends to increase with age, from 30-40% of men suffering at age 40 up to 70% of men suffering by age 70 (Sehgal and Srivastava, 2003; Jensen et al., 2000). Despite the limited data from developing countries and the lack of men seeking treatment globally, the incidence, prevalence, and severity appear to be uniform worldwide, irrespective of race or ethnicity (NIH, 1993; Sehgal and Srivastava, 2003).

Erectile dysfunction is generally classified as organic, psychogenic, or a mix of organic and psychogenic etiologies (NIH, 2003; Maas et al., 2002; Sachs, 2000). Although only two decades ago erectile dysfunction was considered primarily a condition of psychogenic origin (Melman and Gingell, 1999), recent critical advances in understanding not only the physiology of an erection, but also the pathophysiology of erectile dysfunction help to distinguish that the most common form is actually organic (Maas et al., 2002; Bivalacqua et al., 2003). Psychogenic ED is due to the central inhibition of the erectile mechanism without physical injury (Melman and Gingell, 1999).

Some of these psychogenic factors include depression, anxiety, guilt, lifestyle changes, psychological trauma, child abuse, sexual incompatibility, low self esteem, performance anxiety, relationship conflicts, etc. (Sehgal and Srivastava, 2003; Fabbri et al., 1997). These psychogenic aspects are often related to specific events and have an acute onset (Sehgal and Srivastava, 2003). Studies show that psychogenic factors are predominant in younger males (Melman and Gingell, 1999).

The most prevalent cause of erectile dysfunction, as previously stated is of the organic nature. Organic ED is due to vasculogenic, neurogenic, hormonal, or cavernosal smooth muscle abnormalities or lesions (Melman and Gingell, 1999). Some of the organic factors are attributed to aging and/or underlying diseases (Lue, 2000; Sachs, 2000). The most frequent cause of organic ED is vascular in nature and includes arterial or venous abnormalities. These vascular abnormalities are oftentimes associated with atherosclerosis, diabetes mellitus, hypercholesterolemia, hypertension, etc. (Sehgal and Srivastava, 2003; Melman and Gingell, 1999; Maas et al., 2002; Fabbri et al., 1997; Bivalacqua et al., 2003, Simonsen et al., 2002; Jensen et al., 1999). The neurogenic factors include spinal injury, nerve damage, multiple sclerosis, cerebrovascular accidents, chronic renal failure, Alzheimer's disease etc. (Sehgal and Srivastava, 2003; Melman and Gingell, 1999; Fabbri et al., 1997). The endocrinologic causes of ED include hypogonadism, pituitary tumors, hypo and hyperthyroidism, etc. (Sehgal and Srivastava, 2003; Melman and Gingell, 1999; Fabbri et al., 1997; Shabsigh et al., 2006; Glina, 2004, Gooren, 2006). Other etiologies of ED include structural abnormalities, drug induced ED, pelvic trauma, irradiation, and/ or surgery (Sehgal and Srivastava, 2003; Melman and Gingell, 1999; Fabbri et al., 1997). Aging, as well as risk factors associated with a

variety of diseases such as smoking, obesity, alcoholism, narcotic drug abuse, sedentary lifestyles, increase the risk of ED (Maas et al., 2002; Simonsen et al., 2002; Derby et al., 2000; Bacon et al., 2006; Maggi et al., 2000).

Sexual stimulation, which can include sensory and/or mental stimulation, elicits impulses from both the central and peripheral nervous system. The brain initially integrates and processes these stimuli via the hypothalamus, which in turn activates the descending pathways of the nervous system. The variety of sensory information for sexual arousal initially reaches its corresponding cortical area and then project to the appropriate cortical association areas. These primary cortical connections then extend to connect with limbic structures such as the amygdala. Within the limbic system, most especially within the nucleus accumbens, dopamine plays a major role in anticipating sexual behavior, whereas noradrenaline is thought to participate in the motivational aspect of sexual behavior (Guiliano 2004). From the amygdala, connections are linked to midbrain structures such as the periaqueductal gray, as well as the hypothalamus (Moreland et al., 2001). When the brain receives sexual stimuli, it drives the sexual response via the medial pre-optic area (MPOA) and the paraventricular nucleus (PVN) of the hypothalamus, which activates certain neurochemicals which can either stimulate or inhibit sexual behavior. The MPOA is essential for integrating and distributing sexual information to other hypothalamic, as well as brainstem structures, including the PVN located within the hypothalamus and the nucleus paragigantocellularis (nPGi) located within the pons. Whereas the PVN has a stimulatory effect on the erection process, the nPGi has an inhibitory role. The nPGi inhibitory projections themselves must be inhibited to allow for an erection to occur. The PVN receives projections from the

MPOA, which in turn activates selective autonomic pathways, therefore regulating some behavioral aspects of sexual function (Giuliano and Rampin, 2000; Giuliano et al., 1997; Steers, 2000). Within the PVN, DA agonists increase nitric oxide (NO) suggesting a role for the NO-cGMP pathway described further (below) in more detail at the level of the cavernosal smooth muscle tissue (Moreland et al., 2001). Similarly, research has demonstrated that the NO-cGMP pathway activation within the MPOA is involved with the increase in intracavernosal pressure to stimulate an erection (Sato et al., 2001). Oxytocin has been shown to have a significant facilitatory effect on the erection process (Argiolas and Melis, 1995). During an erection, dopamine is also thought to activate oxytocinergic neurons within the PVN, releasing oxytocin, thereby inhibiting the serotonergic projections to the nPGi. As priorly stated, these serotonergic neurons within the nPGi produce an inhibitory effect on the erectile response; therefore the PVN dopaminergic effect helps to stimulate the erectile process (Chen et al., 1999; Guiliano, 2004; McKenna, 1999; Steers, 2000). Likewise prolactin is thought to possibly inhibit the excitatory dopaminergic effect; however more research needs to be done to examine the role of prolactin in the entire erectile process (Kruger et al., 2002). Serotonin (5-HT or 5-hyroxytryptamine) participates in the control of sexual behavior involving both the sympathetic, as well as the parasympathetic, nervous systems. Although serotonin appears to have a variety of functions in the erectile function of the male, the primary role of 5-HT is thought to be an inhibitory effect of the sexual response (Andersson, 2001). However, of the several 5-HT subtypes, the 5-HT_{2C} receptor subtypes are thought to exert a facilitating effect on the male sexual behavior; whereas the 5-HT_{1A} receptor subtypes are thought to provide an inhibitory effect (Moreland et al., 2001).

Afferent nerve fibers from the supraspinal centers convey sensory information to interneurons within the lumbosacral spinal cord. This information is then projected to the autonomic and somatic efferent fibers, which innervate the pelvic organs. These descending inputs, originating from various supraspinal centers including the hypothalamus, brainstem, and various cortical areas, provide excitatory and inhibitory regulation as stated above. The supraspinal centers are also influenced by sensory information from the genitals which creating a positive feedback mechanism (McKenna, 1999). The parasympathetic preganglionic path originates within the sacral spinal cord and is responsible for excitatory input responsible for vasodilation of cavernous artery resulting in erection. These preganglionic neurons contain a variety of neurotransmitters including acetylcholine, NO, VIP, etc., which regulate the ganglion cells within the pelvis plexus and the cavernous nerve. The cavernous nerve then innervates the penis through the postganglionic parasympathetic fibers. The sympathetic preganglionic path originates in the intermediolateral cell column of the thoracocolumbar spinal cord and travel in the hypogastric nerve and sympathetic chain. These fibers tend to be mostly vasoconstrictive; however they play a role in both tumescence and detumescence (McKenna, 1999). Like the parasympathetic fibers, the sympathetic neurons also contain a variety of neurotransmitters and neuropeptides including acetylcholine, NO, VIP, as well as norepinephrine and neuropeptide Y (Steers, 1994). The sympathetic and parasympathetic nerve fibers coalesce to form the cavernous nerves which ultimately influence vascular events within the penis such as the regulation of blood flow into and out of the corpora cavernosa, corpus spongiosum and the glans penis; whereas the somatosensory component is primarily due to the innervation of the pudendal nerve

which is responsible for sensation, as well as contraction and relaxation of the extracorporeal muscle cells (Christ and Lue, 2004; Morelli et al., 2006). Sensory information from the penis to the sacral spinal cord is relayed by a terminal branch of the pudendal nerve called the dorsal nerve of the penis (DNP). These afferents in the DNP have been shown to be critical in initiating erectile responses (Steers, 1994; Yang and Bradley, 1998). Onuf's nucleus located in the sacral spinal cord is considered the center of somatomotor penile innervations. These nerve fibers are carried by the pudendal nerve to the ischiocavernosus and bulbocavernosus muscles that are vital in sexual function (Dean and Lue, 2005; Steers, 2000). The excitement of these nerve fibers cause the release of a variety of neurotransmitters along with the activation of several second messenger pathways which in turn regulate the state of contraction and relaxation of the penile smooth muscle cells.

The penis is composed of three distinct erectile tissues, each separated by a connective tissue septum. The first tissue is the corpus spongiosum, which functions to support and protect the urethra. The remaining two tissues, the corpora cavernosa, are adjacent to each other and act as a blood reservoir, as well as a structural support for the penis during erection. The penile erectile tissue of the two corpora cavernosa tissue are located dorsally and function as one unit, whereas the single corpus spongiosum is located ventrally, encompasses the urethra, and distends distally to form the glans penis. Both the corpora cavernosa and the corpus spongiosum are surrounded by the tunica albuginea, a thick fibrous sheath. All three corpora are essentially composed of cavernosal spaces, or lacunae, which are lined with vascular endothelium and separated by fibrous trabeculae. The majority of the cells that make up the tissue of the corpora

include smooth muscle cells and endothelial cells. In the normal healthy adult male, the trabeculae are made up fibroblasts, collagen, and elastin fibers, with the majority (42-50% of trabecular tissue) being composed of smooth muscle cells fibers (Ryu et al., 2005). The lacunae are filled with, or emptied of, blood depending on the penile state of flaccidity or rigidity (Melman and Gingell, 1999; Gefen, et al., 2001).

The hemodynamics, influenced by the nervous system, are ultimately responsible for the flaccidity or rigidity of the penis and thereby control the tone of the smooth muscle fibers. Blood supply to the penis primarily originates from the internal pudendal artery, which eventually branches into the penile artery and ultimately diverges into several smaller arteries, including the cavernosal arteries. These smaller arteries supply the corpora cavernosa and its sinusoidal spaces. There are three sets of veins responsible for draining the blood from the penis, including the deep vein, which drains the corpora cavernosa and the corpus spongiosum (Morelli et al., 2006; Gefen et al., 2001).

Unlike most other smooth muscles, the erectile muscle of the penile tissue remains in a contracted state for a majority of the time, then relaxes to carry out its physiological function. In the normal flaccid state of the penile tissue, sympathetic innervation is prevalent, blood flow into the penis is minimal due to the tonic contractile state of the arterial, as well as the corpora smooth muscle, and venous out flow of blood is uninhibited (Morelli et al., 2006; Gefen et al., 2001). Upon sexual stimulation, parasympathetic induced release of NO causes the relaxation of the corpora and arterial smooth muscles. This allows the blood to flow into the cavernosa, filling its sinusoidal spaces and ultimately causing the expansion and enlargement of the penile tissue. This expansion of the penile tissue is restricted by the thick, rigid covering of the tunica

albuginea. This restriction causes the compression of the emissary veins, thereby preventing venous outflow of blood from the penile tissue, called the veno-occlusive mechanism. The combination of the increased arterial inflow and the decreased venous outflow causes a high intracavernosal pressure, which ultimately results in an erection (Christ and Lue, 2004; Morelli et al., 2006; Gefen et al., 2001). Three specific types of neuronal control have been identified locally at the corpora cavernosa level; the first being responsible for the contractile state of the penile tissue and the other two are identified as being involved in the relaxation of smooth muscle which leads to erection. The first neuronal control that is involved in the contraction of both the corpora cavernosa and the vascular smooth muscle tissue is noradrenergic stimulation. This sympathetic impact is responsible for maintaining the typical flaccid state of the penis. The two main factors of neurotransmitters/neuromodulators that are involved in the contractile state of the penis include noradrenaline or norepinephrine and endothelin-1 (Morelli et al., 2006; Argiolas and Melis, 1995; Andersson, 2003). The release of noradrenaline induces contraction by stimulating the post-synaptic α-adrenoceptors located in the both the blood vessels and cavernosal tissue. Androgens, as well as several other factors, possibly regulate the responsiveness of these α-adrenoceptors (Andersson, 2003). Once noradrenaline binds to the α-adrenergic receptors, a G-protein pathway is activated, which involves phosphatidylinositol 4,5-biphosphate (PIP_2), a substrate for the enzyme phospholipase C. When noradrenaline binds, phospholipase C stimulates the hydrolysis of PIP_2 into diacylglycerol (DAG) and, more importantly for the contraction of smooth muscle, inositol-1,4,5-triphosphate (IP_3). IP_3 triggers the release of calcium from intracellular stores, specifically the sarcoplasmic reticulum, and/or triggering calcium

channels on the cell's membrane to open leading to an influx of calcium into the cytosol. The sarcoplasmic reticulum also has calcium-induced calcium release (CICR) channels which are activated by the increase in cytosolic calcium. This further increases the amount of calcium available in the cell and enhances contraction (Levin et al., 1997). The sustained contraction of erectile tissue is dependent on the continuous transmembrane calcium influx through voltage gated calcium channels, as well as through intracellular calcium storage sites such as the sarcoplasmic reticulum. This increased calcium concentration leads to the binding of calcium with calmodulin. The binding of calcium to calmodulin results in a change in the conformation of the protein. This conformational transformation enables the calcium-calmodulin complex to activate myosin light chain kinase (MLCK). In turn, MLCK phosphorylates myosin regulatory light chains which activates myo-ATPase. The energy that ATP releases via myo-ATPase enables cross-bridge attachment and cycling, which is the molecular interaction between myosin and actin, thereby inducing contraction (Maas et al., 2002; Lue, 2000; Andersson, 2003; Williams et al., 2005; Jin and Burnett, 2006). Simultaneously, DAG activates protein kinase C (PKC) that is also calcium dependent. PKC then phosphorylates a variety of proteins that regulate cross-bridge cycling such as L-type calcium channels. The L-type calcium channels are voltage gated calcium channels that lead to the additional influx of calcium, further promoting contraction of the CCSM (Webb, 2003). Another important protein that PKC activates is CPI-17, an inhibitory protein targeting the catalytic subunit of myosin light chain phosphatase (MLCP) (Jin and Burnett, 2006; Eto et al., 2007).

Another critical conduit for contraction is related to calcium sensitization, which does not require additional increases of calcium in order to inhibit myosin phosphatase. This calcium sensitization is caused by activation of heterotrimeric G-protein coupled receptors that in turn activate the RhoA/Rho-kinase G-protein pathway. Consequently, RhoAGDP, a small, monomeric G protein, binds with GTP and translocates to the plasma membrane to initiate signal transduction. In its inactive configuration, RhoAGDP is bound to Rho-GDI (guanine nucleotide dissociation inhibitor), which stabilizes the complex within the cytosol. The translocation of RhoAGTP to the plasma membrane is due to the replacing GDP with GTP on RhoA, causing its activation and dissociation from Rho-GDI (guanine nucleotide dissociation inhibitor) (Jin and Burnett, 2006; Wang et al., 2002). Via this second messenger system, activated RhoA stimulates Rho-kinase (ROCK), the serine/threonine kinase. Rho-kinase increases the phosphorylation of myosin by either directly phosphorylating myosin regulatory light chain (RLC) or indirectly by phosphorylating the myosin binding subunit, thereby inhibiting its activity. ROCK is a primary regulator of MLCP activity. This Rho-kinase interference prevents the dephosphorylation of myosin RLC thus preserving penile contraction, by sensitizing the myofilaments to calcium (Andersson, 2003; Somlyo and Somlyo, 2000; Mills et al., 2001). Rho-kinase is thought also to increase calcium sensitization via its ability to phosphorylate CPI-17 (Jin and Burnett, 2006; Eto et al., 2007). The phosphorylation of CPI-17 is critical in converting the protein into an effective inhibitor by phosphorylating the catalytic subunit of MLCP. This phosphorylation of CPI-17 occurs simultaneously to the phosphorylation of myosin via PKC, which is maintained via the RhoA/ROCK pathway. The inhibition of MLCP promotes myosin phosphorylation, which leads to

contraction (Eto et al., 2007; Webb, 2003). Furthermore, the inhibition of MLCP by CPI-17 leads to calcium sensitization, increasing MLC phosphorylation and force regardless of the intracellular calcium concentration (Bonnevier and Arner, 2004). Recently, it has been suggested that this RhoA/Rho-kinase cascade also plays an important role in suppressing the expression and enzymatic activity of the gene for endothelial nitric oxide synthase. This inhibition results in a decreased biosynthesis of endothelial nitric oxide, an important component in penile relaxation whose effects are explained below (Bivalacqua et al., 2003).

Generated within the vascular endothelium, endothelian-1 (ET-1) is responsible for inducing long-term contractions within the smooth muscle tissues, as well as maintaining cavernosal smooth muscle tone. The contractile effect of ET-1 is thought to be dependent on increases in intracellular calcium and mediated by the Rho-kinase pathway (Andersson, 2003; Mills et al., 2001; DiSanto, 2003). Another suggestion is that ET-1 is involved in penile tissue contractions via a mechanism involving phospholipase C as described above for NE. This activation of ET-1 leads to increases in intracellular calcium levels via the PIP_2/DAG-IP_3 pathway described above, ultimately causing contraction (Fabbri et al., 1997). The third molecule which has been proven to play a viable role in CCSM contraction is angiotensin II which also works through a G-protein coupled receptor and RhoA pathway (Lin et al., 2008; Comiter et al., 1997). Other vaso-constrictors are found in penile tissue including neuropeptide Y, prostaglandin $F_{2\alpha}$, and tromboxane A_2, but their roles are not well established as yet (Morelli et al., 2006; Andersson, 2003; Somlyo and Somylo, 2000).

The other two types of neuronal control are involved in the relaxation state of the penile tissue and both are of parasympathetic origin. The first is considered a cholinergic pathway which is responsible for initiating relaxation and the second is a nonadrenergic-noncholinergic pathway which is believed to work in conjunction with the inhibitory cholinergic pathway. The inhibitory cholinergic neuronal pathway involves the neurotransmitter acetylcholine. Acetylcholine plays an indirect role in the relaxation of penile smooth muscles via two methods. First it diminishes the sympathetic action of contraction by inhibiting the receptors for noradrenaline. Secondly, acetylcholine activates the nonadrenergic-noncholinergic pathway by stimulating the release of nitric oxide from corpus cavernosa's vascular endothelium and, more importantly, its release from local inhibitory nerves. The nonadrenergic-noncholinergic inhibitory pathway involving nitric oxide is a crucial conduit for the relaxation of penile vascular and smooth muscle tissue, therefore ultimately essential in creating and sustaining a tonic erection. Nitric oxide (NO), a transient gaseous radical that can act within the cell in which it is manufactured or easily diffuse through membranes to produce its effects in other cells, is found not only in the vascular endothelium, but also is located in the local nonadrenergic-noncholinergic nerve cells (Morelli et al., 2006; Argiolas and Melis, 1995; Andersson, 2003; Kim et al., 1991). NO is synthesized via the oxidation of L-arginine by nitric oxide synthase (NOS), a calcium-calmodulin dependent enzyme, which is thought to exist in several forms. Two types of nitric oxide synthase are thought to mediate relaxation of erectile tissue: nNOS found in the non-adrenergic, non-cholinergic neurons and eNOS found in the endothelium of both the vascular tissue and the cavernosal tissue. Like most enzymes, NOS can be inhibited, activated, down-regulated or up-regulated (Maas et al.,

2002; Morelli et al., 2006). This rigid regulation of the NOS isoforms is critical in producing physiologically relevant amounts of NO. nNOS activity stimulates the production of NO from the nonadrenergic-noncholinergic nerve cells, which acts as a neurotransmitter, ultimately causing the increase of blood flow from local arteries supplying the corpora, leading to its expansion. This increased blood flow and expansion of the corpora subsequently activates eNOS by a shear stress/mechanical mechanism, which in turn produces endothelial-derived NO to provide for sustained NO production and maximal erection (Bivalacqua et al., 2003; Boo et al., 2002; Hurt et al., 2002). This process is mediated by the cascade pathway of phosphatidylinositol 3-kinase (PI3) and the serine/threonine protein kinase Akt (also called PKB). Studies have shown that that eNOS phosphorylation is regulated by a pathway dependent on protein kinase A (PKA), independent of Akt; yet the production of NO is dependent on both PKA and Akt protein kinase pathways (Andersson, 2003; Hurt et al., 2002). In addition, other studies have shown that in diabetic males, eNOS expression and function has been shown to be modulated by RhoA/Rho-kinase (Bivalacqua et al., 2004).

Nitric oxide works to activate soluble guanylate cyclase via the classic cyclic guanosine monophosphate (cGMP) second messenger system in which guanylate cyclase catalyses the conversion of GTP into cGMP (Morelli et al., 2006). The consequential increased levels of cGMP result in the modulation of specific events which further regulate diverse intracellular functions including activities of protein kinases, phosphodiesterases (PDEs), other signal transduction mechanisms, and ion channels, particularly calcium and potassium channels. One of these numerous intracellular functions includes an important step in the relaxation of penile smooth muscle and the

corresponding penile vasodilation, relying on cGMP to activate the serine/threonine protein kinase, cyclic GMP-dependent protein kinase (PKG) (Chuang et al., 1998). Three major pathways are regulated by the second messenger system of NO, cGMP, and PKG which ultimately lead to relaxation of penile smooth muscle. These include reduction of intracellular cytosolic calcium levels, calcium desensitization, and thin filament regulation. Within the corpus cavernosal smooth muscle cells, PKG catalyzes the phosphorylation of a variety of physiologically important proteins that regulate the contractile state, including ion channels and pumps that promote the reduction of cytosolic calcium. One such protein that is phosphorylated is the IP_3 receptor, thereby inhibiting calcium release from intracellular stores. Furthermore, PKG activates the Ca^{2+}/ATPase pump located within the cell membrane to aid in the extrusion of calcium out of the cell, as well as the Ca^{2+}/ATPase pump located on the sarcoplasmic reticulum to sequester calcium back into intracellular stores. Following a decrease in cytosolic calcium, calmodulin dissociates from myosin light chain kinase and inactivates it (Andersson, 2003; Williams et al., 2005; Lincoln et al., 2001; Chuang et al., 1998).

Additionally, PKG activates another important ion channel via phosphorylation, reducing cytosolic calcium; these are membrane potassium channels called the K_{Ca} and K_{ATP} channels. As stated before, tonic contraction of the erectile smooth muscle depends on the continual influx of transmembrane calcium, including extracellular calcium entry from voltage gated calcium channels. The most physiologically relevant calcium channel present in the corporal smooth muscle is the L-type voltage dependent calcium channel (VDCC), which provides a continuous influx of calcium to sustain contraction and tone. There are at least four potassium channel subtypes identified within corporal smooth

muscle, these include the K_{Ca} (also known as Maxi-K or BK channels) which are calcium sensitive potassium channels, the K_{ATP} metabolically regulated potassium channels, the voltage-regulated potassium channels, and the A-type potassium channels. Although all of these potassium channels are relevant to hyperpolarization and the efflux of potassium, the K_{Ca} and the K_{ATP} are the most studied and understood, as well as thought to be the most physiologically relevant (Christ and Lue, 2004). The most predominant of all the potassium channels is the K_{Ca} channel, responsible for approximately 90% of the outward potassium current within corporal smooth muscle cells (Christ et al., 1997; Christ et al., 1993). This K_{Ca} channel is made up of two subunits: the alpha (α) subunit is the pore-forming subunit and the beta (β) subunit is a regulatory transmembrane subunit. This channel responds to both depolarization of the membrane, as well as increases of calcium within the cytosol (Archer, 2002). When cytosolic calcium levels are high, K_{Ca} channels open and concomitantly modulate the activity of voltage gated calcium channels (Christ et al., 1997). Furthermore, increased activity of these K_{Ca} channels is caused by direct activation via PKG. Analogously to other ion pumps and channels, PKG regulates these K_{Ca} channels either directly by catalyzing the phosphorylation of them or indirectly by activating a protein phosphatase that can dephosphorylate them (Lincoln et al., 2001). As a result, these K_{Ca} channels hyperpolarize the cell membrane and reduce cytosolic calcium by inhibiting the influx of the ion from voltage gated calcium channels. The reduction of intracellular calcium then leads to the dephosphorylation of MLC and simultaneously to relaxation (Morelli et al., 2006; Archer et al., 1994; Lee and Kang, 2001; Fan et al., 1995; Lincoln et al., 2001). These K_{Ca} channels have also been implemented in the modulation of α-adrenergic receptor mediated contractions, as well as

ET-1 induced contractions. When these potassium channels were blocked, the magnitude of contractions via an α-adrenergic receptor agonist increased, whereas activating these K_{Ca} channels had the opposite effect (Spektor et al., 2002; Christ et al., 1997). Inhibition of these K_{Ca} channels also has impaired cGMP-induced vasodilation (Archer, 2002).

The K_{ATP} channels are the potassium channels which work like the K_{Ca} channel to reduce calcium influx and assist in the modulation of corporal smooth muscle tone. These K_{ATP} channels are activated when intracellular ATP concentrations are low, such as is seen in the contractile state of smooth muscle (Lee et al., 1999). Phospholipids, such as PIP_2 are shown to increase the activity and reduce the ATP sensitivity of these channels, causing the channels to open and potassium to diffuse out of the cell (Venkateswarlu et al., 2002; Baukrowitz et al., 1998). Studies have shown that NO activates the K_{ATP} channel via a cGMP-dependent cascade (Archer, 2002). Another crucial ion channel that possibly contributes to the hyperpolarization of the membrane, reduction of calcium, and ultimately relaxation of the penile muscle is the Na^+/K^+-ATPase pump. This ATPase pump is also thought to be activated by NO, independent of its ability to increase cGMP. This direct stimulation of the Na^+/K^+-ATPase pump by NO causes hyperpolarization, which in turn closes voltage gated calcium channels, leading to CCSM relaxation (Gupta et al, 1995, Saenz, 2000; Archer, 2002).

Karkanis et al. (2003) were the first to demonstrate a calcium-activated chloride current within both the human and rat CCSM, presenting a novel excitatory mechanism for the erection process. These calcium activated chloride channels contribute to membrane hyperpolarization and are also important in the role of penile tissue relaxation (Christ and Lue, 2004; Karkanis et al., 2003). Many of these calcium activated chloride

channels fire spontaneous chloride currents as a response to the release of calcium from the sarcoplasmic reticulum. Furthermore these channels are amplified by noradrenaline, which promotes calcium release into the cell, and suppressed by the NO-cGMP pathway, which assists in removing calcium from the cell promoting relaxation (Craven et al., 2004).

A crucial pathway in smooth muscle cell relaxation of the penile tissue that is modulated by PKG is calcium desensitization. PKG achieves this calcium desensitization by several methods. One critical avenue is the phosphorylation of RhoA by PKG. This prevents RhoA from activating Rho-kinase, therefore inhibiting contraction (Wang et al., 2002; Bonnevier and Arner, 2004; DiSanto, 2003).

In addition, PKG has also been suggested to phosphorylate the Ser-695 site of the myosin-binding subunit of myosin light chain phosphatase (MLCP), activating the phosphatase, and opposing Rho-kinase induced contraction (Wooldridge et al., 2004; Torrecillas et al., 2000). In their 2004 study, Bonnevier and Arner demonstrated this RhoA/Rho-kinase independent mechanism of PKG activating MLCP and causing calcium desensitization. The activation of myosin light chain phosphatase (MLCP) leads to this calcium desensitization via decreasing myosin light chain phosphorylation and tension, independent of intracellular calcium concentration. MLCP dephosphorylates myosin, which then detaches from the actin filament, resulting in muscle relaxation (Maas et al., 2002; Williams et al., 2005).

PKG also increases the rate of CPI-17 dephosphorylation, reversing calcium sensitization, thereby validating a NO-mediated mechanism for relaxation (Bonnevier and Arner, 2004). An interesting relationship exists between NO and RhoA/Rho kinase

beyond nitric oxide's ability to reduce calcium sensitization via mediation of the RhoA pathway. RhoA/Rho kinase has been shown to inhibit NOS, ultimately reducing NO production. This interaction between both pathways defines a feedback regulation between NO, NOS, and RhoA/Rho kinase which provides a balance for smooth muscle activity (Jin and Burnett, 2006).

Recently there has been an increased interest in the role of oxidative stress and erectile dysfunction, although the exact role in the pathophysiological of ED is still unclear. Oxidative stress manifests itself when the cells are exposed to excessive elevation of reactive oxygen species (ROS). This is due to the disproportion between pro-oxidants and antioxidants. ROS are created during the normal metabolic process of the cell. Some crucial free radicals (ROS), which are involved in vascular disease include superoxide (O_2^-), hydrogen peroxide (H_2O_2), hypochlorous acid (HOCL) and peroxynitritie ($OONO^-$) (Agarwal et al., 2006). The relationship between NO and ROS is thought to be one of the mechanisms associated with erectile dysfunction pathology. NO reacts with superoxide to form peroxynitrite, which ultimately inactivates superoxide dismutase, an important antioxidant that protects the cell from toxic superoxide by assisting in its rapid clearance. This also leaves less NO available for ample relaxation of the erectile tissue (Agarwal et al., 2006; Kahn et al., 2001).

Although the NO/cGMP/PKG signaling cascade is considered the major mediator in corpus cavernosal tissue, another critical second messenger cascade is thought to regulate the tone of erectile tissue, as well as interact with the cGMP pathway to induce relaxation of penile tissue, the cyclic AMP signaling mechanism (Andersson, 2003; Uckert et al., 2004). This cascade is also dependent on the stimulation of G protein

coupled receptors which are activated by a variety of factors including: vasoactive intestinal peptide (VIP), calcitonin gene related peptide (CGRP), prostaglandin E_1 (PGE_1), adenosine, and possibly catecholamines (Christ and Lue, 2004; Morelli et al., 2006; Saenz, 2000; Steers, 2000). Once these vasorelaxant factors bind to their respective receptor, they induce adenylate cyclase to convert adenosine triphosphate (ATP) into cyclic adenosine monophosphate or cAMP. Initially, cAMP binds to protein kinase A (PKA), activating it. Protein kinase A in turn phosphorylates specific calcium and potassium channels, as well as a number of proteins involved in the smooth muscle tone. One method PKA works to regulate the tone of erectile tissue is thought to be through the phosphorylation and dephosphorylation of the actin-smooth muscle myosin cascade. In this role, PKA phosphorylates myosin light chain kinase (MLCK), which prevents the calcium complex from activating it, reducing the cross-bridge cycling. Furthermore, PKA phosphorylates the protein phospholamban, which in turn sequesters calcium back into the sarcoplasmic reticulum (Andersson, 2001). All this leads to the reduction to intracellular calcium, allowing relaxation to occur. Additionally, cAMP is also involved directly in increasing levels of PKG, promoting relaxation (Lin et al., 2008; Maggi et al., 2000).

VIP present in nerve fibers that innervate both the cavernosal smooth muscle tissue and the vascular tissue has been shown to induce vasodilation, leading to tumescence (Reilly et al., 1997). VIP stimulation of adenylate cyclase, resulting in the increase of intracellular cAMP, is thought to ultimately exert its effects via the opening of potassium channels and the subsequent closing of calcium channels to promote relaxation.

CGRP is a vasoactive neuropeptide that not only works to increase the levels of intracellular cAMP by activating adenylyl cyclase, but is also thought to be involved in vasodilation and relaxation of the corpora cavernosa smooth muscle cells by hyperpolarizing the membrane via potassium channels. CGRP primarily promotes potassium efflux and hyperpolarization by activating the K_{ATP} channels (Bivalacqua, 2001; Kawase and Burns, 1998).

The endogenous vasodilator PGE_1 is also thought to be an important regulator of erectile muscle tone by activating the cAMP cascade. PGE_1 is synthesized by the cavernosal endothelial cells in response to the mechanical shear stress flow of blood into the corpora tissue. PGE_1 works via a G-protein coupled receptors (EP) on smooth muscle cells to stimulate adenylyl cyclase to produce cAMP (Maas et al., 2002; Bivalacqua et al., 2003; Rubio et al., 2004). PGE_1 is thought to increase K_{Ca} channel activity, inhibiting transmembrane calcium influx (Christ et al., 1997). Additionally PGE_1 inhibits the release of noradrenaline by binding to receptors on these sympathetic neurons, reducing vasoconstriction. PGE_1 has also been shown to participate in the activation of K_{Ca} channel opening via the cAMP/PKA mechanism, and subsequently causing hyperpolarization of the membrane to promote relaxation (Lee et al., 1999). Furthermore, PGE_1 has been observed to up-regulate eNOS and nNOS, suggesting a synergistic action between NO and PGE_1 to improve erectile response (Morelli et al., 2006).

Increased cytosolic cAMP can also reduce intracellular levels of calcium; but more critically, the elevated intracellular levels of cAMP are shown to cross activate PKG, working to stimulate the NO/cGMP cascade which leads to relaxation of erectile

tissue (Rubio et al., 2004; Uckert et al., 2004). cAMP has also been shown to elevate cGMP levels by inhibiting its hydrolysis by phosphodiesterase type 5 (PDE 5), which effects are described below. Contrarily, it has been suggested that cGMP can modulate cAMP-signaling as well. It has been proposed that cGMP may cause the phosphorylation of EP receptors to decrease intracellular calcium levels, as well as intracellular cAMP levels. However the extent and exact mechanism of cross regulation between intracellular cGMP and cAMP within the cavernosal tissue needs to be examined further (Rubio et al., 2004; Kim et al., 2000; Christ et al., 1997).

The effects of cGMP, as well as cAMP, including amplitude and duration, are modulated by specific phosphodiesterases, primarily the hydrolytic PDE 5, as shown by the pharmacological inhibition of this enzyme as treatment for ED (Morelli et al., 2006; Uckert et al., 2004). Phosphodiesterases are part of a large superfamily of metallophosphohydrolases which are critical to the regulation of both cAMP and cGMP second messenger systems. Within the cavernosal tissue, PDE 5 influences the contractile tone of erectile tissue by catalyzing the enzymatic degradation of cGMP to GMP, causing the inactivation of cGMP, which ultimately returns the erectile tissue back to its normal flaccid state. PDE 5 is ten to one hundred times more abundant within the cavernosal tissue than other male tissues and this overabundance could account for the flaccid state of the penis the majority of the time. Recent studies show that androgens regulate both the expression and activity of PDE 5 (Morelli et al., 2006; Morelli et al., 2004; DiSanto, 2003).

Erectile response is thought to occur by both an androgen dependent and androgen independent collaboration, each of which are mediated by NO. Androgens are

a group of chemically related sex steroid hormones that aid in the growth and development of the male reproductive system, as well as stimulate and modulate male sexual behavior and the activities of male sex organs, including the penile tissue. In the male, androgens are primarily synthesized by the Leydig cells within the testis, as well as in the adrenal cortex of the adrenal gland. The primary androgen in males is testosterone, which exerts its effects by activating the androgen receptor either directly or indirectly as DHT, 5α-dihydrotestosterone, the most potent naturally occurring androgen. A key factor in the biological relevance of testosterone's effect is its conversion to bioactive metabolites such as DHT. Testosterone is reduced to DHT by the enzyme 5α-reductase, which amplifies its action since DHT has a higher potency due to its greater binding affinity and slower dissociation rate from the androgenic receptor (Liu et al., 2003). Androgens are important modulators of erectile tissue influencing both the nitric oxide cascade and the vasoconstriction signaling. Although androgens receptors are found in the corpus cavernosa of the rat, the credited mediator of androgen performance is the cytosolic androgen receptor (Shabsigh et al., 1998). The active androgen in rat tissue, which exerts its influence on the erection process, has been shown to be DHT (Lewis and Mills, 2004; Lugg et al., 1995). Due to the ablation of androgens, castration causes a decline in the rate at which blood flows into the sinuses of the corpus cavernosa, whereas androgen replacement, as well as administration of a NO donor, reverses this effect. This suggests that androgens modulate the rate of cavernosal blood flow by increasing the synthesis of NO. Testosterone has also been recognized as a modulator for blood outflow by reducing the sensitivity of α-adrenergic stimulation, either by a changing the compliance of the erectile tissue or by enhancing the blood flow. Reducing sympathetic

tone then allows for greater blood flow and higher intracavernosal pressure, activating the veno-occlusive mechanism, and ultimately inducing a greater erectile response (Gooren, 2006; Reilly et al., 1997). Supporting this, studies have shown that androgen deprivation via castration has significantly decreased the content of trabecular smooth muscle within the corpus cavernosum, as well as elastic fibers within the tunica albuginea, replacing this tissue with collagenous connective tissue fibers (Gooren and Saad, 2006). Testosterone is thought to work via a paracrine mechanism involving growth factors within the corpora cavernosa to maintain the fibroelastic properties of erectile tissue, as well as smooth muscle content (Glina, 2004). Furthermore, androgen deprivation has been shown to induce apoptosis of the erectile tissue, which ultimately leads to failure of the veno-occlusive mechanism (Traish et al., 2003; Shabsigh et al., 1998; Gooren and Saad, 2006). Although the exact mechanism is still unclear, it has been documented that restored androgen after castration has the capacity to regenerate cells by inducing new DNA synthesis within the erectile cell structure, suggesting that androgens have a critical role in maintaining the growth and functional integrity of erectile smooth muscle cells (Glina, 2004; Morelli et al., 2006; Shabsigh et al., 1998). Other studies suggest that ETs (endothelins) may regulate apoptosis induced by serum starvation. Furthermore, they may act as survival factors for endothelial and smooth muscle cells. Surgical castration has produced a substantial increase in the ET receptor in the prostate cells, which are androgen dependent for both survival and growth in healthy males. This suggests that androgens act to modulate ET expression and ultimately ET induced contraction (Padley et al., 2002).

Interestingly, testosterone has the ability to regulate both the formation and degradation of cGMP (Morelli et al., 2006; Morelli et al., 2004). One main action of testosterone has been shown to be its involvement in the adequate formation of NO. Testosterone and its metabolite, DHT, up-regulate the activity of NOS (Mills et al, 1999). The inhibition of the erectile mechanism due to castration is caused by several actions. One of the most likely ramifications is due to the castration-induced reduction in NOS levels, which are prevented by DHT (Lugg et al., 1995). This androgen is thought to sustain high levels of NOS by either enhancing NOS gene expression, especially from nerve cells, or by decreasing NOS's mRNA degradation (Reilly et al., 1997). Contradicting its stimulatory actions on cGMP formation and relaxation of the penile tissue, testosterone also positively up-regulates the expression and functional activity of PDE5's in the penis, which degrade cGMP, causing contraction (Gooren, 2006; Morelli et al., 2004). The fact that erection can occur in the absence of androgens is thought to be due to the fact that lower amounts of NO formation is counterbalanced by lower amounts of PDE 5 degradation of cGMP (Morelli et al., 2004). Castration has also been shown to result in a decrease in the relaxation of penile tissue, up to about a 50% reduction, due to the loss of nitric oxide production as well as the increase to vasoconstriction stimulation of the RhoA/Rho-kinase pathway. The lack of androgens has been shown to have a negative effect on relaxation by causing the up-regulation of the RhoA/Rho-kinase system. This increase of RhoA/Rho-kinase protein levels, which is evident after castration, contributes to the reduced erectile response by blocking the vasodilation effects of NO. Conversely, the inhibition of the RhoA/Rho-kinase cascade would permit greater activity of the myosin light chain phosphatase, thereby reducing levels of myosin

light chain phosphorylation, resulting in smooth muscle relaxation. This inhibition of the RhoA/Rho-kinase pathway has been shown to be both NO/cGMP dependent or independent, with either causing an increased erectile response (Wingard et al., 2003; Chitaley et al., 2001; Mills et al., 2001). Given all this information, it is quite evident that androgens are essential to not only the formation of cGMP via NOS activity regulation, but are also critical in the integrity of the erectile mechanism.

Testosterone may regulate a number of other cellular mechanisms beyond the NO/cGMP pathway. Alcorn et al. (1999) demonstrated that castration had a direct effect on NO distal to both the site of NOS regulation and the guanylate cyclase activation step in the NO/cGMP pathway. These results suggest that the lack of androgen effects erectile protein function at a step beyond the formation of cGMP. However, the precise mechanisms of testosterone's actions in regulating the CCSM relaxation still remain unclear.

Mills et al. (1999) demonstrated how androgens have been shown to increase the sensitivity of α-adrenergic agonists allowing a greater erectile response in non-castrated rats. This study further reported a difference in the veno-occlusive mechanism possibly to due changes in the physical property and tissue compliance of the tunica albuginea, as well as a greater inflow rate in the non-castrated rats. Additionally, Traish et al. (1999) demonstrated these same results and also determined that there was a significant decrease in the amount of trabecular smooth muscle within castrated rabbits due to the lack of androgens. The replacement of androgens restored the ICP, α-adrenergic receptors, and smooth muscle content to control levels. Finally, Palese et al. (2003) confirmed the

androgen dependent veno-occlusive mechanism within the mouse, getting the same results as the previous studies in the rat and rabbit.

Furthermore, castration demonstrates its effects in a variety of areas of erectile and sexual function beyond just affecting the penile mechanism of action. Castration, or androgen-deprived therapy, causes considerable physical and mental changes in men including: hot flashes, bone mineral density reduction, hair loss, impotence, reduced libido, weight gain, etc. (Sharifi et al., 2005).

As discussed, all these mechanisms point to the fact that there are a wide variety of pathways that are involved in the complex cellular mechanisms that regulate CCSM function. The common factors involve alterations in neurotransmission, impulse propagation, and intracellular signal transduction cascades. CCSM functional integrity depends on the continuity and regulation of these complex series of sequential events that balance the action of a variety of neurovascular agents and their receptors. Any discrepancy in the integration of these cellular processes whether due to modification of receptor activity and/or expression or due to the disruption of downstream events could result in erectile dysfunction.

The current study was designed to establish an extensive profile of the proteins present in the smooth muscle cells of the corpus cavernosal tissue. Specifically, this study will present a proteomic profile of the corpus cavernosal tissue isolated from intact and castrated rats. The hypothesis is that castration will alter the protein expression at multiple sites. Therefore, this study will provide new basic background information concerning the role of androgens in regulating protein expression in the corpus cavernosal smooth muscle cells.

Methods and Materials

Animals:

A total of sixteen male Long-Evans rats were used in this study. The housing conditions of the rats included a light and dark cycle of twelve hours each, with lights on from 1800 hours to 0600 hours. Eight of the animals were castrated at three months of age and the remaining eight rats remained intact. The CCSM tissues of all sixteen rats were removed at six months of age. This experiment was approved by the institutional animal care and use committee at Youngstown State University.

Castration

At three months of age, eight of the Long-Evans rats were anesthetized prior to the castration surgery. All animals were anesthetized with ketamine, 50 mg/kg, and xylazine, 8 mg/kg, injected intramuscularly. Once the animals were anesthetized, the scrotum was shaved and sterilized with iodine. A bilateral castration was performed, removing one testis at a time. The initial incision was made at the midline of the scrotum. The fat and connective tissue was cut exposing the tunica vaginalis, which is the tough outer layer of tissue that surrounds the testes. A small hole was cut into the tunica in order to remove the testes. The testis and epididymus were isolated by tying a suture around the vas deferens and accompanying blood vessels. Once the testis and epididymus were removed, the remaining vas deferens was gently inserted into the scrotum and the tunica was stitched. The procedure was repeated on the opposite side and when both testes were removed, the midline incision on the scrotum was stitched. The rats were monitored daily to assure that they healed properly and remained healthy.

Tissue Preparation

Eight weeks after castration, the corpus cavernosal smooth muscle tissue was removed from the rats for further analysis. Carbon Dioxide was used to euthanize the rats. An incision was made below the rib cage in order to cut the diaphragm to give a pneumothorax and assure the rats were euthanized. A second incision was made in the pelvic area around the penis and the connective tissue was removed around the penis, exposing the base of the penis. The penis was then isolated at the base and immediately put in buffer solution in order to be further cleaned. The glans penis was removed, as well as any excess connective tissue. The urethra and the dorsal penile vein were also removed. Once the tissue was cleaned, it was immediately put into two-dimensional gel electrophoresis buffer (2DGE buffer) and frozen at -80 degrees Celsius until the gel electrophoresis was ready to be performed.

Gel electrophoresis

Small gels were initially run in order to get an overview of the CCSM protein distribution and then large format gels were created. The large gels were run for both castrate and non-castrate CCSM tissue as well, allowing the samples to be spread over a larger surface area, increasing the resolution of the protein bands. This was done in order to locate more proteins as well as to analyze and investigate specific areas of interest for the purpose of creating a more detailed protein profile.

Prior to gel electrophoresis, the tissue was thawed and cut into small pieces. For the small format gels, the tissue was immediately put into a steel homogenizer with 1200 µl of 2DGE buffer. The tissue was homogenized for 20 minutes and then centrifuged for 10 minutes at 12000 RPM's in order to separate the supernatant from the tissue. For the large format gels, four of the castrate and four of the non-castrate tissue were pooled

separately. The pooled tissue was put into the same steel homogenizer with 1600 µl of 2DGE buffer. Both the non-castrate and the castrate pooled tissue were homogenized for 40 minutes each and then centrifuged for an additional 10 minutes at 12000 RPM's in order to separate the supernatant from the tissue.

A Modified Bradford Assay was then performed on the supernatant to determine the amount of proteins to load on first dimension of gel electrophoresis. The spectrophotometer was turned on prior to creation of the standards in order to warm up and equilibrate. For the Modified Bradford Assay, a series of protein concentration standards were created, along with the sample tubes. Each tube contained 80 µl of DI water, 20 µl of 0.1 HCl, and 10 µl of 2DGE buffer. For the standards, one was a blank and contained no bovine serum albumin (BSA); whereas the other tubes contained 1.0 µl, 1.5 µl, 2.0 µl, 2.5 µl, 3.0 µl, 3.5 µl, and 4.0 µl of BSA consecutively and the sample contained 10 µl of the sample protein isolated from the CCSM. The mixtures were vortexed to mix thoroughly and allowed to sit for five minutes. Four millimeters of Bradford dye was then added to each tube, vortexed again, and allowed to sit for an additional five minutes. The blank was used to set a baseline and calibrate the spectrophotometer at zero. Absorbance readings were then taken at 595 nm for each standard and sample using a spectrophotometer. The standard absorbencies were used to create a standard curve with which the sample was measured. Using Microsoft excel, the standard curve was prepared comparing the absorbencies with micrograms of protein. The graph was done in a scatter plot and a trendline was added displaying both the equation for the line and the R^2 value for the curve. The R^2 value should approach 1.00, for example 0.995 or better. For the large format gels, a Bradford Assay produced an R^2

value of 0.9957. Using the equation that was generated from the curve and further calculations, the amount of sample needed to load in the gel was determined.

First Dimension of Electrophoresis: Isoelectric Focusing

In this dimension of electrophoresis, the proteins were separated on basis of their individual isoelectric points (pI). The pI is the pH at which a particular protein carries no net electrical charge. Since the majority of the proteins found in the CCSM have pI's between 4 and 7, this determines the pH polyacrylamide gel (IPG or immobilized pH gradient) strips used in this technique. Strips of 7 cm were used for small gels and strips of 17 cm were used for large gels. The proteins migrate to their specific pI in an electric field and accumulate at that point on the strip since their mobility and electric potential becomes zero there. A rehydration/equilibration tray was used for this part of the experiment. For the rehydration process, a large load of 125 µl (300 µl for large gels) of the CCSM serum protein was added to a lane in the tray with 1.3 µl of an ampholyte with a range of 4-7 pH which matches the IPG strips being used. The ampholytes were used to establish a stable pH gradient for the isoelectric focusing. The IPG strip was then placed gel-face down over the sample/ampholyte mix, to assure no air bubbles were beneath the strip. Mineral oil was then overlayed on the strip assuring that the strips do not dry out or crystallize. Once all the protein samples were loaded into the lanes and the tray was covered, the tray was left on a shaker for 12-24 hours in order to rehydrate and load the protein samples onto the IPG strips. Once rehydration was complete, the strips were placed in the PROTEAN IEF cell. The strips were transferred from the rehydration tray into the focusing tray. Before transferring the strips, a small paper wick was put over each electrode on opposite ends of the tray and eight to ten µl of DI water was pipetted

over each wick. The strips were then transferred gel side down to the electrode focusing tray assuring the positive side of the gel was placed on the positive electrode. Once again each strip was overlayed with mineral oil. The focusing tray was then placed into the PROTEAN IEF cell, positive end on the red and negative on the black electrode contact areas of the cell. The cell was then closed and the machine was ready to be set. The preset method was selected as well as linear increase voltage. Since this was passive rehydration, 'no' was selected for rehydration and the gel length of 7 cm (17 cm for large gels) was entered. The voltage was then changed from the 20000 volts on the fourth screen to 40000 volts since the strips were run for ten volt-hours which was optimal. 'Yes' was selected to hold at 500 volts and the number of gel strips which are in the machine was entered. Finally the machine was started and the information that was displayed was doubled checked for accuracy. When the strips were done, it was essential to equilibrate them in two different buffers in order to reduce streaking. The first buffer was SDS-PAGE Equilibration Buffer I which contained DTT. DTT breaks down disulfide bonds. The second buffer was SDS-PAGE Equilibration Buffer II which contained iodoacetamide. Iodoacetamide binds the disulfide bonds broken down by the first buffer so they cannot reform again. The strips were moved to the equilibration trays, covered with Equilibration Buffer I, and put on a shaker for 15 minutes. The strips were then moved to another clean tray and overlayed with Equilibration Buffer II for an additional 15 minutes.

Second dimension of Electrophoresis: SDS-PAGE

The second dimension of gel electrophoresis separated the proteins by molecular weight. Sodium Dodecyl Sulfate (SDS) is an anionic detergent used to denature the

proteins by disrupting non-covalent bonds, thereby allowing the separation of proteins by primary structure. Once an electric current is applied, the smaller proteins move through the pores in the gel more easily and therefore migrate farther down the gel; whereas the heavier proteins move more slowly and tend to remain closer to the origin or top of the gel. The gels were made in mass prior to running the second dimension. A pouring cell is assembled and 1 mm plates were used for the small gels and 20 mm plates used for the large gels. Both were stacked as follows: 1 mm (20 mm) plate, a short plate, and a plastic sheet separating the next 1 mm (20 mm) plate and short plate. The plates were stacked until the pouring cell was full and secured. A 10% SDS PAGE running gel was prepared and immediately poured into the cell. One hundred milliliters of this running gel was prepared using 48 ml of DI water, 25 ml of 40% Acrylamide, 25 ml of SDS Running buffer which included 1.5 M of TRIS at a pH of 8.8, 1 ml of 10% ammonium persulfide, and 0.04 ml of TEMED. The ammonium persulfide and TEMED were added right before pouring since these cause the polymerization of the gels. The same recipe was used for both the large and small gels, just larger amounts of each ingredient to make four hundred milliliters for the large gels compared to one hundred milliliters for the small gels. Ten milliliters of butynol was added into reservoir of pouring cell first in order to create an even surface at the top of the gels. Then the SDS PAGE electrode buffer solution was poured into reservoir and allowed to polymerize prior to pulling individual gels apart and wrapping in wet towels and stored in refrigerator.

When ready to run the second dimension gel electrophoresis, the individual gels were pulled out of refrigerator and unwrapped. The large format gels were placed in room temperature 1/2x TGS buffer in order for the plates to "warm up." For the large format

gels, the Protean Plus Dodeca Cell was filled with both room temperature and then chilled TGS buffer until about ¾ of the way full. The chiller was then turned on to keep the buffer cool. For both large and small gels, one percent agarose gel was melted in microwave for about 30 seconds. The molten agar was used to help aid the IPG strip between the 1 mm plate and smaller plate to the top of the SDS-PAGE gel and to help seal the IPG strip in place. The gel side of the strip was placed toward the smaller plate and the positive side and negative side of the strip must match the electrodes in the gel box. Once the IPG strip was touching the gel, more agarose was pipetted over the strip and allowed to solidify. For the small gels, the apparatus was placed in the gel box and covered SDS PAGE electrode buffer. The gel box was then connected to the power supply and run at 0.015 Amps for each gel running, for instance if running two gels, machine should be set at 0.030 Amps; three gels, 0.045, etc. The gel plates were run for about two hours or until the gel front reached as close to the bottom without going past. For the large gels, the plates were then loaded into the Dodeca Cell hinged side down and short plate facing away from the person loading them or to the back of the box. Once all of the gels were loaded, the Dodeca Cell was filled with more 1x TGS buffer until max line was reached. The lid was now placed on and both the circulator and the power source were turned on. The circulator should be slowly moved up to the maximum speed of 100. The power source was set at manual, constant volts, and 200 V. On a piece of tape stuck to the front of the cell, the time started was recorded in order to observe the progress throughout the run. Once the dye front was not longer visible, the power source was paused, the circulator turned off, the lid removed, and two gels were lifted out to check the progress of the line. When gels were complete, the circulator, chiller and

power source were all turned off and the gel plates removed. Likewise, when the small gels were complete, the power supply was turned off, the gels were carefully removed, and immediately placed into Coomassie Brilliant Blue to stain overnight in order to visualize the separated proteins as distinct bands within the gel. For the large format, the gels were separated from the plates, they were put in high destain for at least one hour. SYPRO stain was used in place of Coomassie stain. After one hour in destain, the fixing solution (high destain) was removed. The gels were then submersed into the SYPRO stain and placed on an orbital shaker to shake overnight. The next day place the small format gels were placed in high destain for about 2-3 hours or until the background of the gel is light and the proteins are visible. After removing the destain, place gels in DI water and 5% acetic acid in order to prevent streaking. The following day for the large format gels included removing the SYPRO stain and placing the gels in distilled water for about 15 minutes on the shaker to rinse them. Once rinsed, the DI water was drained and the gels are placed in 5% Acetic Acid solution to store.

Imaging: PDQuest

In order to view the results of the large format gels, PDQuest was used for imaging. The gels were placed directly on pre-moistened UV box and the Trans UV light was used to position and sharpen the image. When the image was as desired, the freeze button helped to capture the picture. The remaining pictures were taken in the same respect without changing the settings.

Ferguson Plots

The Ferguson plot was first used by Kenneth A. Ferguson to analyze hormones of the pituitary gland in starch gels. (Ferguson, 1964) A molecular weight standard was

used which consisted of various standard proteins of known molecular weights. As shown in figure 2, the data from these proteins are used to create a standard curve in order to find the molecular weights of the unknown proteins run in the subsequent gels. In this study, the relative mobility was determined which is also known as the retention factor or "Rf." The relative mobility is the distance migrated by a polypeptide band divided by the distance migrated by the dye front. Relative mobility differs from absolute mobility in that absolute mobility is the distance traveled within a particular timeframe. Relative mobility is more useful in this investigation since it can be used to compare the migration of a protein from gel to gel, regardless of the duration of electrophoresis or the physical length of the gel. Since SDS denatures the proteins, causing them all to have a net negative charge consequently equalizing the charge to mass ratio for all the proteins, the relative mobility of the individual proteins are dependent solely on the differences in the relative molecular mass or the molecular weight of the polypeptides.

Results

This research project was a new approach in our laboratory, and therefore it was necessary to find the proper technique needed to maximize protein isolation from CCSM tissue. In order to successfully break down the corpus cavernosal tissue and obtain a greater number of proteins, several different extraction methods and materials were used. One technique that was used was sonication; however, not enough proteins were extracted from the fibrous cavernosal tissue. An electronic homogenizer was then utilized; unfortunately, it homogenized the tissue too finely that a supernatant could not be extracted when centrifuged. Next, a glass hand held homogenizer was used; but the tissue was so difficult to break down that several glass homogenizers were shattered in the process. Finally, a stainless steel homogenizer was used which successfully extracted proteins from the tissue. Ultimately, the best results came from pooling several tissues and homogenizing these tissues with the stainless steel homogenizer.

During the homogenization process, it was necessary to devise the proper amount of 2DGE (two dimensional gel electrophoresis) buffer that was sufficient enough not to dilute the amount of proteins. Various amounts of buffer were tried including 800 microliters, 1200 microliters and 1600 microliters. For the smaller gels, the appropriate amount seemed to be 1200 microliters. For the large format gels, the most suitable amount was 1600 microliters.

Initially, the gels were run on 3-10 pH IPG strips. However after running the initial gels, we found many of the essential proteins were found between 4-7 pI, therefore the 4-7 pH IPG strips were used instead in order to focus more directly on these proteins.

Bradford Assay

A typical Bradford Assay is displayed in figure 1. These are the actual results of the protein concentrations found in the tissues used for the large format gels in this experiment. As stated before, four individual corpus cavernosal tissues were removed from four separate castrated rats, pooled, and homogenized as one. Likewise, four individual corpus cavernosal tissues were removed from four separate non-castrated rats, pooled and homogenized as one. The absorbances from the prepared standards created a standard curve with a R^2 value of 0.9957 which is very good. Using the equation of the line, the microgram amounts for the samples were calculated and then divided by the microliters used to prepare the Bradford samples. For instance, for both the castrate and non-castrated supernatant, two separate samples were created for each: one using 5 microliters of supernatant and one using 10 microliters of supernatant. Since the maximum load for the large format gels is 250 micrograms, the result of micrograms/microliters found in the previous step is then divided by 250. For example, for the 5 microliters castrate sample (C5 below) the result from the line equation was 49.88028169 micrograms of protein**.** Dividing this number by 5 microliters used to create the sample, gives the product of 9.976056 micrograms per microliter. This result is then divided into 250 micrograms to obtain the amount of 25.06000282 micrograms/microliter. This number represents the amount of sample that will be loaded onto the gel. Finally the amount of sample found was subtracted by 300 to get the amount of rehydration buffer which will be loaded as well. In this instance, 25.06000282 microliters is subtracted from 300 to arrive at 274.9399972 microliters of rehydration

buffer needed. The total amount of sample and rehydration buffer should equal 300 microliters.

Figure 1: The Bradford Assay for the Large Format Gels

Micrograms	*Absorbance*
10	0.225
15	0.314
20	0.371
25	0.461
30	0.503
35	0.591
40	0.658

***Using 1600µl to homogenize*

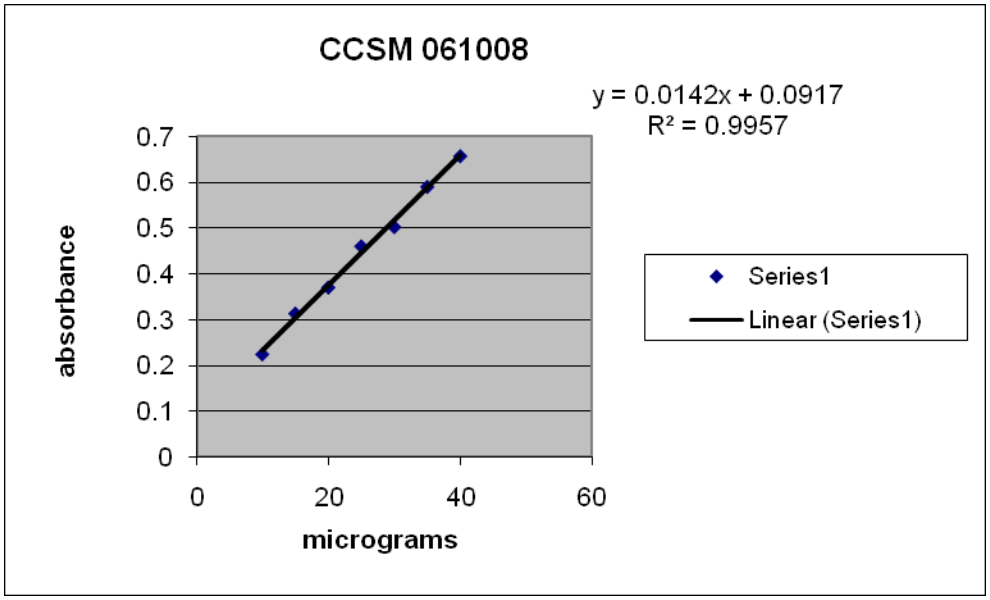

Solve for x **x = y +0.0142 / 0.0917**

Sample Collected	*Absorbance Reading*	*µg*	*µg/µl*	*Amount of sample needed to make 250µg (µl)*	*Amount of Rehydration buffer needed (total to = 300)*
Castrate 5µl	0.8	49.88028169	9.976056	25.06000282	274.9399972
Castrate 10µl	1.144	74.1056338	7.410563	33.73562672	266.2643733
Non-Castrate 5µl	1.036	66.5	13.3	18.79699248	281.2030075
Non-Castrate 10µl	1.523	100.7957746	10.07958	24.80262698	275.197373

Analysis of Electrophoresis Gel Proteins: The Ferguson Plot

Figure 2 shows the graph created of the log MW versus the Rf on a standard curve of known samples. A linear relationship exists between the logarithm of the molecular weight and its relative mobility. Therefore the curve can be described by the equation of the line which is the formula $y = mx + b$. or $Log(MW) = m(Rf) + b$, where $y = Log(MW)$ is the slope, $x = Rf$, and b is the y-intercept. The correlation coefficient (R^2) is computed as well with the equation of the line and the closer the R^2 is to 1, the better the approximation or the better the fit of the data points to a straight line. The accuracy of the calculations of the molecular weights of the unknown proteins depends on the linearity of the relationship, which is represented by the R^2 value. An R^2 greater than 0.97 is needed for a good linear relationship or best line fit; therefore as shown in figure 2 for this experiment, the R^2 of 0.998 gives an excellent linear approximation. (Hames, 1998)

Figure 2: Ferguson Plot Data: Standard Curve used for all gels

	Rounded Numbers Rf	logmw
1	0.30	4.63
2	0.40	4.56
3	0.47	4.49
4	0.67	4.33
5	0.80	4.24

	Actual Numbers Rf	logmw
1	0.300	4.633468
2	0.400	4.556303
3	0.467	4.491362
4	0.667	4.332438
5	0.800	4.243038

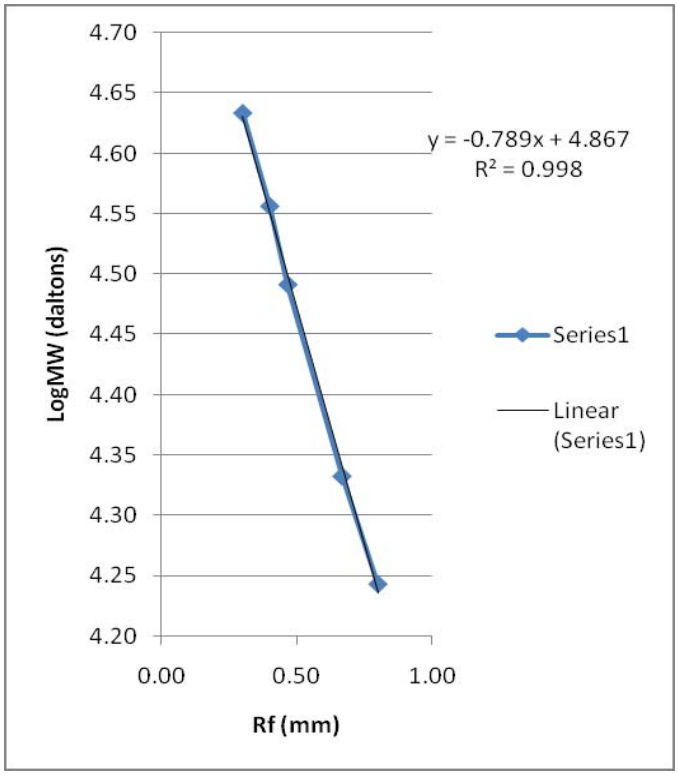

Analysis of Electrophoresis Gel Proteins: The Corpus Cavernosum Protein Profile

Once the molecular weight (MW) was calculated and the isoelectric point (Pi) was determined for each protein marked on the large format gels, the ExPASY (Expert Protein Analysis System) proteomics server of the SIB (Swiss Institute of Bioinformatics) was used to determine the possible protein matches for the given polypeptide bands. The tool which was used within the ExPASY server is called TagIdent. TagIdent generates a list of proteins which are found within a given range of isoelectric points and the molecular weight that has been manually entered into the search form. The form is filled out using the exact molecular weight determined and a range with which the isoelectric point falls. Also the form specifies a particular organism for which the search is conducted; in this case the organism name used is *Rattus norvegicus* (NCBI Tax ID# 10116) of which the Sprague Dawley rats are an outbred strain. All databases were searched and, although the information given is neither always completely accurate nor up-to-date as stated by the website itself, this process has allowed for a starting point to possibly naming and identifying what polypeptides are found in these gels. Therefore mass spectrometry and further analysis should be done in order to assure the true identification of all the proteins.

Labeled Corpus Cavernosum Tissue from Rats:

Most Significant Comparisons:

Figure 3: Gel A of Rat #1

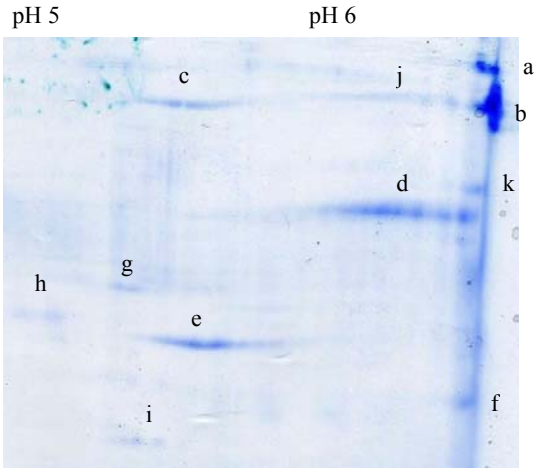

CCSMA1 *bands*	*Rf*	*logMW*	*MW*
a	0.122	4.770742	58985.05653
b	0.183	4.722613	52797.45637
c	0.207	4.703677	50544.86024
d	0.396	4.554556	35855.51791
e	0.671	4.337581	21756.09768
f	0.762	4.265782	18440.89521
g	0.561	4.424371	26568.74252
h	0.610	4.38571	24305.80448
i	0.860	4.18846	15433.3427
j	0.177	4.727347	53376.11988
k	0.348	4.592428	39122.62619
l	0.128	4.766008	58345.58518

Figure 4 : Gel B of Rat #1

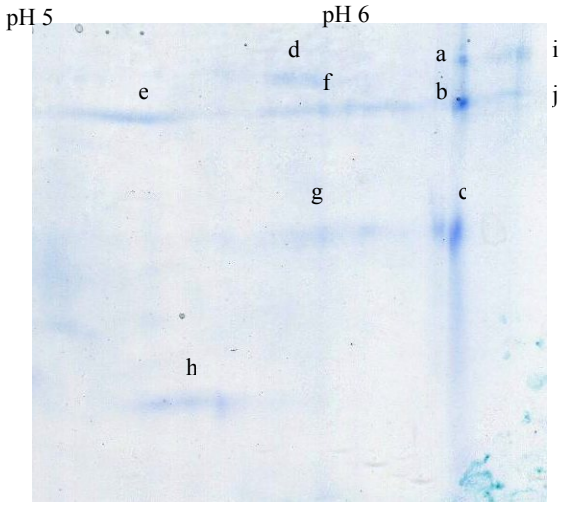

CCSMA2 *bands*	*Rf*	*logMW*	*MW*
a	0.109	4.780999	60394.72387
b	0.169	4.733659	54157.54884
c	0.364	4.579804	38001.7853
d	0.139	4.757329	57191.17246
e	0.200	4.7092	51191.7528
f	0.182	4.723402	52893.46279
g	0.376	4.570336	37182.27855
h	0.636	4.365196	23184.40742
i	0.091	4.795201	62402.3579
j	0.157	4.743127	55351.19481

Comparing Figures 3 and 4:

After analyzing all of the gels, selected gels were chosen to review and compare together. The first two gels that are being compared are in the previous figures 3 and 4. Both of these tissues were from castrated rats and both gels were run on 4-7 pH strips. Figure 3 is Gel A of the first rat (Rat #1) and Figure 4 is Gel B of the same rat. Despite the slight disparities, there are a few analogies to be made. First of all, like most of all of the CCSM gels ran, there appears to be a "line" of proteins which fall between the pH of 6.0-7.0. Within in this "line" in Figure 4, the bands of interest include band a (MW~60695 Da), b (MW ~54158 Da), and c (MW~38002 Da). In Figure 3, the corresponding bands are a (MW~58985 Da), b (MW~ 527977 Da), and k (MW~39123 Da). Additionally band f is found in this "line" at approximately 18441 Da. Two very interesting and very closely related bands also include band c in Figure 3 at approximtely 50545 Da and band e in Figure 4 at approximately 51192 Da . A couple more bands of interest include band d in Figure 3 (MW~35856 Da) compared to band g (MW~37182 Da) in Figure 4 and band j (MW~53376 Da) in Figure 3 compared to band f (MW~52893 Da) in Figure 4.

Figure 5: Gel B of Rat #3

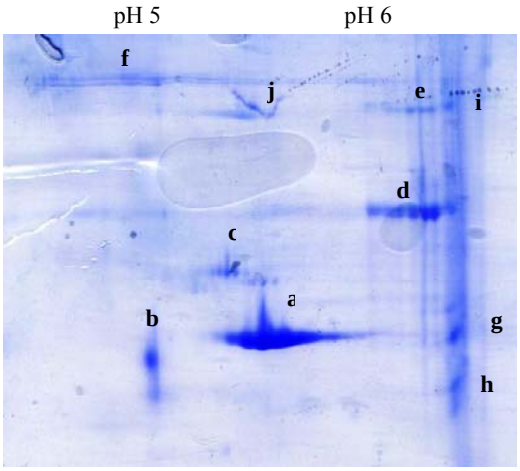

CCSMC2 bands	*Rf*	*logMW*	*MW (Daltons)*
a	0.582	4.407802	25574.19663
b	0.618	4.379398	23955.10065
c	0.473	4.493803	31174.75148
d	0.364	4.579804	38001.7853
e	0.164	4.737604	54651.74081
f	0.236	4.680796	47950.81576
g	0.582	4.407802	25574.19663
h	0.691	4.321801	20979.78339
i	0.182	4.723402	52893.46279
j	0.182	4.723402	52893.46279

Figure 6: Gel C of Rat #4

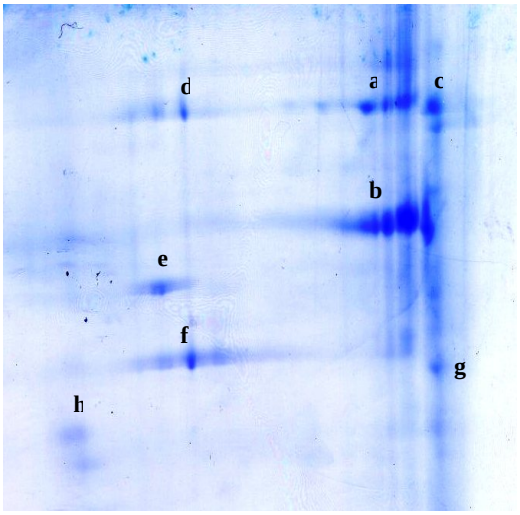

CCSMD3 bands	*Rf*	*logMW*	*MW (Daltons)*
a	0.220	4.69342	49365.0976
b	0.400	4.5514	35595.9018
c	0.220	4.69342	49365.0976
d	0.200	4.7092	51191.7528
e	0.500	4.4725	29682.46743
f	0.620	4.37782	23868.21823
g	0.640	4.36204	23016.53798
h	0.760	4.26736	18508.0217
i	0.420	4.53562	34325.74722
j	0.140	4.75654	57087.36532

Figure 7: Gel A of Rat #2

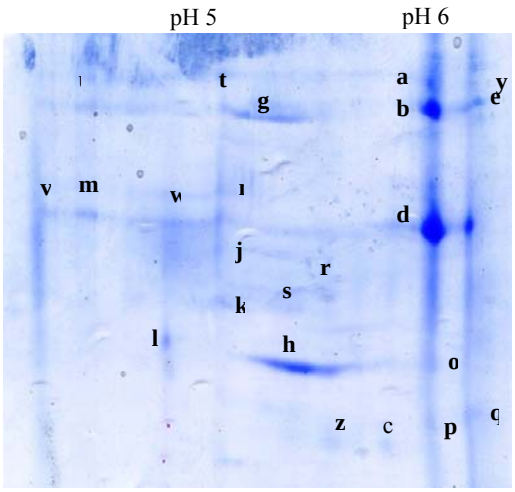

CCSMB1 bands	*Rf*	*logMW*	*MW (Daltons)*
a	0.135	4.760485	57608.2921
b	0.188	4.718668	52320.03189
c	0.800	4.2358	17210.75808
d	0.406	4.546666	35209.99797
e	0.171	4.732081	53961.12557
f	0.394	4.556134	35986.03516
g	0.235	4.681585	48038.00909
h	0.665	4.342315	21994.5459
i	0.382	4.565602	36779.17642
j	0.447	4.514317	32682.6302
k	0.541	4.440151	27551.86489
l	0.612	4.384132	24217.65009
m	0.382	4.565602	36779.17642
n	0.335	4.602685	40057.60687
o	0.659	4.347049	22235.60753
p	0.665	4.342315	21994.5459
q	0.753	4.272883	18744.89448
r	0.529	4.449619	28159.11491
s	0.553	4.430683	26957.71018
t	0.124	4.769164	58771.12445
u	0.176	4.728136	53473.17853
v	0.364	4.579804	38001.7853
w	0.394	4.556134	35986.03516
x	0.835	4.208185	16150.46385
y	0.112	4.778632	60066.45479
z	0.806	4.231066	17024.17206

Comparing Figures 5, 6, and 7:

For Figures 5 through 7, a few distinct characteristics appear that also appear in other CCSM gels a well. As in Figures 3 and 4, there appears a vertical "line" between pH of 6 and 7, however a second line seems to start to display itself. In Figure 4, the light bands i (MW~ 62402 Da) and j (MW~55351 Da) are starting to show in this second horizontal line. In Figure 5 and 6, this second line almost appears to blend into the first; however, in Figure 7 the line is clearly apparent. For the first horizontal line, Figure 5 has band i (MW~52893 Da), band g (MW~25574 Da), and band h (MW~20980 Da) within it. Figure 6 has band j (MW~57087 Da), band a (MW~49365 Da) , and band b (MW~35596 Da) within it, all of which appear to expand toward the left side of the gel or the positive side of the gel. For Figure 7, band a (MW~57608 Da), band b (MW~52320 Da), band d (MW~35210 Da), band o (MW~22236 Da) and band p (MW~ 21995 Da) all fall in this first vertical line. For Figure 6, band c (MW~49365 Da), band i (MW~34326 Da), and band g (MW~23017 Da) appear in the second horizontal line which is more toward the negative side of the gel (or pH 7.0). In Figure 7, this second horizontal line is clearly define more so than on the other gels. In this line, band y (MW~60066 Da), band e (MW~53961), band f (MW~35986 Da), and band g (MW~48038 Da) fall into this second horizontal line.

There is a strong band in Figure 5, band a (MW~25574 Da) between pH 5-6, which appears to possibly correlates to Figure 6's band f (MW~23868 Da) and Figure 7's band h (MW~21995 Da). Also three more closely related bands include band j (MW~52893 Da) in Figure 5, band 2 (MW~51192 Da) in Figure 6, and band g (MW~48038 Da) in Figure 7.

Other significant gels with similar patterns to those described above:

Figure 8: Gel B of Rat #4

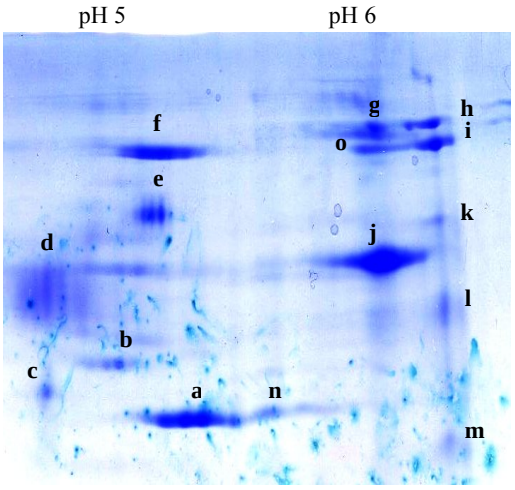

CCSMD2 bands	*Rf*	*logMW*	*MW (Daltons)*
a	0.659	4.347049	22235.60753
b	0.568	4.418848	26233.00246
c	0.614	4.382554	24129.81543
d	0.455	4.508005	32211.05875
e	0.318	4.616098	41314.07181
f	0.227	4.687897	48741.28785
g	0.159	4.741549	55150.44233
h	0.182	4.723402	52893.46279
i	0.227	4.687897	48741.28785
j	0.636	4.365196	23184.40742
k	0.341	4.597951	39623.3326
l	0.500	4.4725	29682.46743
m	0.727	4.293397	19651.55857
n	0.659	4.347049	22235.60753
o	0.227	4.687897	48741.28785

Figure 9: Gel A from Rat #4

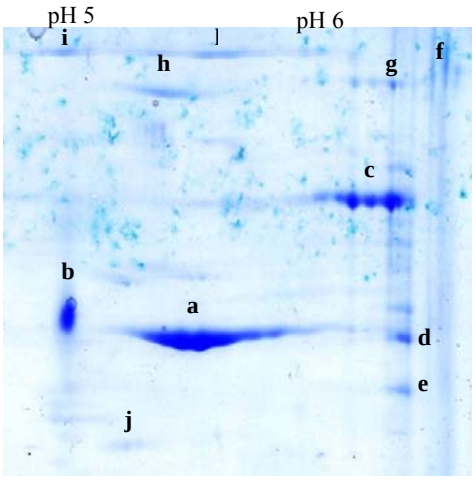

CCSMD1 bands	*Rf*	*logMW*	*MW (Daltons)*
a	0.659	4.347049	22235.60753
b	0.608	4.387288	24394.27975
c	0.392	4.557712	36117.02751
d	0.647	4.356517	22725.68591
e	0.745	4.279195	19019.32064
f	0.157	4.743127	55351.19481
g	0.196	4.712356	51565.11611
h	0.196	4.712356	51565.11611
i	0.118	4.773898	59415.25974
j	0.824	4.216864	16476.46348
k	0.118	4.773898	59415.25974

Figure 10: Gel B of Rat #2

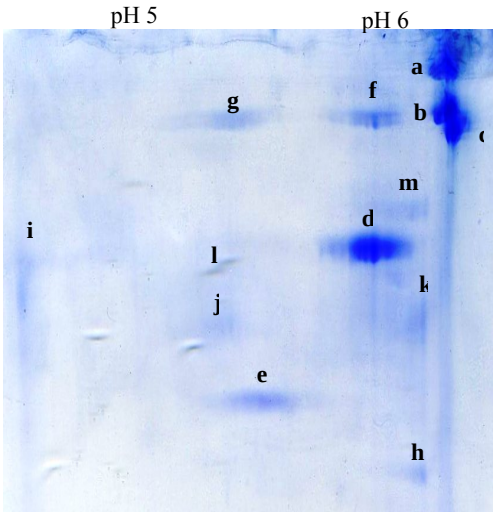

CCSMB2 bands	*Rf*	*logMW*	*MW (Daltons)*
a	0.103	4.86218	72808.15065
b	0.181	4.78886	61497.85951
c	0.206	4.76536	58258.5941
d	0.381	4.60086	39889.62927
e	0.619	4.37714	23830.87562
f	0.187	4.78322	60704.37611
g	0.187	4.78322	60704.37611
h	0.735	4.2681	18539.58464
i	0.426	4.55856	36187.61823
j	0.497	4.49182	31032.73122
k	0.490	4.4984	31506.48833
l	0.400	4.583	38282.47433
m	0.329	4.64974	44641.62552

Figure 11: Gel C of Rat #3

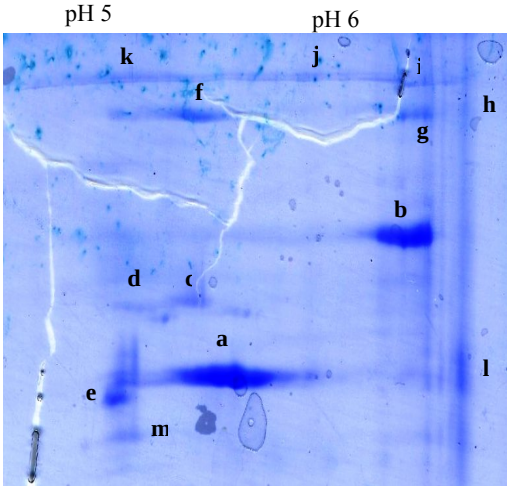

CCSMC3 bands	*Rf*	*logMW*	*MW (Daltons)*
a	0.640	4.36204	23016.53798
b	0.380	4.56718	36913.05587
c	0.500	4.4725	29682.46743
d	0.520	4.45672	28623.31961
e	0.660	4.34626	22195.2479
f	0.200	4.7092	51191.7528
g	0.180	4.72498	53085.99967
h	0.180	4.72498	53085.99967
i	0.120	4.77232	59199.76735
j	0.120	4.77232	59199.76735
k	0.120	4.77232	59199.76735
l	0.600	4.3936	24751.41318
m	0.680	4.33048	21403.26359

Figure 12: Gel C of Rat #5

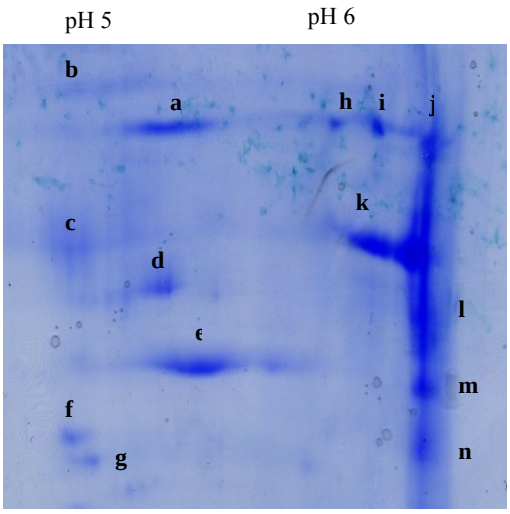

CCSME3 bands	*Rf*	*logMW*	*MW (Daltons)*
a	0.180	4.72498	53085.99967
b	0.180	4.72498	53085.99967
c	0.360	4.58296	38278.94855
d	0.440	4.51984	33100.91507
e	0.760	4.26736	18508.0217
f	0.680	4.33048	21403.26359
g	0.720	4.29892	19903.06677
h	0.180	4.72498	53085.99967
i	0.200	4.7092	51191.7528
j	0.200	4.7092	51191.7528
k	0.380	4.56718	36913.05587
l	0.500	4.4725	29682.46743
m	0.600	4.3936	24751.41318
n	0.780	4.25158	17847.60723

Figure 13: Gel C of Rat #1

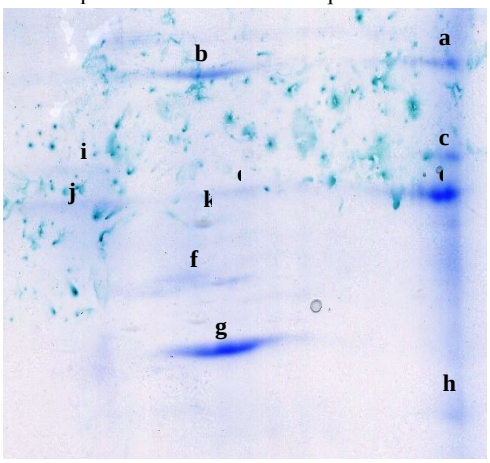

CCSMA3 bands	*Rf*	*logMW*	*MW (Daltons)*
a	0.180	4.72498	53085.99967
b	0.195	4.713145	51658.88165
c	0.329	4.607419	40496.64081
d	0.395	4.555345	35920.71726
e	0.389	4.560079	36314.41062
f	0.515	4.460665	28884.5097
g	0.635	4.365985	23226.56573
h	0.749	4.276039	18881.609
i	0.335	4.602685	40057.60687
j	0.401	4.550611	35531.29202
k	0.437	4.522207	33281.81483

Figure 14: Gel C of Rat #2

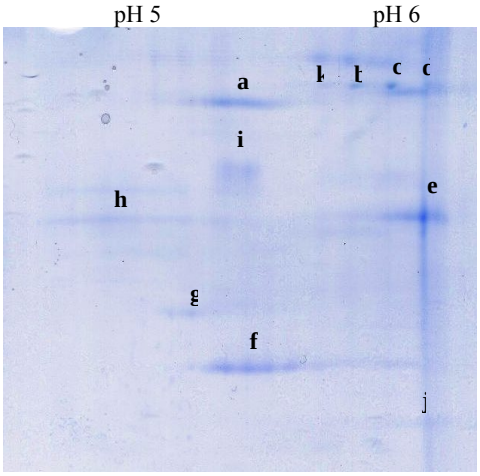

CCSMB3 bands	*Rf*	*logMW*	*MW (Daltons)*
a	0.202	4.76912	58765.17043
b	0.135	4.8321	67936.0043
c	0.178	4.79168	61898.48221
d	0.184	4.78604	61099.82973
e	0.405	4.5783	37870.40939
f	0.669	4.33014	21386.51398
g	0.577	4.41662	26098.76759
h	0.411	4.57266	37381.78196
i	0.331	4.64786	44448.79584
j	0.761	4.24366	17525.07963
k	0.129	4.83774	68824.01428

Figure 15: Gel B from Rat #3

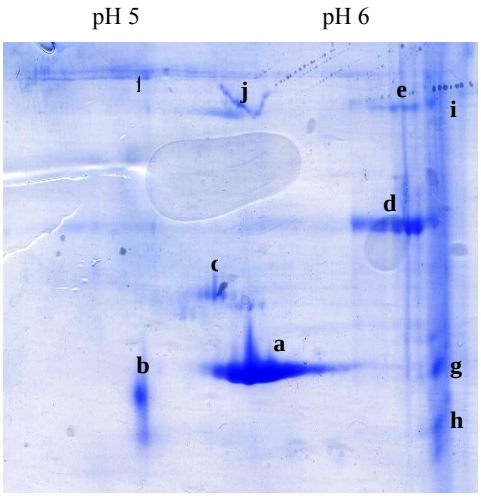

CCSMC2 bands	*Rf*	*logMW*	*MW (Daltons)*
a	0.582	4.407802	25574.19663
b	0.618	4.379398	23955.10065
c	0.473	4.493803	31174.75148
d	0.364	4.579804	38001.7853
e	0.164	4.737604	54651.74081
f	0.236	4.680796	47950.81576
g	0.582	4.407802	25574.19663
h	0.691	4.321801	20979.78339
i	0.182	4.723402	52893.46279
j	0.182	4.723402	52893.46279

Large Format Gels:

Castrate I:

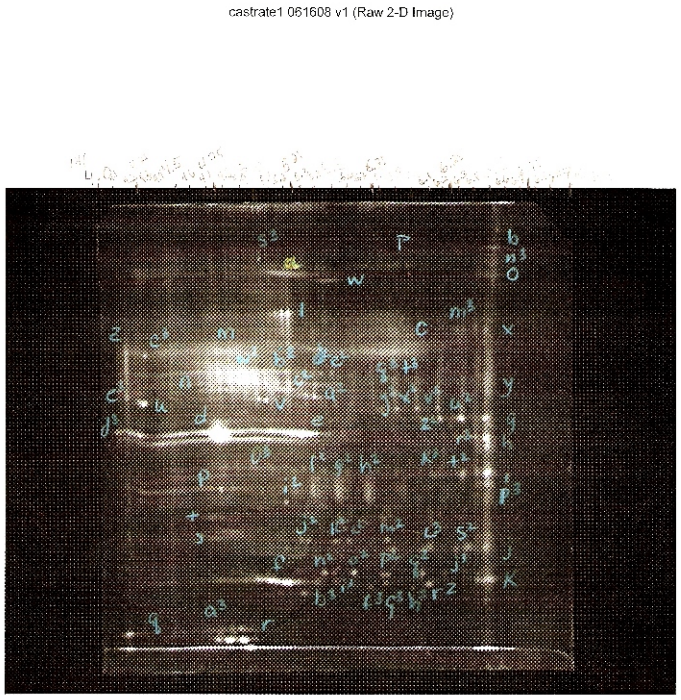

Figure 16:
Labeled Rat CCSM Castrate I

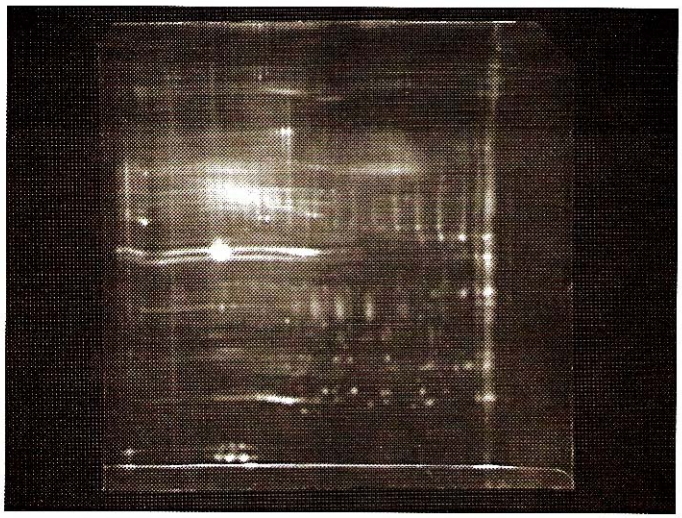

Figure 17:
Unlabeled Rat CCSM Castrate I

Figure 18: Labeled Rat Corpus Cavernosum Tissue from Castrate I for Large Format Gels:

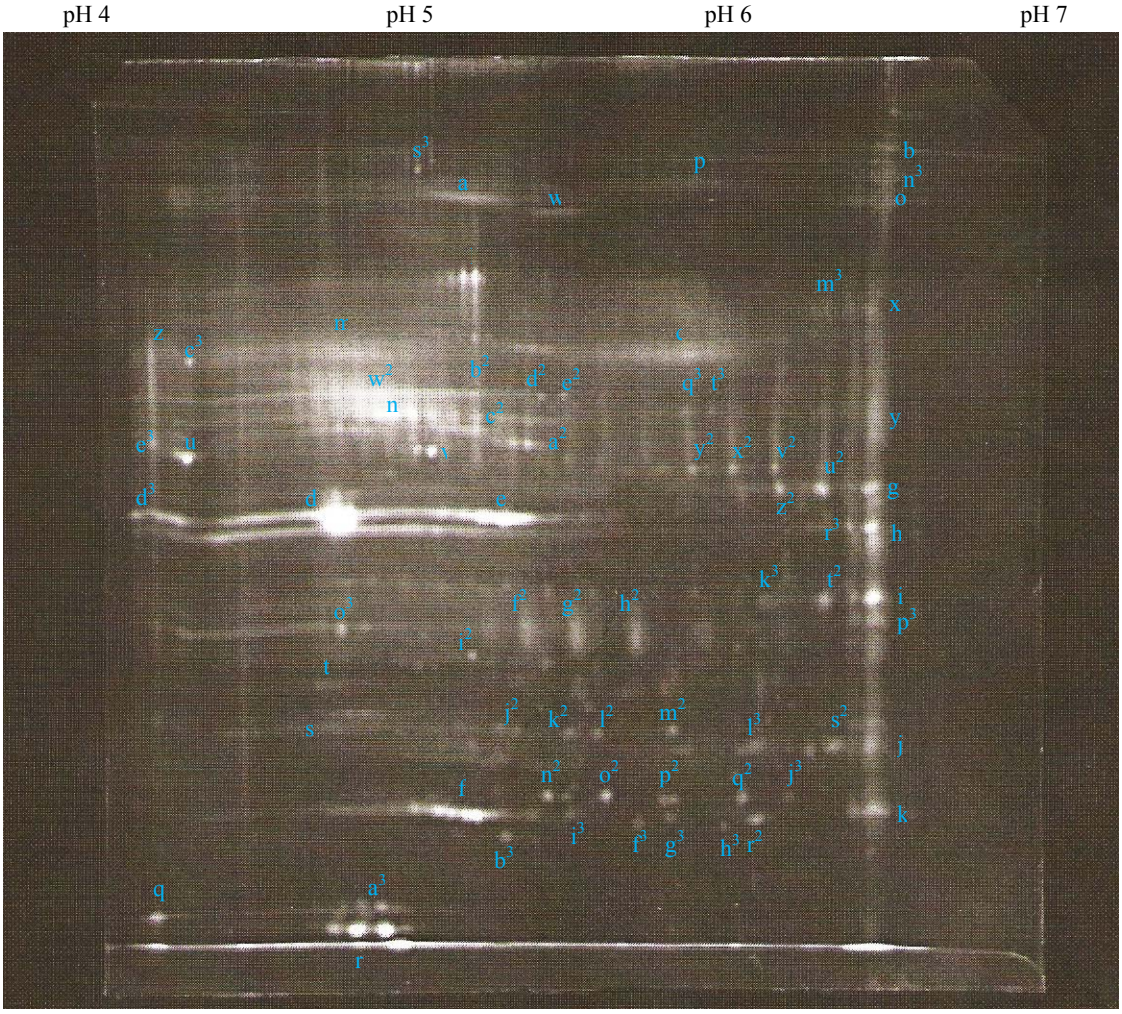

Table 1: Ferguson Plot Data for CCSM Castrate I gel

	rf	logMW	MW	pI		rf	logMW	MW	pI
a	0.15	4.746283	55754.89471	5.0-5.3	a^2	0.43	4.526152	33585.51406	5.3-5.4
b	0.10	4.786522	61167.67878	6.5-6.6	b^2	0.37	4.572703	37385.48336	5.2-5.25
c	0.33	4.605841	40349.7641	5.6-6.1	c^2	0.42	4.539565	34638.97242	5.1-5.3
d	0.52	4.459087	28779.74887	4.4-5.1	d^2	0.38	4.566391	36846.05534	5.4-5.5
e	0.52	4.459087	28779.74887	5.1-5.5	e^2	0.38	4.566391	36846.05534	5.5
f	0.85	4.198717	15802.17984	5.0-5.4	f^2	0.64	4.365196	23184.40742	5.3-5.5
g	0.48	4.485913	30613.50108	6.4-6.5	g^2	0.64	4.365196	23184.40742	5.5-5.6
h	0.53	4.452775	28364.49135	6.4-6.6	h^2	0.64	4.365196	23184.40742	5.7-5.75
i	0.60	4.392022	24661.64262	6.4-6.6	i^2	0.67	4.339159	21835.2918	5.2-5.25
j	0.77	4.258681	18141.82611	6.5-6.6	j^2	0.75	4.272094	18710.8708	5.3-5.4
k	0.84	4.205029	16033.52451	6.4-6.6	k^2	0.75	4.272094	18710.8708	5.5-5.6
l	0.24	4.680007	47863.7807	5.2-5.25	l^2	0.75	4.272094	18710.8708	5.6-5.7
m	0.33	4.605841	40349.7641	4.6-5.1	m^2	0.75	4.272094	18710.8708	5.8-6.0
n	0.40	4.552978	35725.47403	4.8-5.2	n^2	0.83	4.211341	16268.25608	5.5
o	0.16	4.739971	54950.41795	6.5-6.6	o^2	0.83	4.211341	16268.25608	5.6-5.7
p	0.10	4.786522	61167.67878	5.9-6.0	p^2	0.83	4.211341	16268.25608	5.8-5.9
q	0.96	4.111138	12916.29632	4.25	q^2	0.83	4.211341	16268.25608	6.0-6.1
r	0.98	4.097725	12523.47923	4.8-5.0	r^2	0.86	4.191616	15545.90466	6.1-6.2
s	0.75	4.272094	18710.8708	5	s^2	0.77	4.258681	18141.82611	6.4
t	0.70	4.312333	20527.35533	4.7-4.8	t^2	0.61	4.38571	24305.80448	6.3-6.4
u	0.44	4.519051	33040.83392	4.3	u^2	0.48	4.485913	30613.50108	6.3-6.4
v	0.44	4.519051	33040.83392	5.0-5.2	v^2	0.46	4.505638	32035.97898	6.1-6.2
w	0.17	4.733659	54157.54884	5.4-5.6	w^2	0.37	4.572703	37385.48336	4.4-5.4
x	0.28	4.64608	44266.99077	6.4-6.5	x^2	0.46	4.505638	32035.97898	6.0-6.1
y	0.36	4.586116	38558.13326	6.4-6.5	y^2	0.46	4.505638	32035.97898	5.9-6.0
z	0.33	4.605841	40349.7641	4.1-4.2	z^2	0.48	4.485913	30613.50108	6.2-6.25

Table 1: Ferguson Plot Data for CCSM Castrate I gel (continued)

	rf	logMW	MW	pI
a[3]	0.95	4.118239	13129.22225	4.7-5.0
b[3]	0.87	4.178203	15073.11456	5.3
c[3]	0.34	4.599529	39767.56504	4.3-4.4
d[3]	0.51	4.466188	29254.18476	4.1-4.3
e[3]	0.42	4.532464	34077.2076	4.1-4.2
f[3]	0.86	4.191616	15545.90466	5.75-5.8
g[3]	0.85	4.198717	15802.17984	5.8-5.9
h[3]	0.86	4.191616	15545.90466	6.0-6.1
i[3]	0.85	4.198717	15802.17984	5.5-5.6
j[3]	0.77	4.258681	18141.82611	6.3
k[3]	0.60	4.392022	24661.64262	6.1-6.2
l[3]	0.77	4.258681	18141.82611	6.1-6.2
m[3]	0.28	4.64608	44266.99077	6.3-6.4
n[3]	0.13	4.766797	58451.68026	6.5-6.6
o[3]	0.70	4.317856	20790.07232	4.7-4.8
p[3]	0.63	4.372297	23566.60377	6.5
q[3]	0.40	4.552978	35725.47403	5.9
r[3]	0.53	4.452775	28364.49135	6.4-6.5
s[3]	0.13	4.766797	58451.68026	6.3-6.4
t[3]	0.40	4.552978	35725.47403	5.9-6.0

Table 2: Castrate I from smallest to largest mw

	MW	pI		MW	pI		MW	pI
r	12523.48	4.8-5.0	i^2	21835.292	5.2-5.25	t^3	35725.47	5.9-6.0
q	12916.3	4.25	f^2	23184.407	5.3-5.5	d^2	36846.06	5.4-5.5
a^3	13129.22	4.7-5.0	g^2	23184.407	5.5-5.6	e^2	36846.06	5.5
b^3	15073.11	5.3	h^2	23184.407	5.7-5.75	b^2	37385.48	5.2-5.25
r^2	15545.9	6.1-6.2	p^3	23566.604	6.5	w^2	37385.48	4.4-5.4
f^3	15545.9	5.75-5.8	t^2	24305.804	6.3-6.4	y	38558.13	6.4-6.5
h^3	15545.9	6.0-6.1	i	24661.643	6.4-6.6	c^3	39767.57	4.3-4.4
f	15802.18	5.0-5.4	k^3	24661.643	6.1-6.2	c	40349.76	5.6-6.1
g^3	15802.18	5.8-5.9	h	28364.491	6.4-6.6	m	40349.76	4.6-5.1
i^3	15802.18	5.5-5.6	r^3	28364.491	6.4-6.5	z	40349.76	4.1-4.2
k	16033.52	6.4-6.6	d	28779.749	4.4-5.1	x	44266.99	6.4-6.5
n^2	16268.26	5.5	e	28779.749	5.1-5.5	m^3	44266.99	6.3-6.4
o^2	16268.26	5.6-5.7	d^3	29254.185	4.1-4.3	l	47863.78	5.2-5.25
p^2	16268.26	5.8-5.9	g	30613.501	6.4-6.5	w	54157.55	5.4-5.6
q^2	16268.26	6.0-6.1	u^2	30613.501	6.3-6.4	o	54950.42	6.5-6.6
j	18141.83	6.5-6.6	z^2	30613.501	6.2-6.25	a	55754.89	5.0-5.3
s^2	18141.83	6.4	v^2	32035.979	6.1-6.2	n^3	58451.68	6.5-6.6
j^3	18141.83	6.3	x^2	32035.979	6.0-6.1	s^3	58451.68	6.3-6.4
l^3	18141.83	6.1-6.2	y^2	32035.979	5.9-6.0	b	61167.68	6.5-6.6
s	18710.87	5	u	33040.834	4.3	p	61167.68	5.9-6.0
j^2	18710.87	5.3-5.4	v	33040.834	5.0-5.2			
k^2	18710.87	5.5-5.6	a^2	33585.514	5.3-5.4			
l^2	18710.87	5.6-5.7	e^3	34077.208	4.1-4.2			
m^2	18710.87	5.8-6.0	c^2	34638.972	5.1-5.3			
t	20527.36	4.7-4.8	n	35725.474	4.8-5.2			
o^3	20790.07	4.7-4.8	q^3	35725.474	5.9			

Table 3: Castrate I from smallest to largest pI

	MW	pI		MW	pI		MW	pI
Z	40349.7641	4.1-4.2	f^2	23184.40742	5.3-5.5	l^3	18141.82611	6.1-6.2
e^3	34077.2076	4.1-4.2	d^2	36846.05534	5.4-5.5	z^2	30613.50108	6.2-6.25
d^3	29254.18476	4.1-4.3	w	54157.54884	5.4-5.6	j^3	18141.82611	6.3
Q	12916.29632	4.25	e^2	36846.05534	5.5	t^2	24305.80448	6.3-6.4
U	33040.83392	4.3	n^2	16268.25608	5.5	u^2	30613.50108	6.3-6.4
c^3	39767.56504	4.3-4.4	g^2	23184.40742	5.5-5.6	m^3	44266.99077	6.3-6.4
D	28779.74887	4.4-5.1	k^2	18710.8708	5.5-5.6	s^3	58451.68026	6.3-6.4
w^2	37385.48336	4.4-5.4	i^3	15802.17984	5.5-5.6	s^2	18141.82611	6.4
M	40349.7641	4.6-5.1	l^2	18710.8708	5.6-5.7	g	30613.50108	6.4-6.5
T	20527.35533	4.7-4.8	o^2	16268.25608	5.6-5.7	x	44266.99077	6.4-6.5
o^3	20790.07232	4.7-4.8	c	40349.7641	5.6-6.1	y	38558.13326	6.4-6.5
a^3	13129.22225	4.7-5.0	h^2	23184.40742	5.7-5.75	r^3	28364.49135	6.4-6.5
R	12523.47923	4.8-5.0	f^3	15545.90466	5.75-5.8	h	28364.49135	6.4-6.6
N	35725.47403	4.8-5.2	p^2	16268.25608	5.8-5.9	i	24661.64262	6.4-6.6
S	18710.8708	5	g^3	15802.17984	5.8-5.9	k	16033.52451	6.4-6.6
V	33040.83392	5.0-5.2	m^2	18710.8708	5.8-6.0	p^3	23566.60377	6.5
A	55754.89471	5.0-5.3	q^3	35725.47403	5.9	b	61167.67878	6.5-6.6
F	15802.17984	5.0-5.4	p	61167.67878	5.9-6.0	j	18141.82611	6.5-6.6
c^2	34638.97242	5.1-5.3	y^2	32035.97898	5.9-6.0	o	54950.41795	6.5-6.6
E	28779.74887	5.1-5.5	t^3	35725.47403	5.9-6.0	n^3	58451.68026	6.5-6.6
L	47863.7807	5.2-5.25	q^2	16268.25608	6.0-6.1			
b^2	37385.48336	5.2-5.25	x^2	32035.97898	6.0-6.1			
i^2	21835.2918	5.2-5.25	h^3	15545.90466	6.0-6.1			
b^3	15073.11456	5.3	r^2	15545.90466	6.1-6.2			
a^2	33585.51406	5.3-5.4	v^2	32035.97898	6.1-6.2			
j^2	18710.8708	5.3-5.4	k^3	24661.64262	6.1-6.2			

Castrate II:

castrate2 061608 v1 (Raw 2-D Image)

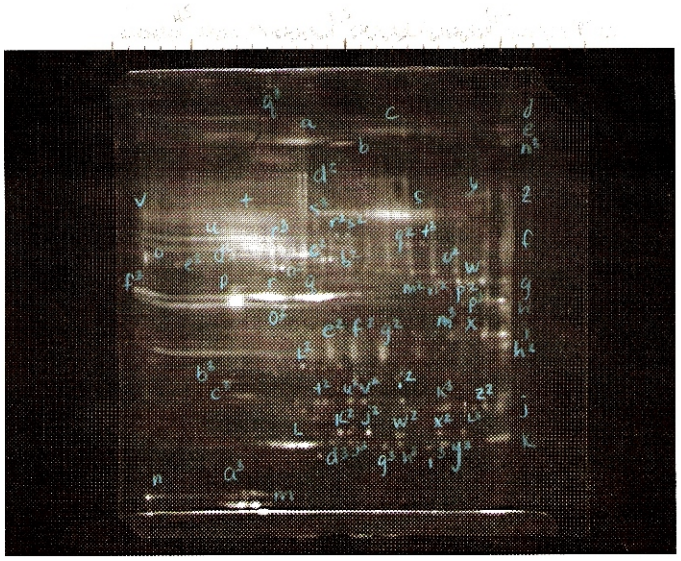

Figure 19:
Labeled Rat CCSM Castrate II

castrate2 061608 v1 (Raw 2-D Image)

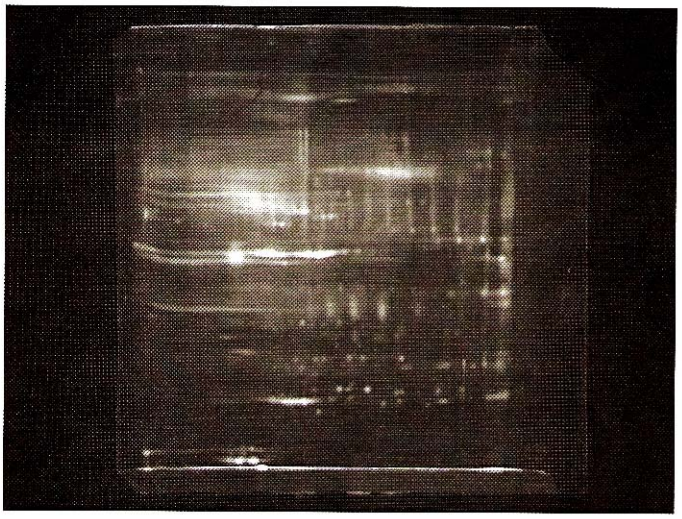

Figure 20:
Unlabeled Rat CCSM Castrate II

Figure 21: Labeled Rat Corpus Cavernosum Tissue from Castrate II for Large Format Gels:

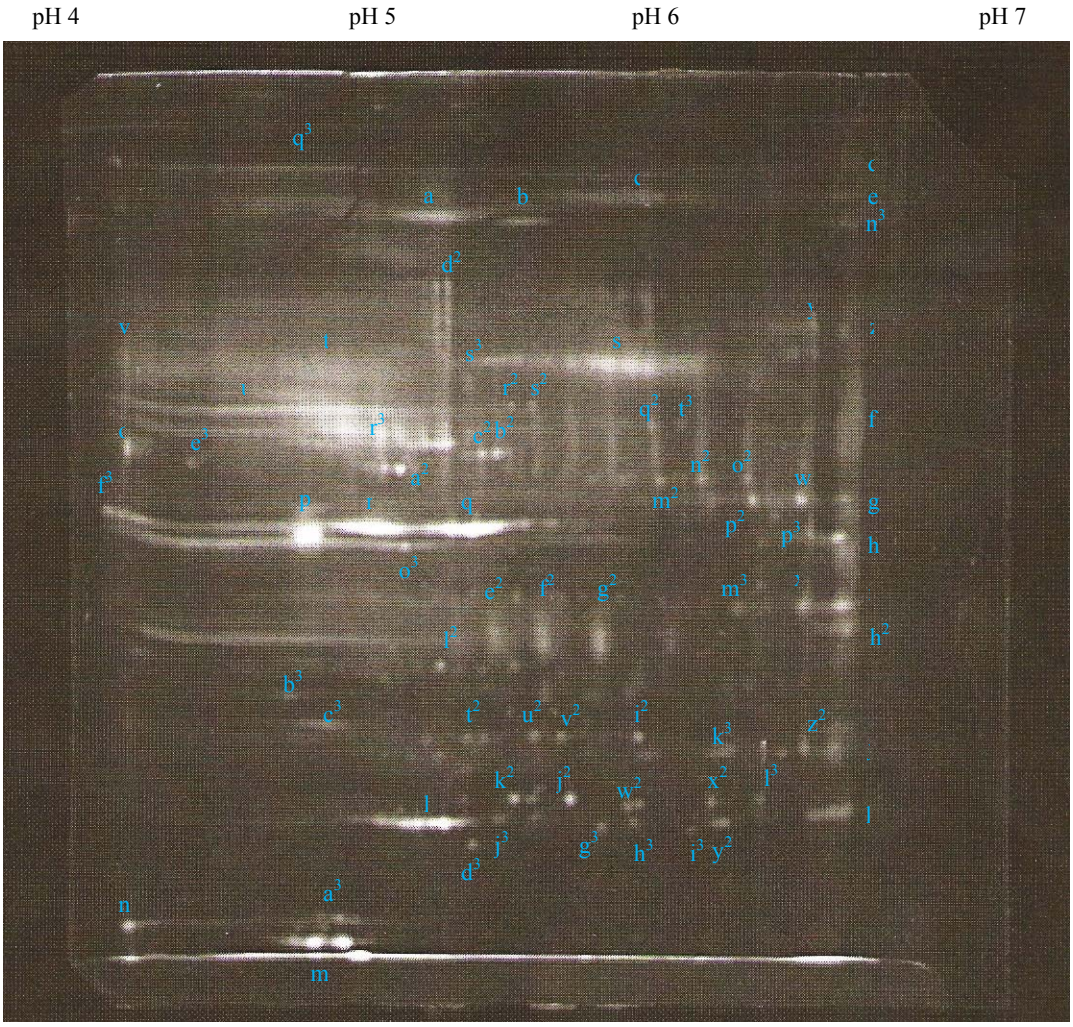

Table 4: Ferguson Plot Data for CCSM Castrate II gel

	rf	logMW	MW	pI		rf	logMW	MW	pI
a	0.16	4.739182	54850.67798	5.0-5.4	a^2	0.44	4.516684	32861.24399	5.1
b	0.17	4.732081	53961.12557	5.4-5.6	b^2	0.43	4.530097	33891.98457	5.4-5.5
c	0.14	4.758907	57399.35338	5.6-6.0	c^2	0.42	4.536409	34388.16485	5.1-5.3
d	0.14	4.758907	57399.35338	6.5-6.6	d^2	0.28	4.644502	44106.43943	5.2-5.3
e	0.17	4.732081	53961.12557	6.5-6.6	e^2	0.64	4.361251	22974.76088	5.4-5.5
f	0.43	4.530097	33891.98457	6.5-6.6	f^2	0.64	4.361251	22974.76088	5.5-5.6
g	0.48	4.489069	30836.77841	6.5	g^2	0.64	4.361251	22974.76088	5.7-5.8
h	0.52	4.455931	28571.3657	6.5	h^2	0.62	4.374664	23695.39758	6.5-6.6
i	0.60	4.395178	24841.51051	6.5-6.6	i^2	0.75	4.273672	18778.98003	5.9-6.0
j	0.77	4.260259	18207.86396	6.5	j^2	0.82	4.219231	16566.50897	5.6-5.7
k	0.84	4.205818	16062.67972	6.4-6.6	k^2	0.82	4.219231	16566.50897	5.5-5.6
l	0.85	4.199506	15830.91438	4.9-5.4	l^2	0.76	4.266571	18474.42797	5.2-5.3
m	0.98	4.091413	12342.78034	4.6-5.0	m^2	0.46	4.502482	31804.01869	5.9
n	0.97	4.104826	12729.92954	4.2	n^2	0.46	4.502482	31804.01869	6.0-6.1
o	0.42	4.536409	34388.16485	4.2	o^2	0.46	4.502482	31804.01869	6.2
p	0.52	4.455931	28571.3657	4.4-4.9	p^2	0.49	4.482757	30391.84041	6.2-6.3
q	0.51	4.462243	28989.65187	5.2-5.6	q^2	0.39	4.556923	36051.47184	6.0
r	0.51	4.462243	28989.65187	4.9-5.2	r^2	0.38	4.570336	37182.27855	5.4-5.5
s	0.33	4.604263	40203.4201	5.5-6.1	s^2	0.38	4.570336	37182.27855	5.5
t	0.34	4.597162	39551.41268	4.7-5.1	t^2	0.75	4.273672	18778.98003	5.3-5.4
u	0.43	4.530097	33891.98457	4.4-5.0	u^2	0.75	4.273672	18778.98003	5.5-5.6
v	0.33	4.610575	40792.0001	4.2	v^2	0.75	4.273672	18778.98003	5.6-5.7
w	0.48	4.489069	30836.77841	6.4	w^2	0.83	4.212919	16327.47397	5.9-6.0
x	0.60	4.395178	24841.51051	6.4	x^2	0.82	4.219231	16566.50897	6.1
y	0.28	4.644502	44106.43943	6.3-6.5	y^2	0.85	4.199506	15830.91438	6.1-6.2
z	0.29	4.637401	43391.13397	6.5-6.6	z^2	0.76	4.266571	18474.42797	6.4

Table 4: Ferguson Plot Data for CCSM Castrate II gel (continued)

	rf	logMW	MW	pI
a[3]	0.96	4.111927	12939.7832	4.7-5.0
b[3]	0.64	4.361251	22974.76088	4.2-5.0
c[3]	0.74	4.287085	19368.00997	4.7-4.9
d[3]	0.87	4.178992	15100.52338	5.3-5.4
e[3]	0.44	4.522996	33342.33418	4.4
f[3]	0.50	4.475656	29898.95434	4.1-4.3
g[3]	0.86	4.192405	15574.17319	5.7-5.8
h[3]	0.85	4.199506	15830.91438	5.9-6.0
i[3]	0.86	4.192405	15574.17319	6.0-6.1
j[3]	0.85	4.199506	15830.91438	5.5-5.6
k[3]	0.77	4.260259	18207.86396	6.0-6.2
l[3]	0.82	4.219231	16566.50897	6.3
m[3]	0.60	4.395178	24841.51051	6.1-6.2
n[3]	0.13	4.766008	58345.58158	6.5-6.6
o[3]	0.54	4.442518	27702.43854	4.2-5.2
p[3]	0.48	4.489069	30836.77841	6.4
q[3]	0.11	4.779421	60175.67908	4.1-5.0
r[3]	0.41	4.54351	34955.05582	4.8-5.1
s[3]	0.33	4.610575	40792.0001	5.3-5.6
t[3]	0.39	4.556923	36051.47184	5.9-6.1

Table 5: Castrate II from smallest to largest mw

	mw	pI		mw	pI		mw	pI
m	12342.7803	4.6-5.0	f^2	22974.76	5.5-5.6	c^2	34388.16	5.1-5.3
n	12729.9295	4.2	g^2	22974.76	5.7-5.8	r^3	34955.06	4.8-5.1
a^3	12939.7832	4.7-5.0	b^3	22974.76	4.2-5.0	q^2	36051.47	6
d^3	15100.5234	5.3-5.4	h^2	23695.4	6.5-6.6	t^3	36051.47	5.9-6.1
g^3	15574.1732	5.7-5.8	i	24841.51	6.5-6.6	r^2	37182.28	5.4-5.5
i^3	15574.1732	6.0-6.1	x	24841.51	6.4	s^2	37182.28	5.5
l	15830.9144	4.9-5.4	m^3	24841.51	6.1-6.2	t	39551.41	4.7-5.1
y^2	15830.9144	6.1-6.2	o^3	27702.44	4.2-5.2	s	40203.42	5.5-6.1
h^3	15830.9144	5.9-6.0	h	28571.37	6.5	v	40792	4.2
j^3	15830.9144	5.5-5.6	p	28571.37	4.4-4.9	s^3	40792	5.3-5.6
k	16062.6797	6.4-6.6	q	28989.65	5.2-5.6	z	43391.13	6.5-6.6
w^2	16327.474	5.9-6.0	r	28989.65	4.9-5.2	y	44106.44	6.3-6.5
j^2	16566.509	5.6-5.7	f^3	29898.95	4.1-4.3	d^2	44106.44	5.2-5.3
k^2	16566.509	5.5-5.6	p^2	30391.84	6.2-6.3	b	53961.13	5.4-5.6
x^2	16566.509	6.1	g	30836.78	6.5	e	53961.13	6.5-6.6
l^3	16566.509	6.3	w	30836.78	6.4	a	54850.68	5.0-5.4
j	18207.864	6.5	p^3	30836.78	6.4	c	57399.35	5.6-6.0
k^3	18207.864	6.0-6.2	m^2	31804.02	5.9	d	57399.35	6.5-6.6
l^2	18474.428	5.2-5.3	n^2	31804.02	6.0-6.1	n^3	58345.59	6.5-6.6
z^2	18474.428	6.4	o^2	31804.02	6.2	q^3	60175.68	4.1-5.0
i^2	18778.98	5.9-6.0	a^2	32861.24	5.1			
t^2	18778.98	5.3-5.4	e^3	33342.33	4.4			
u^2	18778.98	5.5-5.6	f	33891.98	6.5-6.6			
v^2	18778.98	5.6-5.7	u	33891.98	4.4-5.0			
c^3	19368.01	4.7-4.9	b^2	33891.98	5.4-5.5			
e^2	22974.7609	5.4-5.5	o	34388.16	4.2			

Table 6: Castrate II from smallest to largest pI

	mw	pI		mw	pI		mw	pI
f^3	29898.954	4.1-4.3	b^2	33891.985	5.4-5.5	m^3	24841.511	6.1-6.2
q^3	60175.679	4.1-5.0	e^2	22974.761	5.4-5.5	o^2	31804.019	6.2
n	12729.93	4.2	r^2	37182.279	5.4-5.5	p^2	30391.84	6.2-6.3
o	34388.165	4.2	b	53961.126	5.4-5.6	l^3	16566.509	6.3
v	40792	4.2	s^2	37182.279	5.5	y	44106.439	6.3-6.5
b^3	22974.761	4.2-5.0	f^2	22974.761	5.5-5.6	w	30836.778	6.4
o^3	27702.439	4.2-5.2	k^2	16566.509	5.5-5.6	x	24841.511	6.4
e^3	33342.334	4.4	u^2	18778.98	5.5-5.6	z^2	18474.428	6.4
p	28571.366	4.4-4.9	j^3	15830.914	5.5-5.6	p^3	30836.778	6.4
u	33891.985	4.4-5.0	s	40203.42	5.5-6.1	k	16062.68	6.4-6.6
m	12342.78	4.6-5.0	j^2	16566.509	5.6-5.7	g	30836.778	6.5
c^3	19368.01	4.7-4.9	v^2	18778.98	5.6-5.7	h	28571.366	6.5
a^3	12939.783	4.7-5.0	c	57399.353	5.6-6.0	j	18207.864	6.5
t	39551.413	4.7-5.1	g^2	22974.761	5.7-5.8	d	57399.353	6.5-6.6
r^3	34955.056	4.8-5.1	g^3	15574.173	5.7-5.8	e	53961.126	6.5-6.6
r	28989.652	4.9-5.2	m^2	31804.019	5.9	f	33891.985	6.5-6.6
l	15830.914	4.9-5.4	i^2	18778.98	5.9-6.0	i	24841.511	6.5-6.6
a	54850.678	5.0-5.4	w^2	16327.474	5.9-6.0	z	43391.134	6.5-6.6
a^2	32861.244	5.1	h^3	15830.914	5.9-6.0	h^2	23695.398	6.5-6.6
c^2	34388.165	5.1-5.3	t^3	36051.472	5.9-6.1	n^3	58345.59	6.5-6.6
d^2	44106.439	5.2-5.3	q^2	36051.472	6			
l^2	18474.428	5.2-5.3	n^2	31804.019	6.0-6.1			
q	28989.652	5.2-5.6	i^3	15574.173	6.0-6.1			
t^2	18778.98	5.3-5.4	k^3	18207.864	6.0-6.2			
d^3	15100.523	5.3-5.4	x^2	16566.509	6.1			
s^3	40792	5.3-5.6	y^2	15830.914	6.1-6.2			

Non-castrate I:

noncastrate1 061608 v1 (Raw 2-D Image)

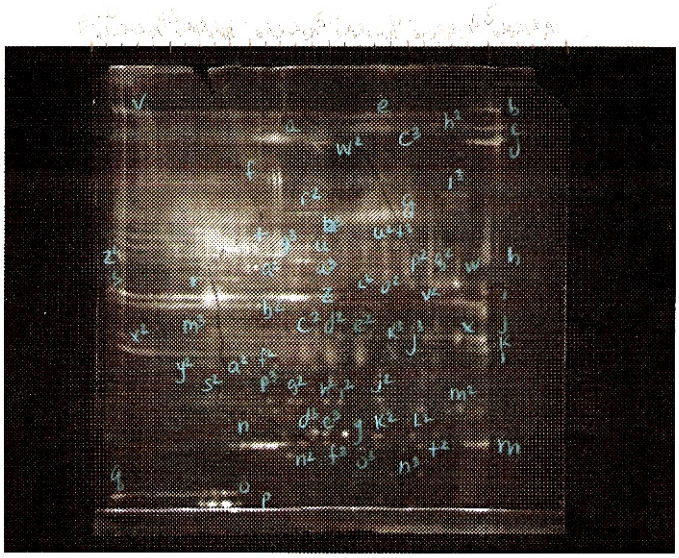

Figure 22:
Labeled rat CCSM non-castrate I

noncastrate1 061608 v1 (Raw 2-D Image)

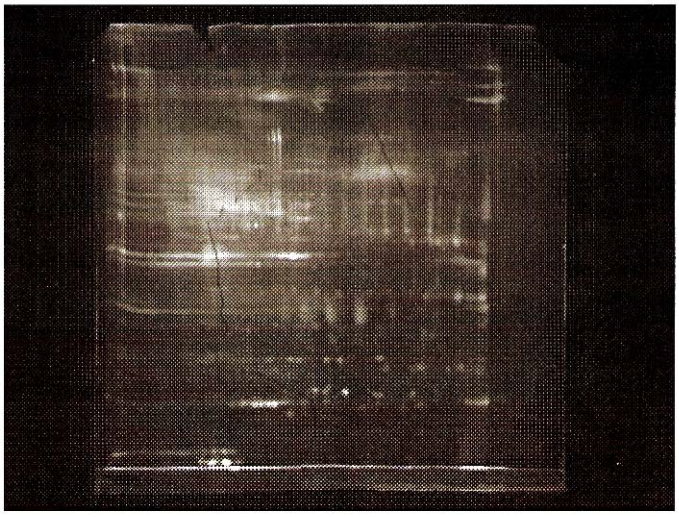

Figure 23:
Unlabeled rat CCSM non-castrate I

Figure 24: Labeled Rat Corpus Cavernosum Tissue from Non-Castrate I for Large Format Gels:

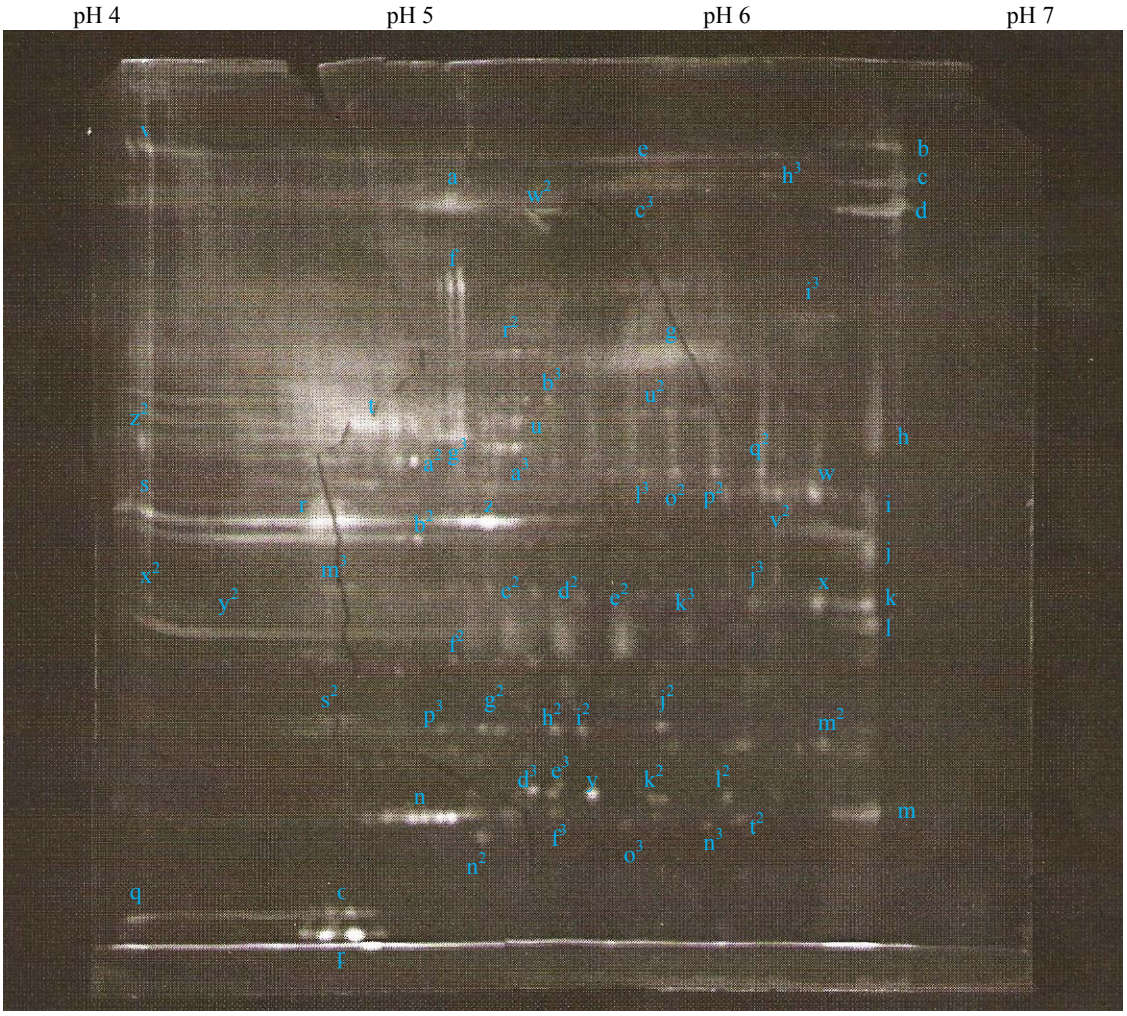

Table 7: Ferguson Plot Data for CCSM Non-Castrate I gel:

	rf	logMW	MW	pI		rf	logMW	MW	pI
a	0.16	4.739182	54850.67798	5.0-5.3	a^2	0.45	4.509583	32328.30985	5.0-5.1
b	0.09	4.792834	62063.17654	6.4-6.6	b^2	0.54	4.442518	27702.43854	4.9-5.1
c	0.14	4.758907	57399.35338	6.4-6.6	c^2	0.64	4.361251	22974.76088	5.3-5.4
d	0.17	4.732081	53961.12557	6.4-6.6	d^2	0.64	4.361251	22974.76088	5.5-5.6
e	0.11	4.779421	60175.67908	5.6-6.0	e^2	0.64	4.361251	22974.76088	5.7-5.8
f	0.25	4.671328	46916.75862	5.1-5.2	f^2	0.68	4.327324	21248.29073	5.1-5.2
g	0.33	4.604263	40203.4201	5.6-6.0	g^2	0.76	4.266571	18474.42797	5.2-5.4
h	0.42	4.536409	34388.16485	6.5	h^2	0.76	4.266571	18474.42797	5.4-5.5
i	0.50	4.469344	29467.54803	6.4-6.5	i^2	0.76	4.266571	18474.42797	5.5-5.6
j	0.56	4.428316	26811.18442	6.4-6.5	j^2	0.75	4.273672	18778.98003	5.8-5.9
k	0.62	4.381765	24086.01764	6.4-6.5	k^2	0.84	4.205818	16062.67972	5.8-5.9
l	0.64	4.361251	22974.76088	6.4-6.5	l^2	0.84	4.205818	16062.67972	6.0-6.1
m	0.85	4.199506	15830.91438	6.4-6.5	m^2	0.77	4.260259	18207.86396	6.3-6.4
n	0.86	4.192405	15574.17319	4.9-5.3	n^2	0.88	4.17268	14882.6408	4.2-4.3
o	0.97	4.104826	12729.92954	4.6-4.9	o^2	0.46	4.502482	31804.01869	5.8-5.9
p	0.99	4.085101	12164.68871	4.6-5.0	p^2	0.46	4.502482	31804.01869	6.0
q	0.97	4.098514	12546.25182	4.1-4.2	q^2	0.46	4.502482	31804.01869	6.1-6.2
r	0.52	4.455931	28571.3657	4.3-5.0	r^2	0.38	4.570336	37182.27855	5.2-5.5
s	0.51	4.462243	28989.65187	4.2	s^2	0.74	4.279984	19053.90519	4.8
t	0.41	4.54351	34955.05582	4.8-5.0	t^2	0.86	4.192405	15574.17319	6.1
u	0.41	4.54351	34955.05582	5.3-5.4	u^2	0.39	4.556923	36051.47184	5.7-5.8
v	0.10	4.785733	61056.65392	4.2	v^2	0.53	4.44883	28108.00357	6.2-6.3
w	0.49	4.482757	30391.84041	6.3-6.4	w^2	0.17	4.732081	53961.12557	5.4-5.5
x	0.62	4.381765	24086.01764	6.3-6.4	x^2	0.65	4.35415	22602.16286	4.2
y	0.83	4.212919	16327.47397	5.6	y^2	0.68	4.334425	21598.57008	4.1-5.1
z	0.52	4.455931	28571.3657	5.1-5.4	z^2	0.44	4.522996	33342.33418	4.1-4.2

Table 7: Ferguson Plot Data for CCSM Non-Castrate I gel (continued)

	rf	logMW	MW	pI
a[3]	0.44	4.522996	33342.33418	5.3-5.4
b[3]	0.38	4.564024	36645.78253	5.4-5.5
c[3]	0.14	4.758907	57399.35338	5.6-6.0
d[3]	0.82	4.219231	16566.50897	5.4-5.5
e[3]	0.83	4.212919	16327.47397	5.5
f[3]	0.86	4.192405	15574.17319	5.5
g[3]	0.43	4.530097	33891.98457	5.0-5.2
h[3]	0.14	4.758907	57399.35338	6.1-6.3
i[3]	0.30	4.631089	42765.05156	6.2-6.4
j[3]	0.62	4.381765	24086.01764	6.1-6.2
k[3]	0.65	4.35415	22602.16286	5.9
l[3]	0.46	4.502482	31804.01869	5.7-5.8
m[3]	0.60	4.395178	24841.51051	4.8-4.9
n[3]	0.92	4.138753	13764.2642	5.9-6.0
o[3]	0.86	4.186093	15349.45642	5.7
p[3]	0.75	4.273672	18778.98003	5.1-5.2

Table 8: Non-Castrate I from smallest to largest mw

	mw	pI		Mw	pI		mw	pI
P	12164.6887	4.6-5.0	L	22974.7609	6.4-6.5	u	34955.056	5.3-5.4
Q	12546.2518	4.1-4.2	c^2	22974.7609	5.3-5.4	u^2	36051.472	5.7-5.8
O	12729.9295	4.6-4.9	d^2	22974.7609	5.5-5.6	b^3	36645.783	5.4-5.5
n^3	13764.2642	5.9-6.0	e^2	22974.7609	5.7-5.8	r^2	37182.279	5.2-5.5
n^2	14882.6408	4.2-4.3	K	24086.0176	6.4-6.5	g	40203.42	5.6-6.0
o^3	15349.4564	5.7	X	24086.0176	6.3-6.4	i^3	42765.052	6.2-6.4
N	15574.1732	4.9-5.3	j^3	24086.0176	6.1-6.2	f	46916.759	5.1-5.2
t^2	15574.1732	6.1	m^3	24841.5105	4.8-4.9	d	53961.126	6.4-6.6
f^3	15574.1732	5.5	J	26811.1844	6.4-6.5	w^2	53961.126	5.4-5.5
M	15830.9144	6.4-6.5	b^2	27702.4385	4.9-5.1	a	54850.678	5.0-5.3
k^2	16062.6797	5.8-5.9	v^2	28108.0036	6.2-6.3	c	57399.353	6.4-6.6
l^2	16062.6797	6.0-6.1	R	28571.3657	4.3-5.0	c^3	57399.353	5.6-6.0
Y	16327.474	5.6	Z	28571.3657	5.1-5.4	h^3	57399.353	6.1-6.3
e^3	16327.474	5.5	S	28989.6519	4.2	e	60175.679	5.6-6.0
d^3	16566.509	5.4-5.5	I	29467.548	6.4-6.5	v	61056.654	4.2
m^2	18207.864	6.3-6.4	W	30391.8404	6.3-6.4	b	62063.177	6.4-6.6
g^2	18474.428	5.2-5.4	o^2	31804.0187	5.8-5.9			
h^2	18474.428	5.4-5.5	p^2	31804.0187	6			
i^2	18474.428	5.5-5.6	q^2	31804.0187	6.1-6.2			
j^2	18778.98	5.8-5.9	l^3	31804.0187	5.7-5.8			
p^3	18778.98	5.1-5.2	a^2	32328.3099	5.0-5.1			
s^2	19053.9052	4.8	z^2	33342.3342	4.1-4.2			
f^2	21248.2907	5.1-5.2	a^3	33342.3342	5.3-5.4			
y^2	21598.5701	4.1-5.1	g^3	33891.9846	5.0-5.2			
x^2	22602.1629	4.2	H	34388.1649	6.5			
k^3	22602.1629	5.9	T	34955.0558	4.8-5.0			

Table 9: Non-Castrate I from smallest to largest pI

	Mw	pI		mw	pI		mw	pI
q	12546.252	4.1-4.2	a^3	33342.334	5.3-5.4	j^3	24086.018	6.1-6.2
z^2	33342.334	4.1-4.2	h^2	18474.428	5.4-5.5	h^3	57399.353	6.1-6.3
y^2	21598.57	4.1-5.1	w^2	53961.126	5.4-5.5	v^2	28108.004	6.2-6.3
s	28989.652	4.2-4.3	b^3	36645.783	5.4-5.5	i^3	42765.052	6.2-6.4
v	61056.654	4.2	d^3	16566.509	5.4-5.5	w	30391.84	6.3-6.4
x^2	22602.163	4.2	e^3	16327.474	5.5	x	24086.018	6.3-6.4
n^2	14882.641	4.2	f^3	15574.173	5.5	m^2	18207.864	6.3-6.4
r	28571.366	4.3-5.0	d^2	22974.761	5.5-5.6	i	29467.548	6.4-6.5
o	12729.93	4.6-4.9	i^2	18474.428	5.5-5.6	j	26811.184	6.4-6.5
p	12164.689	4.6-5.0	y	16327.474	5.6	k	24086.018	6.4-6.5
s^2	19053.905	4.8	e	60175.679	5.6-6.0	l	22974.761	6.4-6.5
m^3	24841.511	4.8-4.9	g	40203.42	5.6-6.0	m	15830.914	6.4-6.5
t	34955.056	4.8-5.0	c^3	57399.353	5.6-6.0	b	62063.177	6.4-6.6
b^2	27702.439	4.9-5.1	o^3	15349.456	5.7	c	57399.353	6.4-6.6
n	15574.173	4.9-5.3	e^2	22974.761	5.7-5.8	d	53961.126	6.4-6.6
a^2	32328.31	5.0-5.1	u^2	36051.472	5.7-5.8	h	34388.165	6.5
g^3	33891.985	5.0-5.2	l^3	31804.019	5.7-5.8			
a	54850.678	5.0-5.3	j^2	18778.98	5.8-5.9			
f	46916.759	5.1-5.2	k^2	16062.68	5.8-5.9			
f^2	21248.291	5.1-5.2	o^2	31804.019	5.8-5.9			
p^3	18778.98	5.1-5.2	k^3	22602.163	5.9			
z	28571.366	5.1-5.4	n^3	13764.264	5.9-6.0			
g^2	18474.428	5.2-5.4	p^2	31804.019	6			
r^2	37182.279	5.2-5.5	l^2	16062.68	6.0-6.1			
u	34955.056	5.3-5.4	t^2	15574.173	6.1			
c^2	22974.761	5.3-5.4	q^2	31804.019	6.1-6.2			

Non-Castrate II:

noncastrate2 061608 v1 (Raw 2-D Image)

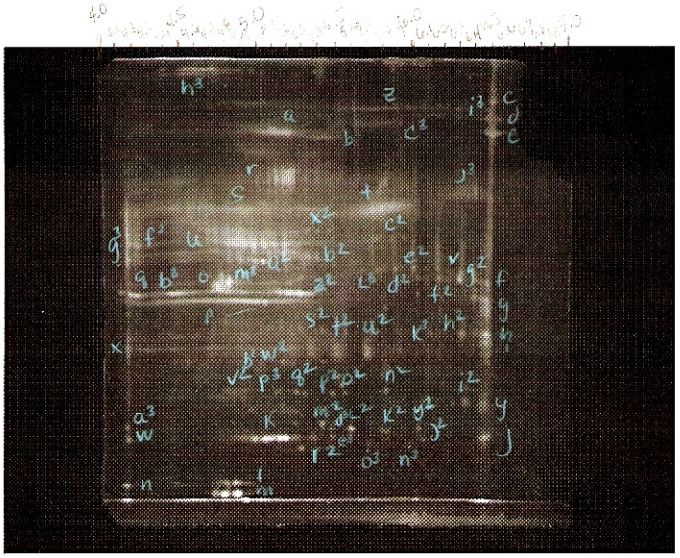

Figure 25:
Labeled rat CCSM non-castrate II

noncastrate2 061608 v1 (Raw 2-D Image)

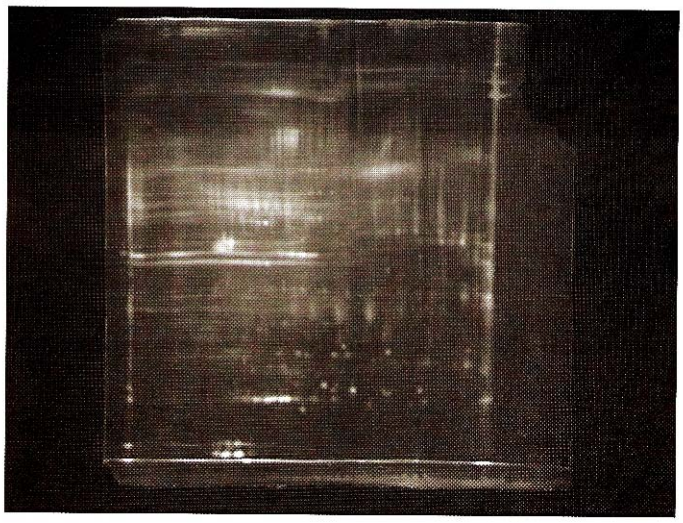

Figure 26:
Unlabeled rat CCSM non-castrate II

Figure 27: Labeled Rat Corpus Cavernosum Tissue from Non-Castrate II for Large Format Gels:

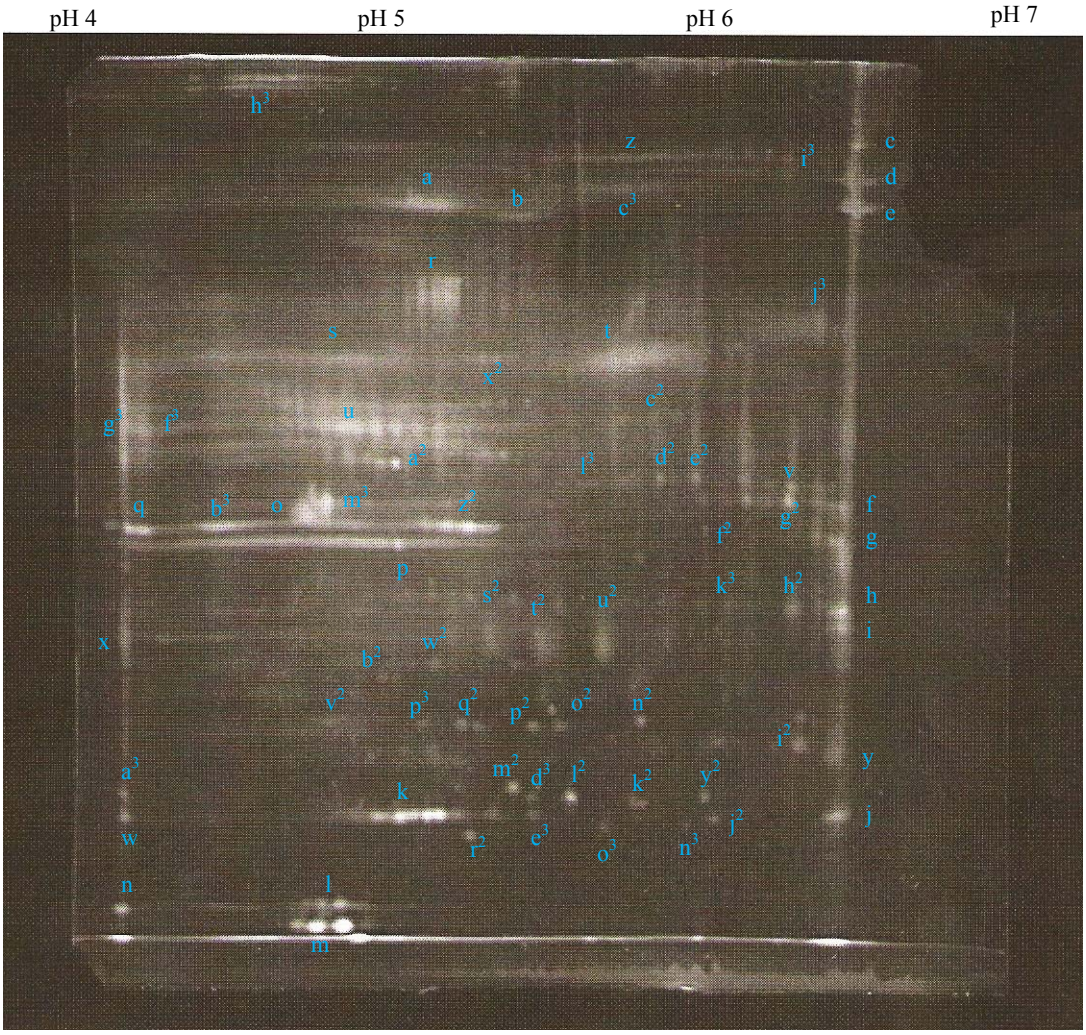

Table 10: Ferguson Plot Data for CCSM Non-Castrate II gel

	rf	logMW	MW	pI		rf	logMW	MW	pI
a	0.16	4.739182	54850.67798	5.0-5.3	a^2	0.45	4.509583	32328.30985	5.0-5.1
b	0.18	4.725769	53182.53077	5.3-5.5	b^2	0.44	4.516684	32861.24399	5.0
c	0.09	4.792834	62063.17654	6.5	c^2	0.40	4.549822	35466.79952	5.8-6.0
d	0.14	4.758907	57399.35338	6.4-6.6	d^2	0.47	4.49617	31345.12456	5.9
e	0.16	4.739182	54850.67798	6.4-6.6	e^2	0.47	4.49617	31345.12456	6.0
f	0.50	4.469344	29467.54803	6.4-6.5	f^2	0.50	4.475656	29898.95434	4.2-4.3
g	0.55	4.435417	27253.16841	6.4-6.5	g^2	0.50	4.475656	29898.95434	6.3
h	0.62	4.374664	23695.39758	6.4-6.5	h^2	0.66	4.347838	22276.04056	6.3-6.4
i	0.64	4.361251	22974.76088	6.4-6.5	i^2	0.78	4.253158	17912.5741	6.3-6.4
j	0.86	4.192405	15574.17319	6.4-6.5	j^2	0.86	4.192405	15574.17319	6.1
k	0.86	4.192405	15574.17319	4.9-5.3	k^2	0.84	4.205818	16062.67972	5.8-5.9
l	0.96	4.111927	12939.7832	4.7-5.0	l^2	0.83	4.212919	16327.47397	5.6
m	0.98	4.091413	12342.78034	4.7-5.0	m^2	0.82	4.219231	16566.50897	5.4-5.5
n	0.97	4.104826	12729.92954	4.2	n^2	0.74	4.279984	19053.90519	5.8-5.9
o	0.50	4.469344	29467.54803	4.7-4.8	o^2	0.75	4.273672	18778.98003	5.5-5.6
p	0.55	4.435417	27253.16841	4.1-5.4	p^2	0.75	4.273672	18778.98003	5.5
q	0.54	4.442518	27702.43854	4.1-4.3	q^2	0.75	4.273672	18778.98003	5.2-5.3
r	0.27	4.657915	45489.90187	5.1-5.3	r^2	0.88	4.17268	14882.6408	5.3
s	0.34	4.597162	39551.41268	4.8-5.1	s^2	0.66	4.347838	22276.04056	5.3-5.4
t	0.33	4.604263	40203.4201	5.6-6.1	t^2	0.66	4.347838	22276.04056	5.5-5.6
u	0.42	4.536409	34388.16485	4.7-5.3	u^2	0.66	4.347838	22276.04056	5.7-5.8
v	0.48	4.489069	30836.77841	6.1-6.2	v^2	0.74	4.279984	19053.90519	4.8-4.9
w	0.86	4.186093	15349.45642	4.2	w^2	0.68	4.327324	21248.29073	5.2
x	0.66	4.347838	22276.04056	4.1-4.2	x^2	0.39	4.563235	36579.26712	5.3-5.5
y	0.78	4.253158	17912.5741	6.4-6.5	y^2	0.83	4.212919	16327.47397	6.0-6.1
z	0.11	4.779421	60175.67908	5.6-6.0	z^2	0.53	4.44883	28108.00357	5.1-5.4

Table 10: Ferguson Plot Data for CCSM Non-Castrate II gel (continued)

	rf	logMW	MW	pI
a[3]	0.84	4.205818	16062.67972	4.2
b[3]	0.53	4.44883	28108.00357	4.4-5.0
c[3]	0.15	4.752595	56571.14904	5.6-5.9
d[3]	0.84	4.205818	16062.67972	5.5
e[3]	0.86	4.192405	15574.17319	5.5
f[3]	0.42	4.536409	34388.16485	4.6-5.3
g[3]	0.45	4.509583	32328.30985	4.1-4.2
h[3]	0.03	4.846486	70224.07058	4.4-4.9
i[3]	0.11	4.779421	60175.67908	6.2-6.3
j[3]	0.31	4.623988	42071.50034	6.4
k[3]	0.62	4.381765	24086.01764	6.1
l[3]	0.48	4.489069	30836.77841	5.7-5.8
m[3]	0.50	4.469344	29467.54803	4.8-4.9
n[3]	0.86	4.186093	15349.45642	6.0
o[3]	0.87	4.178992	15100.52338	5.7
p[3]	0.75	4.273672	18778.98003	5.1-5.2

Table 11: Non-Castrate II from smallest to largest mw

	mw	pI		mw	pI		mw	pI
m	12342.78	4.7-5.0	x	22276.041	4.1-4.2	f^3	34388.165	4.6-5.3
n	12729.93	4.2	h^2	22276.041	6.3-6.4	c^2	35466.8	5.8-6.0
l	12939.783	4.7-5.0	s^2	22276.041	5.3-5.4	x^2	36579.267	5.3-5.5
r^2	14882.641	5.3	t^2	22276.041	5.5-5.6	s	39551.413	4.8-5.1
o^3	15100.523	5.7	u^2	22276.041	5.7-5.8	t	40203.42	5.6-6.1
w	15349.456	4.2	i	22974.761	6.4-6.5	j^3	42071.5	6.4
n^3	15349.456	6	h	23695.398	6.4-6.5	r	45489.902	5.1-5.3
j	15574.173	6.4-6.5	k^3	24086.018	6.1	b	53182.531	5.3-5.5
k	15574.173	4.9-5.3	g	27253.168	6.4-6.5	a	54850.678	5.0-5.3
j^2	15574.173	6.1	p	27253.168	4.1-5.4	e	54850.678	6.4-6.6
e^3	15574.173	5.5	q	27702.439	4.1-4.3	c^3	56571.149	5.6-5.9
k^2	16062.68	5.8-5.9	z^2	28108.004	5.1-5.4	d	57399.353	6.4-6.6
a^3	16062.68	4.2	b^3	28108.004	4.4-5.0	z	60175.679	5.6-6.0
d^3	16062.68	5.5	f	29467.548	6.4-6.5	i^3	60175.679	6.2-6.3
l^2	16327.474	5.6	o	29467.548	4.7-4.8	c	62063.177	6.5
y^2	16327.474	6.0-6.1	m^3	29467.548	4.8-4.9	h^3	70224.071	4.4-4.9
m^2	16566.509	5.4-5.5	f^2	29898.954	4.2-4.3			
y	17912.574	6.4-6.5	g^2	29898.954	6.3			
i^2	17912.574	6.3-6.4	v	30836.778	6.1-6.2			
o^2	18778.98	5.5-5.6	l^3	30836.778	5.7-5.8			
p^2	18778.98	5.5	d^2	31345.125	5.9			
q^2	18778.98	5.2-5.3	e^2	31345.125	6			
p^3	18778.98	5.1-5.2	a^2	32328.31	5.0-5.1			
n^2	19053.905	5.8-5.9	g^3	32328.31	4.1-4.2			
v^2	19053.905	4.8-4.9	b^2	32861.244	5			
w^2	21248.291	5.2	u	34388.165	4.7-5.3			

Table 12: Non-Castrate II from smallest to largest pI

	mw	pI		mw	pI		mw	pI
x	22276.041	4.1-4.2	q^2	18778.98	5.2-5.3	k^3	24086.018	6.1
g^3	32328.31	4.1-4.2	r^2	14882.641	5.3	v	30836.778	6.1-6.2
q	27702.439	4.1-4.3	s^2	22276.041	5.3-5.4	i^3	60175.679	6.2-6.3
P	27253.168	4.1-5.4	b	53182.531	5.3-5.5	g^2	29898.954	6.3
n	12729.93	4.2	x^2	36579.267	5.3-5.5	h^2	22276.041	6.3-6.4
w	15349.456	4.2	m^2	16566.509	5.4-5.5	i^2	17912.574	6.3-6.4
a^3	16062.68	4.2	p^2	18778.98	5.5	j^3	42071.5	6.4
f^2	29898.954	4.2-4.3	d^3	16062.68	5.5	f	29467.548	6.4-6.5
h^3	70224.071	4.4-4.9	e^3	15574.173	5.5	g	27253.168	6.4-6.5
b^3	28108.004	4.4-5.0	o^2	18778.98	5.5-5.6	h	23695.398	6.4-6.5
f^3	34388.165	4.6-5.3	t^2	22276.041	5.5-5.6	i	22974.761	6.4-6.5
o	29467.548	4.7-4.8	l^2	16327.474	5.6	j	15574.173	6.4-6.5
l	12939.783	4.7-5.0	c^3	56571.149	5.6-5.9	y	17912.574	6.4-6.5
m	12342.78	4.7-5.0	z	60175.679	5.6-6.0	d	57399.353	6.4-6.6
u	34388.165	4.7-5.3	t	40203.42	5.6-6.1	e	54850.678	6.4-6.6
v^2	19053.905	4.8-4.9	o^3	15100.523	5.7	c	62063.177	6.5
m^3	29467.548	4.8-4.9	u^2	22276.041	5.7-5.8			
S	39551.413	4.8-5.1	l^3	30836.778	5.7-5.8			
K	15574.173	4.9-5.3	k^2	16062.68	5.8-5.9			
b^2	32861.244	5	n^2	19053.905	5.8-5.9			
a^2	32328.31	5.0-5.1	c^2	35466.8	5.8-6.0			
a	54850.678	5.0-5.3	d^2	31345.125	5.9			
p^3	18778.98	5.1-5.2	e^2	31345.125	6			
r	45489.902	5.1-5.3	n^3	15349.456	6			
z^2	28108.004	5.1-5.4	y^2	16327.474	6.0-6.1			
w^2	21248.291	5.2	j^2	15574.173	6.1			

Large Format Gel Results:

Once again, corpus cavernosum smooth muscle (CCSM) tissues were removed from four castrated rats and four non-castrated rats. All of the tissues were removed from all eight rats on the same day and immediately frozen. The following day the tissue was thawed, pooled, and homogenized: the four castrated CCSM's together and the four non-castrated CCSM's together. The gels were run as previously described, two gels for the castrated tissue and two gels for the non-castrate, and the results are shown above. After reviewing both the castrate and non-castrate gels done on the large format gels, I found all of these gels to be quite similar. Most likely due to the pooling of tissue, there are substantially more proteins visible in the large format gels as compared to the mini-gels. Like the mini-gels, there is a vertical "line" of proteins found in all of these gels right at about the pH of 6.5, however there is not a clear second line noticeable like the one that is appearing in a few of the mini-gels. In Figure 18, the castrate #1 (C1) gel, the polypeptide bands in this vertical line include: band b (MW~61168 Da), band n^3 (MW~58452 Da), band o (MW~54950 Da), band x (MW~44267 Da), band y (MW~38558 Da), band g (MW~30614 Da), band h (MW~28364 Da), band i (MW~24662 Da), band p^3 (MW~23567 Da), band j (MW~18142 Da), and band k (MW~16034 Da). In Figure 21, the castrate #2 (C2) gel, the polypeptide bands that appear in this line include: band d (MW~57399), band e (MW~53961 Da), band n^3 (MW~58346 Da), band z (MW~43391 Da), band f (MW~33892 Da), band g (MW~30837 Da), band h (MW~28571 Da), band i (MW~24842 Da), band h^2 (MW~23695 Da), band j (MW~18208 Da), and band k (MW~16063 Da). In Figure 24, the non-castrate #1 (NC1) gel, the polypeptide bands which appear in this similar line

include: band b (MW~62063 Da), band c (MW~ 57399 Da), band d (MW~53961 Da), band h (MW~34388 Da), band i (MW~29468 Da), band j (MW~26811 Da), band k (MW~24086 Da), band l (MW~22975 Da), and band m (MW~15831 Da). In Figure 27, the non-castrate #2 (NC2) gel, the corresponding bands falling into this vertical line include: band c (MW~62063 Da), band d (MW~57399 Da), band e (MW~54851 Da), band f (MW~29468 Da), band g (MW~27253 Da), band h (MW~23695 Da), band i (MW~22975 Da), band y (MW~17913 Da), and band j (MW~15574 Da). Although numerous possible proteins were named within the search parameters for each of the polypeptide bands, only the most appropriate protein matches derived from the TagIdent website will be listed. Within this vertical line of polypeptide bands, some critical proteins for the erectile process were listed as possible matches. There were two interesting suggestions for C1's band o, C2's band e, NC1's band d, and NC2's band e. The first was calcium/calmodulin dependent protein kinase type II alpha chain and the second was an actin like protein 7A. For the protein bands of C1's g, C2's g, NC1's i, and NC2's f, the most relatable match was a phosphatidylinositol (PIP_2) transfer protein beta isoforms. For the proteins listed in C1 as p^3 and i, in C2 as i and h^2, in NC1 as k and l, and in NC2 as h and i, a few interesting matches came up: a couple GTP binding proteins one of which was testis specific and a couple prolactin proteins. The proteins listed in the last few lines were more pronounced in the castrated gels than in the non-castrated tissue, possibly suggesting upregulation. For bands C1 j, C2 j and NC2 y, the search result came up as a regulator of G protein signaling 1. Finally, the noteworthy proteins expressed with the parameters for C1 k, C2 k, NC1 m, and NC2 j were a voltage

dependent calcium channel subunit, delta 2 and a potassium voltage gated channel subfamily E, member 2.

Another similarity in both the castrate and the non-castrate gels, there appears to be two parallel horizontal bands that are visible between the pH range of 4.0 – 5.5. In figure 18, the castrate # 1 gel, the bands, which are marked on these two lines, include band d (MW~28780 Da), band e (MW~28780 Da), and band d^3 (MW~29254 Da). For figure 21, the castrate #2 gel, the band represented in these area are bands q (MW~28990 Da), band r (MW~28990 Da), band p (MW~28571 Da), band o^3 (MW~27702 Da), and band f^3 (MW~29899 Da). In Figure 24, the non-castrate #1 gel, the bands representing these two parallel lines include band s (MW~28990 Da), band r (MW~28571 Da), band z (MW~28571 Da), and band b^2 (MW~27702 Da). Finally in Figure 27, the bands located in this same area include band q (MW~27702 Da), band b^3 (MW~28108 Da), band o (MW~29468 Da), band m^3 (MW~29468 Da), band z^2 (MW~28108 Da), and band p (MW~27253 Da). The ExPASy TagIdent search returned some interesting protein correlates. For C1's band e, C2's band q, NC1's band z, and NC2's band z^2 these were regulator G protein, another prolactin protein, a calcium channel, and finally a chloride intracellular channel. There was a wide variety of results that came up for C1's d, C2's p, r, and o^3, NC1's r, and NC2's p and b^3. These included several types and isoforms of tropomyosin, the calcium binding protein calbindin, sperm protein 10, and a couple voltage gated potassium channel interacting proteins. Interestingly, these bands appear to shift when comparing castrated to non-castrated tissue. The castrated proteins C1's d and C2's p appear lower and brighter than their corresponding non-castrated protein

counterparts. When performing the search for NC2's m^3, an isoforms of prostaglandin reductase 2 was the closest related protein found.

Another cluster of polypeptide bands found on both the castrate and non-castrate gels are in the area between pH 4.5 to pH 5.5/5.6 right above the two horizontal lines mentioned above. However the bands found in the castrated gels appear much more pronounced than what is seen in the non-castrated gels. In Figure 18, the castrate #1 gel, the bands consist of band m (MW~40350 Da), band w^2 (MW~37385 Da), band b^2 (MW~37385 Da), band n (MW~37725 Da), band d^2 (MW~36846 Da), band e^2 (MW~36846 Da), band a^2 (MW~33586 Da), band c^2 (MW~34639 Da), and band v (MW~33041 Da). In Figure 21, the castrate #2 gel, the band in this cluster include band t (MW~39551 Da), band u (MW~33892 Da), band s^3 (MW~40792 Da), band r^3 (MW~34955 Da), band r^2 (MW~37182 Da), band s^2 (MW~37182 Da), band b^2 (MW~33892 Da), band c^2 (MW~34388 Da), band o^2 (MW~31804 Da), and band d^2 (MW~44106 Da). In Figure 24, the non-castrate #1 gel, the polypeptide bands found in this cluster of proteins include band t (MW~34955 Da), band a^2 (MW~32328 Da), band a^3 (MW~33342 Da), band u (MW~34955 Da), band b^3 (MW~36646 Da), band g^3 (MW~33892 Da), and band r^2 (MW~37182 Da). Finally in Figure 27, the non-castrate #2 gel, the bands located in this region include band u (MW~34388 Da), band a^2 (MW~32328 Da), band b^2 (MW~32861 Da), band x^2 (MW~36579 Da), and band s (MW~39551 Da). Within this cluster of proteins, the ExPASY TagIdent search expressed several closely related proteins. For C1's m band, C2's t band, and NC2's s band, the main polypeptides listed were tropomodulin 1 and 3, a couple calcium binding proteins, and an actin related protein. The polypeptide bands including C1's w^2, b^2, d^2,

e^2, and n; C2's r^2 and s^2; NC1's r^2 and b^3; and finally NC2's x^2 share several of the same protein results. These consist of prostaglandin reductase 2, a cAMP response element binding protein, the calcium binding protein calponin 3, as well as a couple guanine nucleotide binding proteins. Once again the protein bands found in this area of the castrated CCSM tissue are much more outstanding than the ones found in the same area in the non-castrated tissue, suggesting either up-regulation of the proteins in the castrated tissue or down-regulation of the proteins in the non-castrated tissue. Another interesting group of polypeptide bands found in this cluster are C1's c^2, C2's r^3 and c^2, NC1's t, and NC2's u. The search results for these proteins include an isoforms of cAMP response binding element protein, a cAMP dependent regulating protein kinase, and a zona pellucida sperm binding protein. Two important bands are found in the castrate #2 (C2) gel. The first is the polypeptide band u, which ExPASY search comes back to several forms and isoforms of tropomyosin. The second is band d^2, which search returns several forms of actin including smooth muscle actin, a calcium calmodulin dependent protein kinase, and a potassium channel.

Another interesting group of congruent polypeptide bands found on both the castrate and non-castrate gels are located toward the bottom of the gel between the pH of 4.0 and 5.2. In Figure 18, the castrate #1 gel, these bands include band q (MW~12916 Da), band a^3 (MW~13129 Da), and band r (MW~12523 Da). In Figure 21, the castrate #2 gel, these concurrent bands are band n (MW~12730 Da), band a^3 (MW~12940 Da), and band m (MW~12343 Da). In the non-castrate #1 gel, Figure 24, these respective bands include band q (MW~12546 Da), band o (MW~12730 Da), and band p (MW~12165 Da). Finally in the non-castrate #2 gel, Figure 27, these corresponding bands are labeled as band n

(MW~12730 Da), band l (MW~12940 Da), and band m (MW~12343 Da). The search results in these parameters however did not return any proteins which were targeted in our research.

Three additional bands are worth noting that appear in all four gels are located between pH of 5.0 and pH of 6.0. In Figure 18, the castrate #1 gel, these spots are labeled band a (MW~55755 Da), band w (MW~54158 Da), and band p (MW~61168 Da). In Figure 21, the castrate #2 gel, these corresponding bands are band a (MW~54851 Da), band b (MW~53961 Da), and band c (MW~57399 Da). In Figure 24, the non-castrate #1 gel, these protein bands are labeled band a (MW~54851 Da), band w^2 (MW~53961 Da), and band c^3 (MW~57399 Da). Finally in Figure 27, the non-castrate #2 gel, the respective bands are labeled band a (MW~54851 Da), band b (MW~53183 Da), and band c^3 (MW~56571 Da). Within this group of protein bands, there are quite a few interesting proteins listed in the ExPASy TagIdent feedback. For C1, C2, NC1, and NC2s' band a, the proteins include a couple acetylcholine receptor subunit (β), quite a few voltage gated potassium channel subunits, a cAMP responsive element binding protein, and a protein kinase C substrate. For C1's band w, C2's band b, NC1's band w^2, and NC2's band b, the results also returned a voltage gated potassium channel and a couple acetylcholine receptor subunits, but also a chloride channel, a Rho-guanine nucleotide exchange factor, a heat shock 70 kDa protein, and a PIP_2 kinase regulatory subunit. Additionally for C2's band c, NC1's band c^3, and NC2's band c^3, the results consisted of a voltage dependent L-type calcium channel subunit, a voltage gated potassium channel, a calcium/calmodulin dependent protein kinase, and a vesicular acetylcholine transporter.

In each individual gel, another spot or two shows up in this particular area. In Figure 18, the castrate #1 gel, there is a spot, band s^3 (MW~58452 Da), which is located right at pH 5.0. In Figure 21, the castrate #2 gel, there is a long band that extends from pH 4.0 to about pH 5.0 labeled band q^3 (MW~60176 Da). This long band has several different proteins which are generated by the ExPASY TagIdent search. The first is a voltage gated potassium channel, as well as several isoforms of a cAMP specific phosphodiesterase. In addition there is a protein phosphatase regulatory subunit and a chloride intracellular channel which appear in the search outcome. The same band appears in Figure 24, the non-castrate #1 gel, labeled band v (MW~61057 Da) which comes out as a chloride intracellular channel in the ExPASY TagIdent search. There are two additional bands which appear as well. The first, band e (MW~60176 Da), is another long stretch of proteins which falls between pH 5.5 and pH 6.5 and the second, band h^3 (MW~57399 Da), is a short band found right about pH of 6.2-6.3. Finally in Figure 27, the same patterns that are found in Figure 24 are found in this gel. First of all the same long band which is noted in Figure 21 and Figure 24 appears labeled as band h^3 (MW~70224 Da). The other long band of protein between pH 5.5-6.5 is labeled band z (MW~60176 Da) in this gel and the short band is labeled i^3 (MW~60176 Da). This short band is found only in the non-castrate gel, not in the castrated gel. Besides the proteins listed, there were no other significant results from the ExPASY TagIdent search that related to this research project.

An interesting pair of polypeptide bands occurs right below this area at pH of about 5.0 to 5.3, which are found in all the large format gels. In Figure 18, this pair of protein bands is labeled band l (MW~47864 Da); in Figure 21, the pair is labeled band d^2

(MW~44106 Da); in Figure 24, the pair is labeled band f (MW~46917 Da); and in Figure 27, the pair is labeled band r (MW~45490 Da). Three of these protein bands had similar suggestions for possible polypeptides found in the ExPASy TagIdent. C1's band l, NC1's band f, and NC2's band r results included a G-protein activated inward rectifier potassium channel as well as another potassium channel. The castrate #1 (C1) band d^2 came up with several significant search results including a protein phosphatase, a cAMP dependent protein kinase, a calcium/calmodulin dependent protein kinase, a potassium channel, and several different types of actin including a smooth muscle and a cytoplasmic form. Once again the proteins located in castrated tissue were much more distinct than their counterparts in the non-castrated tissue.

Another cluster of protein spots which are visible in each individual gel falls in the rage of pH 5.6 to about pH 6.5. In the castrate #1 gel, Figure 18, these spots include band m^3 (MW~44267 Da), band c (MW~40350 Da), band q^3 (MW~35725 Da), band t^3 (MW~35725 Da), band y^2 (MW~32036 Da), band x^2 (MW~32036 Da), band v^2 (MW~32036 Da), band u^2 (MW~30614 Da), band z^2 (MW~30614 Da), band r^3 (MW~28364 Da), band k^3 (MW~24662 Da), and band t^2 (MW~24306 Da). In the castrate #2 gel, Figure 21, the bands found in this cluster are band s (MW~40203 Da), band y (MW~44106 Da), band q^2 (MW~36051 Da), band t^3 (MW~36051 Da), band o^2 (MW~31804 Da), band w (MW~30837 Da), band m^2 (MW~31804 Da), band n^2 (MW~31804 Da), band p^2 (MW~30392 Da), band p^3 (MW~30837 Da), band m^3 (MW~24842 Da), and band x (MW~24842 Da). In the non-castrate #1 gel, Figure 24, the polypeptide bands that are located in this same area include band i^3 (MW~42765 Da), band g (MW~40203 Da), band u^2 (MW~36051 Da), band p^2 (MW~31804 Da), band q^2

(MW~31804 Da), band w (MW~30392 Da), band v^2 (MW~28108 Da), band o^2 (MW~31804 Da), band l^3 (MW~31804 Da), band j^3 (MW~24086 Da), and band x (MW~24086). Finally, in the non-castrate #2 gel, Figure 27, the cluster of proteins include band t (MW~40203 Da), band j^3 (MW~42072 Da), band c^2 (MW~35467 Da), band e^2 (MW~31345 Da), band v (MW~30837 Da), band g^2 (MW~29899 Da), band f^2 (MW~29899 Da), band d^2 (MW~31345 Da), band l^3 (MW~30837 Da), band k^3 (MW~24086 Da), and band h^2 (MW~22276 Da). The most relevant results from the ExPASy TagIdent search are listed as follows. For C1's m^3 band, C2's y band, NC1's i^3 band, and NC2's j^3 band, the proteins found were a couple Acyl CoA proteins. For C1's c band, C2's s band, NC1's g band, and NC2's t band, the relevant proteins were a calcium/calmodulin dependent protein kinase, an inward rectifier potassium channel, several guanine-nucleotide binding proteins, an isoforms of a cAMP responsive element binding protein, a couple Ras-related GTP binding proteins, a potassium channel, and a isoforms of a chloride channel. For the proteins bands located at C1's $q^3$and t^3, C2's q^2 and t^3, and NC2's c^2, the significant findings were a prolactin receptor, a potassium channel, a calcium/calmodulin dependent protein kinase, and a calcium binding protein. For the bands found at C1's y^2, x^2, and v^2; C2's m^2, n^2, and o^2; NC1's p^2, q^2, and o^2; and NC2's e^2 and d^2, the significant results included a couple phosphatidylinositol transfer proteins, a calcium binding protein, a neuronal growth regulator, and a GTP binding protein. For the polypeptide bands found at C1's k^3 and t^2, C2's m^3 and x, NC1's j^3 and x, and NC2's k^3, the proteins listed were prolactin and a GTP binding protein. For the bands found in castrate #2 (C2) gel labeled w and p^3, the most interesting corollary was a phosphatidylinositol transfer protein. In the non-castrate 2 (NC2) gel there were two

individual bands worth mentioning. The first was the h^2 band which results were a GTPase and a prolactin. The second is band u^2 which resulted in a GTP binding protein in the ExPASy TagIdent search.

Right below the initial horizontal lines of polypeptides mentioned are a group of interesting protein bands which correspond with all four gels. Directly below these lines at a pH of about 4.2 to about 5.0, are a few shorter horizontal bands found in each gel. In Figure 18, the castrate #1 gel, these bands include band o^3 (MW~20790 Da), band t (MW~20527 Da), and band s (MW~18711 Da). The band o^3 appears only in the castrated CCSM gel, not in the non-castrated CCSM gels. Directly to the right of these bands are an interesting trio of proteins which appear in both the castrate and non-castrate gels. These polypeptides include band f^2 , band g^2, and band h^2 all of which are located at MW~23184 Da, as well as band i^2 (MW~21835 Da) which is also found in that area. In Figure 21, the castrate #2 gel, there are only two horizontal bands located directly below the horizontal pattern mentioned initially; these include band b^3 (MW~22975 Da) and c^3 (MW~19368 Da). The trio is visual in this gel as well all at MW~22975 Da and includes band e^2, band f^2, and band g^2, with band l^2 (MW~18474 Da) located close to these three protein spots as well. In Figure 24, the non-castrate #1 gel, there is an additional polypeptide bands located below the initial horizontal lines of proteins. These include band x^2 (MW~22602 Da), band y^2 (MW~21599 Da), band s^2 (MW~19054 Da), and band a^2 (MW~32328 Da). The protein trio which are also visible in the non-castrate gels at MW~22975 Da include band c^2, d^2, and e^2 as well as that additional protein spot nearby, band f^2 (MW~21248 Da). Finally in Figure 27, the non-castrate #2 gel, the corresponding proteins include band x (MW~22276 Da), band b^2 (MW~32861 Da), and

band v^2 (MW~19054 Da). In this gel, the trio, which are labeled at MW~22276 Da, include band s^2, band t^2, and band u^2 with band w^2 (MW~21248 Da) sitting close by. In this collection of protein bands, there were several analogous results from the ExPASy TagIdent search. For C1's bands o^3 and t, C2's band c^3,and NC2's v^2, the proteins found were a calcium binding protein, a couple myosin regulatory light chain isoforms for smooth muscle, and a neuronal calcium sensor. For C2's b^3 band and NC1's y^2 band, several interesting proteins came up. These included several myosin light chains, a calcium binding protein, a neuronal calcium sensor, Rho-B, a neuron specific calcium binding protein, a couple sodium channel subunits, and a calcium integrin binding protein. Non-castrate #1 (NC1)'s protein band f^2, as well as NC2's protein band w^2, are worth mentioning in the fact that they returns to several Ras related proteins like many of the polypeptide bands found in all of these gels; however none of these Ras related proteins are Rho-A. NC2's protein band w^2 also returns to neurocalcin, which is a neuronal calcium binding protein. Another important polypeptide band located in this group is NC1's s^2 which results in a calcium binding protein and a couple myosin regulatory light chains for smooth muscle. In the trio's listed above, there were several Ras family proteins returned, however once again Rho-A was not one of the results. Also there was a regulator of G-protein signaling, a sodium channel, prolactin, and a GTP binding protein.

The last assemblage of polypeptide bands is a large aggregation that is found in the lower part of each gel at pH of approximately 5.0-6.4. A large band of protein appears in all the gels with smaller spots located to the right of this band; some slightly below but many at the same level or above this prominent polypeptide spot. In Figure 18, the

castrate #1 gel, the large band is labeled band f (MW~15802 Da) and the array of additional protein spots include band j^2 (MW~18711 Da), band k^2 (MW~18711 Da), band l^2 (MW~18711 Da), band m^2 (MW~18711 Da), band l^3 (MW~18142 Da), band s^2 (MW~18142 Da), band n^2 (MW~16268 Da), band o^2 (MW~16268 Da), band p^2 (MW~16268 Da), band q^2 (MW~16268 Da), band j^3 (MW~18142 Da), band b^3 (MW~15073 Da), band i^3 (MW~15802 Da), band f^3 (MW~15546 Da), band g^3 (MW~15802 Da), band h^3 (MW~15546 Da), and band r^2 (MW~15546 Da). In Figure 21, the castrate #2 gel, the prominent polypeptide band is band l (MW~15831 Da) and the collection of proteins spots nearby include band t^2 (MW~18779 Da), band u^2 (MW~18779 Da), band v^2 (MW~18779 Da), band i^2 (MW~18474 Da), band k^3 (MW~18208 Da), band z^2 (MW~18474 Da), band k^2 (MW~16567 Da), band j^2 (MW~16567 Da), band w^2 (MW~16327 Da), band x^2 (MW~16567 Da), band l^3 (MW~16567 Da), band d^3 (MW~15101 Da), band j^3 (MW~15831 Da), band g^3 (MW~15574 Da), band h^3 (MW~15831 Da), band i^3 (MW~15574 Da), and finally band y^2 (MW~15831 Da). In non-castrate #1 gel, Figure 24, the pronounced protein band is labeled band n (MW~15574 Da) and the additional polypeptides are labeled band p^3 (MW~18779 Da), band g^2 (MW~18474 Da), band h^2 (MW~18474 Da), band i^2 (MW~18474 Da), band j^2 (MW~18779 Da), band d^3 (MW~16567 Da), band e^3 (MW~16327 Da), band y (MW~16327 Da), band k^2 (MW~16063 Da), band l^2 (MW~16063 Da), band n^2 (MW~14883 Da), band f^3 (MW~15574 Da), band o^3 (MW~15349 Da), band n^3 (MW~13764 Da), and band t^2 (MW~15574 Da). Lastly, in the non-castrate #2 gel, Figure 27, the distinguishable band is labeled band k (MW~15574 Da) and the cluster of proteins spots nearby are labeled band p^3 (MW~18779 Da), band

q^2 (MW~18779 Da), band p^2 (MW~18779 Da), band o^2 (MW~18779 Da), band n^2 (MW~19054 Da), band i^2 (MW~17913 Da), band m^2 (MW~16567 Da), band d^3 (MW~16063 Da), band l^2 (MW~16327 Da), band k^2 (MW~16063 Da), band y^2 (MW~16327 Da), band j^2 (MW~15574 Da), band r^2 (MW~14883 Da), band e^3 (MW~15574 Da), band o^3 (MW~15101 Da), and finally band n^3 (MW~15349 Da). In this last collection of polypeptide bands, the most intriguing proteins found in the ExPASy TagIdent search included a couple voltage gated potassium channels, a couple protein phosphatase regulatory subunit, a receptor activity modifying protein, a prolactin receptor, a G-protein signaling modulator, an actin related protein complex subunit, a voltage gated calcium channel, a major urinary protein, and a signaling threshold regulating transmembrane adapter.

Any discrepancies could include the possibility that there were a few protein bands that were not labeled on certain gels since these spots were not as clear or as pronounced on one gel as they were on another. Additionally there might be proteins which are not found in the ExPASY database yet and, as stated by the website, their data is not always accurate or up to date.

Discussion

During the last three to four decades, extensive research has led to significant advances in better understanding the anatomy, physiology, and pharmacology of the erection process including the neurological, endocrinological, psychological, vascular, and the pathology of the entire male sexual process. In this research study, the focus is on better understanding the proteomics of the corpora cavernosa smooth muscle in order to generate an overall profile of the complex proteins found in this critical tissue involved in the erectile process.

Several proteins involved in signaling cascades were present in the gels including target proteins as well as regulator proteins. Guanine nucleotide binding proteins, also known as G-protein, are involved in one of the most significant signaling cascades found in most cells (Jin and Burnett, 2006; Wang et al., 2002; Fabbri et al., 1997; Morelli et al., 2006; Chang et al., 1998). There are several components involved in this messenger system, which target numerous cell processes and ultimately regulate various cell processes. Many key elements involved in the G-protein signal transduction were found in the gels of this study. For instance, several GTP binding proteins were expressed, as well as G protein signaling modulators, numerous guanine nucleotide binding proteins, various GTPase IMAP family members, Rho-related GTP binding protein Rho B and Rho Q, and G-activated channels.

One of the most important chemical components of the cell, as described earlier, is the element calcium. The increase of intracellular calcium levels is critical in inducing contraction; conversely the reduction of calcium levels within the cell promotes relaxation and erection (Andersson, 2003; Williams et al., 2005; Lincoln et al., 2001,

Chuang et al., 1998; Webb, 2003; Lue, 2000; Jin and Burnett, 2006). Several polypeptides found in the large format gels in this study are actively involved in either the amplification or the minimization of calcium levels or are directly or indirectly involved in the facilitation of calcium to perform its functions. One G-protein pathway involved in calcium influx involves phosphatidylinositol (PIP_2) (Levin et al., 1997). There were a couple of interesting proteins located on these gels associated with PIP_2, including a PIP_2 transfer protein isoforms and a PIP_2 kinase regulatory subunit, as well as protein kinase C substrates. Several voltage gated calcium channels and other calcium channels appeared, as well as calcium binding proteins, neuronal calcium sensors, calcium/calmodulin dependent protein kinases, and voltage dependent L-type calcium channel subunits. Calcium-calmodulin is important in activating myosin light chain kinase and displacing tropomyosin on actin so crossbridge cycling can occur. This calcium-calmodulin-myosin light chain kinase complex in turn phosphorylates myosin light chains so myosin light chains can now bind to actin to ultimately cause contraction (Maas et al., 2002; Lue, 2000; Andersson, 2003; Williams et al., 2005; Jin and Burnett, 2006). Following this chain of events, several key proteins were found in our research including actin related protein complex subunits and several different types of actin including a smooth muscle and a cytoplasmic form; a number of myosin light chains subunits and myosin regulatory light chains for smooth muscle and their isoforms; as well as numerous forms and isoforms of tropomyosin.

Another signaling cascade that is thought to be involved in the relaxation of the corporal smooth muscle tissue is cyclic adenosine monophosphate or cAMP (Andersson, 2001; Lin et al., 2008; Maagi et al, 2000). This experience showed the expression of

several forms of cAMP response element binding protein as well as a cAMP dependent protein kinase, cAMP dependent transcription factors, adenylate kinase isoenzymes, and numerous isoforms of cAMP specific phosphodiesterases. As was discussed previously, cAMP's and cGMP's activities are regulated by phosphodiesterases, ultimately influencing the contractile tone of erectile tissue (Morelli et al., 2006; Uckert et al., 2004).

The Ras superfamily of proteins envelopes a number of influential polypeptides related based on structure, function, and sequence, all of which function as g-protein signaling modulators, regulating various functions within the cell (Jin and Burnett, 2006; Wang et al., 2002). The subfamilies include Ras, Rho, Rab, Rap, Arf, Ran, Rheb, Rad, Rit, and Miro all of which display specific functional responsibilities within the cell. There was a considerable number of proteins within the Ras subfamilies found in these gels including a Ras associated domain family and an isoform of a Ras related GTP binding protein, several Ras GTPases; a wide variety of Rab proteins which are involved with membrane trafficking; several Rap proteins which assist in vesicular transporting; a testis specific isoform of the GTP binding nuclear binding protein Ran; and finally Rho-guanine nucleotide exchange factor as well as a Rho GDP dissociation inhibitor, Rho B and Rho Q GTP binding proteins, and transforming protein Rho A. As previously stated, the Rho A signaling cascade is a critical component in the contractile pathway for penile erectile tissue. Rho A activates Rho-kinase which promotes the actions of myosin and is thought to inhibit the effects of nitric oxide (Jin and Burnett, 2006; Wan et al., 2002; Andersson, 2003; Somlyo and Somlyo, 2000; Mills et al., 2001). Although Rho-kinase itself was not named as one of the exact proteins residing in the gels of this experiment,

Rho kinase is a serine/threonine kinase and several serine/threonine protein kinases were found in these gels as well as serine/threonine protein phosphatase regulatory subunits.

Potassium channels are another critical conduit to reducing cytosolic calcium levels, as well as regulating adrenergic receptor activity, and possibly being implemented as being one of the most physiologically relevant ion channels promoting relaxation of the erectile tissue (Christ and Lue, 2004; Christ et al., 1997; Lincoln et al., 2001). A myriad of potassium channels were found in this research undertaking including voltage gated potassium channels, potassium channel subunits and accessory subunits, potassium channel subfamilies, G-protein activated potassium channels, and potassium channel interacting proteins.

Another ion channels which is well known in playing a role in depolarization of plasma membranes creating a more negative charge inside the membrane causing a decrease in intracellular calcium and ultimately leading to relaxation is the sodium ion channel (Gupta et al., 1995; Saenz, 2000; Archer, 2002). Several sodium related proteins were identified including sodium channel β subunits, a voltage gated sodium channel subunit (β), and a sodium-coupled amino acid transporter, as well as a sodium dependent phosphate transporter. As was briefly mentioned, another ion channel of interest thought to contribute to hyperpolarization and relaxation of the corpora smooth muscle is chloride channels (Karkanis et al., 2003; Christ and Lue, 2004). A number of chloride intracellular channels, an isoform of chloride channel, and a KCl co-transporter were expressed in the gels.

As stated previously, acetylcholine indirectly plays a vital role in the relaxation of penile tissue. Not only does it inhibit the noradrenaline receptors, which diminishes the

sympathetic role of contraction; it also activates the non-adrenergic-noncholinergic inhibitory pathway by stimulating the release of nitric oxide (Morelli et al., 2006; Argiolas and Melis, 1995; Andersson, 2003; Kim et al., 1991). Several neuronal acetylcholine α receptor subunits, as well as neuronal acetylcholine receptor subunit β and a vesicular acetylcholine transporter, were identified as one of the proteins found in theses gels.

Another vasoconstrictor which was mentioned previously, although its role is not firmly established yet, is angiotensin II (Lin et al., 2008; Comiter et al., 1997). Type I angiotensin II receptor associated protein and angiotensinogen also appeared in these gels. Several inhibitory neurochemicals were mentioned that impede the erectile response; one such neurochemical which displays repressive effect is prolactin (Kruger et al., 2002). Several forms of prolactin were expressed in these gels including prolactin 8A4, prolactin 2A1, prolactin 7B1, prolactin 6A1, prolactin 3B1, prolactin 3D1, and a protein induced protein homolog as well as isoforms of prolactin receptors.

As mentioned earlier, there appears to be some correlation between oxidative stress and ED. Oxidative stress is due to the imbalance to ROS and antioxidants (Agarwal et al., 2006; Kahn et al., 2001). One of the players in the protective mechanism of the body against ROS is the antioxidant superoxide dismutase which was expressed in these gels. Peroxiredoxin 4, peroxiredoxin 3, and peroxiredoxin 2, another group of antioxidants, which helps control peroxide levels and aides in regulating signal transduction were also expressed in these gels. Glutathione synthetase, which also present in these gels, is an enzyme that assists in the production of glutathione, another antioxidant that protects

cells from free radicals. Glutathione peroxidase 3 was also present which again helps protect the cell from oxidative damage.

Additional proteins of interest that were expressed included a couple receptor activity modifying proteins, a nuclear receptor subfamily member, ATP binding domains, a neuroendocrine secretory protein, a dual specificity testis-specific protein kinase, an isoform of a testis specific Y encoded protein, a mitochondrial import receptor subunit, a mitochondrial intermembrane space import and assembly protein, an integral membrane protein, several transmembrane proteins, several protein phosphatases and their regulatory subunits, a few neuronal growth factors and a growth hormone receptor, isoform 2 of an upstream stimulating factor, a signaling threshold regulatory transmembrane adaptor, a vesicular associated membrane protein, a vesicular inhibitory amino acid transporter, and an excitatory amino acid transporter. All of which could play vital roles either the contractile or the erectile of the corpus cavernosal tissue.

In conclusion, the proteomic approach to the study of the erectile tissue can provide important insight into what is occurring at a molecular level and subcellular level during both the contraction and relaxation phases of the erection process. As was demonstrated in this study, there were a variety of proteins found in both the castrate and non-castrate tissue. As discussed, alterations of these polypeptide bands were visible suggesting either up-regulation or down-regulation of a variety of proteins, as well as shifts were seen possibly suggesting phosphorylation or dephosphorylation of proteins. Additionally there were a number of proteins found in either the castrate or the non-castrate gels which did not exist in either's counterpart. These differences suggest that androgens play a critical role in the expression of these proteins, i.e. the presence/absence of the proteins, the state

of the proteins (phosphorylated or not), and/or the number of isoforms found. Although there is much to be learned and investigated in the role of potentially essential tools involved in this process, the current study has helped not only to verify the existing ideas and suggestions of how the entire mechanism flows together, but also established some possible goals for additional investigations. Future proposals for experimental studies would be to investigate a narrower range of specific proteins of interest. Elaborating on this suggestion would be to focus on specific proteins, which are currently being investigated in our laboratory, especially the proteins which are distal to the cGMP point of the erectile pathway. These proteins could be monitored for changes that occur during the contracted and relaxed states of the CCSM tissue. Furthermore, future goals should continue investigating the role of androgens in the entire erection process. Although an extensive amount of research has been done in this area and much progress has been made, there is still much to be learned in order to fully understand the complex cellular mechanisms that regulate the process of erection in mammals.

References

1. Agarwal A, Nandipati KC, Sharma RK, Zippe CD, Raina R (2006) Role of Oxidative Stress in the Pathophysiological Mechanism of Erectile Dysfunction. *The Journal of Andrology* 27: 335-347.
2. Alcorn JF, Toepfer JR, Leipheimer RE (1999) The Effects of Castration on Relaxation of Rat Corpus Cavernosum Smooth Muscle in Vitro. *The Journal of Urology* 161: 686-689.
3. Andersson KE (2003) Erectile Physiological and Pathophysiological Pathways involved in Erectile Dysfunction. *The Journal of Urology* 170: S6-S14.
4. Andersson, K-E (2001) Pharmacology of Penile Erection. *Pharmacological Reviews* 53: 417-450.
5. Archer SL (2002) Potassium channels and erectile dysfunction. *Vascular Pharmacology* 38: 61-71.
6. Archer SL, Huang JMC, Hampl V, Nelson DP, Shultz PJ, Weir EK (1994) Nitric oxide and cGMP cause vasorelaxation by activation of a charybdotoxin-sensitive K channel by cGMP-dependent protein kinase. *Proceedings of the National Academy of Sciences of the United States of America* 91: 7583-7587.
7. Argiolas A and Melis MR (1995) Neuromodulation of Penile Erection: An Overview of the Role of Neurotransmitters and Neuropeptides. *Progress in Neurobiology* 47: 235-255.
8. Aytac IA, McKinlay JB, Krane RJ. (1999) The Likely Worldwide Increase in Erectile Dysfunction Between 1995 and 2025 and Some Possible Policy Consequences. *British Journal of Urology, International* 84:50-56.

9. Bacon CG, Mittleman MA, Kawachi I, Giovannucci E, Glaser DB, Rimm EB (2006) A Prospective Study of Risk Factors of Erectile Dysfunction. *The Journal of Urology* 176: 217-221.
10. Baukrowitz T, Schulte U, Oliver D, Herlitze S, Krauter T, Tucker SJ, Ruppersberg JP, Fakler B (1998) PIP_2 and PIP as Determinants for ATP Inhibition of K_{ATP} Channels. *Science* 282: 1141-1144.
11. Bivalacqua TJ, Champion HC, Abdel-Mageed AB, Kadowitz PJ, Hellstrom WJG (2001) Gene Transfer of Prepro-Calcitonin Gene-Related Peptide Restores Erectile Function in Aged Rat. *Biology of Reproduction* 65: 1371-1377.
12. Bivalacqua TJ, Usta MF, Champion HC, Kadowitz PJ, Hellstrom WJG (2003) Endothelial Dysfunction in Erectile Dysfunction: Role of Endothelium in Erectile Physiology and Disease. *Journal of Andrology* 24 (6) 17-37.
13. Bivalacqua TJ, Champion HC, Usta MF, Cellek S, Chitaley K, Webb RC, Lewis RL, Mills TM, Hellstrom WJG, Kadowitz PJ (2004) RhoA/Rho-kinase suppresses endothelial nitric oxide synthase in the penis: A mechanism for diabetes-associated erectile dysfunction. *Proceedings of the National Academy of Sciences in the United States of America* 101: 9121-9126.
14. Bonnevier J, Arner A (2004) Actions Downstream of Cyclic GMP/Protein Kinase G Can Reverse Protein Kinase C-mediated Phosphorylation of CPI-17 and Ca^{2+} Sensitization in Smooth Muscle. *The Journal of Biological Chemistry* 279 (28): 28998-29003.
15. Boo YC, Sorescu G, Boyd N, Shiojima I, Walsh K, Du J, Jo H (2002) Shear Stress Stimulates Phosphorylation of Endothelial Nitric-oxide Synthase at Ser-

1179 by Akt-independent mechanism. *The Journal of Biological Chemistry* 277: 3388-3396.

16. Chuang AT, Strauss JD, Steers WD, Murphy RA (1998) cGMP mediates corpus cavernosum smooth muscle relaxations with altered cross bridge function. *Life Sciences* 63 (3): 185-194.
17. Chen KK, Chan JYH, Chang LS (1999) Dopaminergic Neurotransmission at the Paraventricular Nucleus of Hypothalamus in Central Regulation of Penile Erection in the Rat. *The Journal of Urology* 162: 237-242.
18. Chitaley K, Wingard CJ, Webb RC, Branam H, Stopper VS, Lewis RW, Mills TM (2001) Antagonism of Rho-kinase stimulates rat penile erection via a nitric oxide-independent pathway. *Nature Medicine* 7: 119-122.
19. Christ GJ, Lue TF (2004) Physiology and Biochemistry of Erections. *Endocrine* 23 (2) 93-100.
20. Christ GC, Richards S, Winkler A (1997) Integrative erectile biology: the role of signal transduction and cell-to-cell communication in coordinating corporal smooth muscle tone and penile erection. *International Journal of Impotence Research* 9: 69-84.
21. Christ GC, Spray DC, Brink PR (1993) Characterization of K Currents in Cultured Human Corporal Smooth Muscle Cells. *Journal of Andrology* 14: 319-328.
22. Comiter CV, Sullivan MP, Yalla SV, Kifor I (1997) Effect of angiotensin II on corpus cavernosum smooth muscle in relation to nitric oxide environment: in

vitro studies in canines. *International Journal of Impotence Research* 9: 135-140.

23. Craven M, Sergeant GP, Hollywood MA, McHale NG, Thornbury KD (2004) Modulation of spontaneous Ca^{2+}-activated Cl^- currents in the rabbit corpus cavernosum by the nitric oxide-cGMP pathway. *Journal of Physiology* 556 (2): 495-506.
24. Dean RC, Lue TF (2005) Physiology of Penile Erection and Pathophysiology of Erectile Dysfunction. *Urologic Clinics of North America* 32 (4): 379-395.
25. Derby CA, Mohr BA, Goldstein I, Feldman HA, Johannes CB, McKinaly JB (2000) Modifiable risk factors and erectile dysfunction: can lifestyle changes modify risk? *Urology* 56 (2): 302-306.
26. DiSanto, ME (2003) Corpus Cavernosum Smooth Muscle Physiology: A Role for Sex Hormones? *Journal of Andrology* 24 (6): S6-S16.
27. Eto M, Kitazawa T, Matsuzawa F, Aikawa S, Kirkbride JA, Isozumi N, Nishimura Y, Brautigan DL, Ohki S (2007) Phosphorylation-induced conformational switching of CPI-17 produces a potent myosin phosphatase inhibitor. *Structure* 15 (12): 1591-1602.
28. Fabbri A, Aversa A, Aldo I (1997) Erectile dysfunction: an overview. *Human Reproduction Update* 3(5): 455-466.
29. Fan SF, Brink PR, Melman A, Christ GJ (1995) An Analysis of the Maxi-K^+ (K_{Ca}) Channel in Cultured Human Corporal Smooth Muscle Cells. *The Journal of Urology* 153: 818-825.

30. Ferguson KA (1964) Starch-gel Electrophoresis-Application to the Classification of Pituitary Proteins and Polypeptides. *Metabolism 13: 985-1002.*

31. Gefen A, Chen J, Elad D (2001) Computational tools in rehabilitation of erectile dysfunction. *Medical Engineering & Physics* 23: 69-82.

32. Giuliano, Francois (2004) Control of Penile Erection by the Melanocortinergic System: Experimental Evidences and Therapeutic Perspectives. *The Journal of Andrology* 25: 683-691.

33. Giuliano F, Rampin O (2000) Central Neural Regulation of Penile Erection. *Neuroscience and Biobehavioral Reviews* 24: 517-533.

34. Giuliano F, Bernabe J, Brown K, Droupy S, Benoit G, Rampin O (1997) Erectile response to hypothalamic stimulation in rats: role of peripheral nerves. *American Journal of Physiology* 273: R1990-R1997.

35. Glina, S (2004) Testosterone and erectile dysfunction. *The Journal of Men's Health and Gender* 1(4): 407-412.

36. Gooren, L (2006) The role of testosterone in erectile function and dysfunction. *The Journal of Men's Health and Gender* 3(3): 292-298.

37. Gooren LJG, Saad F (2006) Recent insights into androgen action on the anatomical and physiological substrate to penile erection. *Asian Journal of Andrology* 8: 3-9.

38. Guay, AT (2005) Relation of Endothelial Cell Function to Erectile Dysfunction: Implications for Treatment. *The American Journal of Cardiology* 96: 52-56.

39. Gupta S, Moreland RB, Munarriz R, Daley J, Goldstein I, Saenz de Tejada I (1995) Possible role of Na^+ -K^+ - ATPase in the regulation of human corpus

cavernosum smooth muscle contractility by nitric oxide. *British Journal of Pharmacology* 116: 2201-2206.

40. Hames BD (eds) (1998) *Gel Electrophoresis of Proteins: A Practical Approach*. Third edition, Oxford University Press, Oxford, New York.
41. Hurt KJ, Musicki B, Palese MA, Crone JK, Becker RE, Moriarity JL, Snyder SH, Burnett AL (2002) Akt-dependent phosphorylation of endothelial nitric-oxide synthase mediates penile erection. *Proceedings of the National Academy of Sciences of the United States of America* 99: 4061-4066.
42. Jensen J, Lendorf A, Stimpel H, Frost J, Ibsen H, Rosenkilde P (1999) The Prevalence and Etiology of Impotence in 101 Male Hypertensive Outpatients. *American Journal of Hypertension* 12: 271-275.
43. Jin L, Burnett AL (2006) RhoA/Rho-kinase in erectile tissue: mechanisms of disease and therapeutic insights. *Clinical Science* 110: 153-165.
44. Kahn MA, Thompson CS, Mumtaz FH, Mikhailidis DP, Morgan RJ, Bruckdorfer RK, Naseem KM (2001) The effect of nitric oxide and peroxynitrite on rabbit cavernosal smooth muscle relaxation. *The World Journal of Urology* 19 (3) 220-224.
45. Karkanis T, DeYoung L, Brock GB, Sims SM (2003) Ca2+-activated Cl- channels in corpus cavernosum smooth muscle: a novel mechanism for control of penile erection. *The Journal of Applied Physiology* 94: 301-313.
46. Kawase T, Burns DM (1998) Calcitonin Gene-Related Peptide Stimulates Potassium Efflux through Adenosine Triphosphate-Sensitive Potassium Channels

and Produces Membrane Hyperpolarization in Osteoblastic UMR106 Cells. *Endocrinology* 139: 3492-3502.

47. Kim N, Azadzoi, KM, Goldstein I, de Tejada IS (1991) A Nitric Oxide-like Factor Mediates Nonadrenergic-Noncholinergic Neurogenic Relaxation of Penile Corpus Cavernosum Smooth Muscle. *The Journal of Clinical Investigations* 88: 112-118.
48. Kim NN, Huang Y-h, Moreland RB, Kwak SS, Goldstein I, Traish A (2000) Cross-Regulation of Intracellular cGMP and cAMP in Cultured Human Corpus Cavernosum Smooth Muscle Cells. *Molecular Cell Biology Research Communications* 4: 10-14.
49. Kruger THC, Haake P, Hartmann U, Schedlowski M, Exton MS (2002) Orgasm induced prolactin secretion: feedback control of sexual drive? *Neuroscience and Biobehavioral Review* 26: 31-44.
50. Lee SW, Kang TM (2001) Effects of nitric oxide on the Ca2+-activated potassium channels in smooth muscle cells of the human corpus cavernosum. *Urological Research* 29: 359-365.
51. Lee SW, Wang HZ, Christ GJ (1999) Characterization of ATP-sensitive potassium channels in human corporal smooth muscle cells. *International Journal of Impotence Research* 11: 179-188.
52. Lee SW, Wang HZ, Zhao W, Ney P, Brink PR, Christ GJ (1999) Prostaglandin E_1 activates the large-conductance K_{Ca} channel in human corporal smooth muscle cells. *International Journal of Impotence Research* 11: 189-200.

53. Levin RM, Hypolite JA, Broderick GA (1997) Evidence for a Role of Intracellular-Calcium Release in Nitric Oxide-Stimulated Relaxation of the Rabbit Corpus Cavernosum. *Journal of Andrology* 18 (3): 246-249.

54. Lewis RW, Mills TM (2004) Effects of Androgens on Penile Tissue. *Endocrine* 23: 101-105.

55. Lin CS, Xin ZC, Wang Z, Lin G, Lue TF (2008) Molecular Yin and Yang of erectile function and dysfunction. *Asian Journal of Andrology* 10 (3): 433-440.

56. Lincoln TM, Dey N, Sellak H (2001) Invited Review: cGMP-dependent protein kinase signaling mechanisms in smooth muscle: from the regulation of tone to gene expression. *Journal of Applied Physiology* 91: 1421-1430.

57. Liu PY, Death AK, Handelsman DJ (2003) Androgens and Cardiovascular Disease. *Endocrine Reviews* 24 (3): 313-340.

58. Lue, TF (2000) Erectile Dysfunction. *The New England Journal of Medicine* 342 (24): 1802-1813.

59. Lugg JA, Rajfer J, Gonzalez-Cadavid NF (1995) Dihydrotestosterone Is Active Androgen in the Maintenance of Nitric Oxide-Mediated Penile Erection in the Rat. *Endocrinology* 136: 1495-1501.

60. Maas R, Schwehelm E, Albsmeier J, Boger RH (2002) The pathophysiology of erectile dysfunction related to endothelial dysfunction and mediators of vascular function. *Vascular Medicine* 7: 213-225.

61. Maggi M, Filippi S, Ledda F, Magini A, Forti G (2000) Erectile dysfunction: from biochemical pharmacology to advances in medical therapy. *European Journal of Endocrinology* 143: 143-154.

62. McKenna K (1999) Central nervous system pathways involved in the control of penile erection. *Annual Review of Sex Research* 10: 157-183.

63. Melman A, Gingell JC. (1999) The Epidemiology and PathoPhysiology of Erectile Dysfunction. *The Journal of Urology* 161: 5-11.

64. Mills TM, Chitaley K, Wingard CJ, Lewis RW, Webb RC (2001) Effect of Rho-kinase inhibition on vasoconstriction in the penile circulation. *Journal of Applied Physiology* 91: 1269-1273.

65. Mills TM, Dai Y, Stopper VS, Lewis RW (1999) Androgenic maintenance of the erectile response in the rat. *Steroids* 64: 605-609.

66. Morelli A, Filippi S, Mancina R, Luconi M, Vignozzi L, Marini M, Orlando C, Vannelli GB, Aversa A, Natali A, Forti G, Giorgi M, Jannini EA, Ledda F, Maggi M (2004) Androgens regulate Phosphodiesterase Type 5 Expression and Functional Activity in Corpora Cavernosa. *Endocrinology* 145: 2253-2263.

67. Morelli A, Filippi S, Vignozzi L, Mancina R, Maggi M (2006) Physiology of Erectile Function: An Update on Intracellular Molecular Processes. *European Association of Urology* 4: 96-108.

68. Moreland RB, Hsieh G, Nakane M, Brioni JD (2001) The Biochemical and Neurologic Basis for the Treatment of Male Erectile Dysfunction. *The Journal of Pharmacology and Experimental Therapeutics* 296: 225-234.

69. NIH Consensus Development Panel on Impotence. NIH Consensus Conference. (1993) Impotence. *Journal of American Medical Association* 270: 83-90.

70. Padley RJ, Dixon DB, Wu-Wong JR (2002) Effect of castration on endothelin receptors. *Clinical Science* 103: 4425-4455.

71. Palese MA, Crone JK, Burnett AL (2003) A Castrated Mouse Model of Erectile Dysfunction. *Journal of Andrology* 24 (5): 699-703.

72. Reilly CM, Stopper VS, Mills TM (1997) Androgens Modulate the α-Adrenergic Responsiveness of Vascular Smooth Muscle in the Corpus Cavernosum. *Journal of Andrology* 18: 26-31.

73. Reilly CM, Zamorano P, Stopper VS, Mills TM (1997) Androgenic Regulation of NO Availability in Rat Penile Erection. *Journal of Andrology* 18: 110-115.

74. Rubio JLR, Hernandez M, de Los Arcos LR, Martinez AC, Garcia-Sacristan A, Prieto D (2004) Mechanisms of Prostaglandin E_1 Induced Relaxation in Penile Resistance Arteries. *The Journal of Urology* 171: 968-973.

75. Ryu JK, Song SU, Han JY, Chu YC, Lee M, Kim JS, Kim SJ, Suh JK (2005) Establishment of Penile Fibrosis Model in a Rat using Mouse NIH 3T3 Fibroblasts expressing Transforming Growth Factor β1. *Biology of Reproduction* 72: 916-921.

76. Sachs BD (2000) Contextual approaches to the physiology and classification of erectile function, erectile dysfunction, and sexual arousal. *Neuroscience and Biobehavioral Reviews* 24: 541-560.

77. Saenz de Tejada I (2000) Molecular mechanisms for the regulation of penile smooth muscle contractility. *International Journal of Impotence Research* 12: S34-S38.

78. Sato Y, Zhao W, Christ GJ (2001) Central modulation of the NO/cGMP pathway affects the MPOA-induced intracavernous pressure response. *American Journal*

of Physiology –Regulatory, Integrative and Comparative Physiology 281: 269-278.

79. Sehgal VN, Srivastava G (2003) Erectile Dysfunctions. *SKINmed* 2 (6): 350-356.
80. Shabsigh R, Rajfer J, Aversa A, Traish AM, Yassin A, Kalinchenko SY, Buvat J (2006) The Evolving Role of Testosterone in the Treatment of Erectile Dysfunction. *International Journal of Clinical Practice* 60(9): 1087-1092.
81. Shabsigh R, Raymond JF, Olsson CA, O'Toole K, Buttyan R (1998) Androgen Induction of DNA Synthesis in the Rat Penis. *Urology* 52: 723-728.
82. Sharifi N, Gulley JL, Dahut WL (2005) Androgen Deprivation Therapy for Prostate Cancer. *The Journal of the American Medical Association* 294 (2): 238-244.
83. Simonsen U, Garcia-Sacristan A, Prieto D (2002) Penile Arteries and Erection. *The Journal of Vascular Research* 39: 283-303.
84. Somlyo AP, Somlyo AV (2000) Signal transduction by G-proteins, Rho-kinase and protein phosphatase to smooth muscle and non-muscle myosin II. *Journal of Physiology* 522: 177-185.
85. Spektor M, Rodriguez R, Rosenbaum RS, Wang HZ, Melman A, Christ GC (2002) Potassium Channels and Human Corporeal Smooth Muscle Cell Tone: Further evidence of the Physiological Relevance of the Maxi-K Channel Subtype to the Regulation of Human Corporeal Smooth Muscle Tone in Vitro. *The Journal of Urology* 167: 2628-2635.

86. Steers WD (2000) Neural pathways and central sites involved in penile erection: neuroanatomy and clinical implications. *Neuroscience and Biobehavioral Reviews* 24: 507-516.

87. Steers WD (1994) Neuroanatomy and Neurophysiology of Erection. *Sexuality and Disability* 12 (1): 17-27.

88. Torrecillas G, Diez-Marques ML, Garcia-Escribano C, Bosch RJ, Rodriguez-Puyol D, Rodriguez-Puyol M (2000) Mechanisms of cGMP-dependent mesangial-cell relaxation: a role for myosin light-chain phosphatase activation. *Biochemical Journal* 346: 217-222.

89. Traish AM, Park K, Dhir V, Kim NN, Moreland RB, Goldstein I (1999) Effects of Castration and Androgen Replacement on Erectile Function in a Rabbit Model. *Endocrinology* 140: 1861-1868.

90. Traish AM, Munarriz R, O'Connell L, Choi S, Kim SW, Kim NN, Huang YH, Goldstein I (2003) Effects of Medical or Surgical Castration on Erectile Function in an Animal Model. *Journal of Andrology* 24: 381-387.

91. Uckert S, Hedlund P, Waldkirch E, Sohn M, Jonas U, Andersson KE, Stief CG (2004) Interactions between cGMP and cAMP pathways are involved in the regulation of penile smooth muscle tone. *The World Journal of Urology* 22: 261-266.

92. Venkateswarlu K, Giraldi A, Zhao W, Wang HZ, Melman A, Spektor M, Christ GC (2002) Potassium channels and Human Corporeal Smooth Muscle Cell Tone: Diabetes and Relaxation of Human Corpus Cavernosum Smooth Muscle by

Adenosine Triphosphate Sensitive Potassium Channel Openers. *The Journal of Urology* 168: 355-361.

93. Wang H, Eto M, Steers WD, Somlyo AP, Somlyo AV (2002) RhoA-mediated Ca2+ Sensitization in Erectile Function. *The Journal of Biological Chemistry* 277 (34): 30614-30621.
94. Webb RC (2003) Smooth Muscle Contraction and Relaxation. *Advances in Physiology Education* 27 (4): 201-206.
95. Williams BA, Liu C, DeYoung L, Brock GB, Sims SM (2005) Regulation of intracellular Ca2+ release in corpus cavernosum smooth muscle: synergism between nitric oxide and cGMP. *American Journal of Physiology – Cell Physiology* 288: 650-658.
96. Wingard CJ, Johnson JA, Holmes A, Prikosh A (2003) Improved erectile function after Rho-kinase inhibition in rat castrate model of erectile dysfunction. *American Journal of Physiology –Regulatory, Integrative and Comparative Physiology* 284: 1572-1579.
97. Wooldridge AA, MacDonald JA, Erdodi F, Ma C, Borman MA, Hartshorne DJ, Haystead TAJ (2004) Smooth muscle phosphatase is regulated in vivo by exclusion of phosphorylation of threonine 696 of MYPT1 of serine 695 in response to cyclic nucleotides. *The Journal of Biological Chemistry* 279 (33): 34496-34504.
98. Yang CC, Bradley WE (1998) Neuroanatomy of the penile portion of the human dorsal nerve of the penis. *British Journal of Urology* 82 (1): 109-113.